Title

Electric Truck Fleet Management under Limited and Uncertain Charging Infrastructure Availability

Authors

Ioannou, Petros
Liu, Xiaocheng
Waqas, Muhammad
et al.

Publication Date

2025-07-01

DOI

10.7922/G2XP7382

Data Availability

The data associated with this publication are available at:
https://doi.org/10.5061/dryad.6hdr7srbv

National Center for Sustainable Transportation
A USDOT University Transportation Center

Research Report

July 2025

Electric Truck Fleet Management under Limited and Uncertain Charging Infrastructure Availability

Petros Ioannou, Xiaocheng Liu, and Muhammad Waqas, University of Southern California

Matthew Barth, Kanok Boriboonsomsin, and Dongbo Peng, University of California, Riverside

METRANS Transportation Consortium USC CSULB

UCR College of Engineering – Center for Environmental Research and Technology

Figure 4-

TECHNICAL REPORT DOCUMENTATION PAGE

1. Report No.	2. Government Accession No.	3. Recipient's Catalog No.
NCST-USC-RR-25-17	N/A	N/A

4. Title and Subtitle Electric Truck Fleet Management under Limited and Uncertain Charging Infrastructure Availability	**5. Report Date** July 2025 **6. Performing Organization Code** N/A
7. Author(s) Dongbo Peng, https://orcid.org/0000-0002-9857-3303 Kanok Boriboonsomsin, Ph.D., https://orcid.org/0000-0003-2558-5343 Matthew Barth, Ph.D., https://orcid.org/0000-0002-4735-5859 Petros Ioannou, Ph.D., https://orcid.org/0000-0001-6981-0704 Xiaocheng Liu, https://orcid.org/0009-0006-6034-6910 Muhammad Waqas, Ph.D., http://orcid.org/0000-0002-2169-1053	**8. Performing Organization Report No.** N/A
9. Performing Organization Name and Address University of Southern California METRANS Transportation Consortium University Park Campus, VKC 367 MC:0626 Los Angeles, California 90089-0626 University of California, Riverside Bourns College of Engineering – Center for Environmental Research & Technology 1084 Columbia Avenue Riverside, CA 92507	**10. Work Unit No.** N/A **11. Contract or Grant No.** USDOT Grant 69A3552348319 and 69A3552344814
12. Sponsoring Agency Name and Address U.S. Department of Transportation Office of the Assistant Secretary for Research and Technology 1200 New Jersey Avenue, SE, Washington, DC 20590	**13. Type of Report and Period Covered** Final Research Report (January 2024 – December 2024) **14. Sponsoring Agency Code** USDOT OST-R

15. Supplementary Notes

DOI: https://doi.org/10.7922/G2XP7382
Dataset DOI: https://doi.org/10.5061/dryad.6hdr7srbv

16. Abstract

The transition to zero-emission freight transportation is a critical component of California's climate strategy, yet the adoption of battery electric trucks (BETs) in both long-haul and short-haul operations faces significant challenges. Limited charging infrastructure, long charging durations, grid reliability concerns, and regulatory constraints—such as Hours of Service (HOS) requirements—pose operational hurdles for fleet operators. This study develops a comprehensive optimization framework for electric truck fleet management, addressing the interplay between infrastructure limitations, operational uncertainties, and energy cost fluctuations. This research will also provide scalable insights for policymakers and industry leaders, supporting the broader transition to sustainable freight transportation. Investments in ultra-fast charging infrastructure, extended-range BETs, and microgrid-based energy management are key to accelerating the electrification of freight operations while ensuring cost efficiency and operational resilience.

For long-haul electric trucking, this study leverages real-world data to optimize charging stops, minimize delays, and ensure regulatory compliance. Using a combination of mixed-integer programming and linearization techniques, the proposed model dynamically identifies cost-effective charging strategies, balancing factors such as driver wages, energy costs, and charging delays. For short-haul trucking, this study introduces a novel dispatching model—the electric vehicle routing problem with backhauls and time windows under uncertainty.

17. Key Words	18. Distribution Statement
Sustainable freight transportation, Electric Vehicle Routing Problem, Metaheuristics, Robust Optimization, Microgrid, Platooning	No restrictions.

19. Security Classif. (of this report)	20. Security Classif. (of this page)	21. No. of Pages	22. Price
Unclassified	Unclassified	129	N/A

Form DOT F 1700.7 (8-72) Reproduction of completed page authorized

About the National Center for Sustainable Transportation

The National Center for Sustainable Transportation is a consortium of leading universities committed to advancing an environmentally sustainable transportation system through cutting-edge research, direct policy engagement, and education of our future leaders. Consortium members include: the University of California, Davis; California State University, Long Beach; Georgia Institute of Technology; Texas Southern University; the University of California, Riverside; the University of Southern California; and the University of Vermont. More information can be found at: ncst.ucdavis.edu.

Disclaimer

Acknowledgments

This study was funded, partially or entirely, by a grant from the National Center for Sustainable Transportation (NCST), supported by the U.S. Department of Transportation (USDOT) through the University Transportation Centers program. The authors would like to thank the NCST and the USDOT for their support of university-based research in transportation, and especially for the funding provided in support of this project.

Electric Truck Fleet Management under Limited and Uncertain Charging Infrastructure Availability

A National Center for Sustainable Transportation Research Report

Petros Ioannou, Xiaocheng Liu, and Muhammad Waqas, Department of Electrical and Computer Engineering, University of Southern California

Matthew Barth, Kanok Boriboonsomsin, Dongbo Peng, College of Engineering –Center for Environmental Research and Technology, University of California, Riverside

Table of Contents

List of Tables

List of Figures

List of Acronyms

Term	Acronym
Adaptive large neighborhood search	ALNS
Average customers' delay time	ADT
Battery Energy Storage System	BESS
Battery electric truck	BET
Battery electric vehicle	BEV
Best-known solutions	BKS
California Public Utilities Commission	CPUC
Charging station	CS
Combined heat and power	CHP
Control barrier function	CBF
Delay cost	DC
Demand response	DR
Distribution Center	DC
Distributed generator	DG
Distributed storage	DS
Electric vehicle	EV
Electric vehicle routing problem	EVRP
Electric vehicle routing problem with backhauling, time windows and uncertain service times only	EVRPBTW-US
Electric vehicle routing problem with backhauling, time windows and uncertain travel times only	EVRPBTW-UT
Electric vehicle routing problem with backhauling, time windows, and uncertainty in service and travel times	EVRPBTW-USUT
Electric vehicle routing problem with time windows	EVRP-TW
Energy Storage Systems	ESS
Extreme fast charging	XFC
Green vehicle routing problem	GVRP
Hours of Service	HOS
Iterative local search	ILS
Level of service	LOS
Local search	LS
Microgrid	MG
Mixed-integer linear programming	MILP
Mixed-integer programmer	MIP
Monte Carlo	MC

Photovoltaic	PV
Robust optimization	RO
Simulated annealing	SA
Southern California Edison	SCE
State of Charge	SOC
Time-of-use	TOU
Vehicle routing problem with backhauls	VRPB
Vehicle-to-grid	V2G
Vehicle-to-vehicle	V2V

Electric Truck Fleet Management under Limited and Uncertain Charging Infrastructure Availability

Executive Summary

California has set aggressive targets and timelines for the sales and adoption of zero-emission trucks in the state. However, developing a charging infrastructure network for medium- and heavy-duty electric trucks is challenging and will take time. In addition, there has also been much debate about whether the electric grid capacity expansion can keep pace with this anticipated mass adoption of electric vehicles (EVs). The goal of this research is to simultaneously address the issues of freight decarbonization and supply chain resiliency by designing electric truck fleet management strategies that: 1) consider the limited availability of charging infrastructure for medium- and heavy-duty electric trucks, at least in the near future; 2) can respond to various uncertainties including those associated with electric grid service interruption or disruption; and 3) analyze the requirements and constraints associated with long-haul and short-haul trucking with respect to electric trucks.

Use of electric trucks in long-haul trucking

This report addresses key challenges in the adoption of electric trucks for freight transportation to include the case of disruptions, using the Long Beach to San Francisco route as a case study. The shift from diesel trucks to electric trucks is one of the crucial ways to cut greenhouse gas emissions and support California's climate goals. However, this transition faces obstacles, including limited charging infrastructure, long charging durations, and regulatory constraints related to government Hours of Service (HOS) requirements as well as infrastructure charging disruptions. To overcome these challenges, this project presents a comprehensive optimization framework that strategically plans charging stops and routes to minimize costs, reduce delays, and ensure regulatory compliance. The approach is dynamic in order to take into account disruptions.

While the methodologies presented in the report can be applicable to many other areas, the Long Beach/Los Angeles port to San Francisco corridor for long haul is selected to demonstrate the approach by incorporating the location and availability of charging stations (CSs), real-time traffic volume, and truck-specific data such as battery charging history and driver needs. Key variables included battery state of charge (SOC), charging times, driving schedules, and compliance with HOS regulations. By employing a combination of mixed-integer programming (MIP) and linearization techniques to handle non-linear constraints, the model ensured computational efficiency and adaptability. Using Gurobi for optimization, the framework dynamically identified the most cost-effective charging stops and routes, balancing energy consumption, driver wages, and charging delays for any given time that takes into account possible disruptions, i.e., some

CSs stop been accessible. This robust approach demonstrated significant potential for reducing costs and improving operational efficiency in long-haul electric freight transport.

The results showed that electric trucks could be both cost-competitive and operationally efficient. In the baseline scenario, driver wages accounted for approximately 65% of total operational costs, emphasizing the importance of minimizing downtime through synchronized charging and rest periods. The sensitivity analysis revealed that ultra-fast chargers (1,000 kilowatts (kW)) could reduce operational costs by up to 25% by shortening charging times and associated labor costs. Additionally, extended-range trucks (600-mile configurations) reduced costs by 10% compared to 300-mile trucks due to fewer required charging stops and improved route efficiency.

A comparative analysis between electric and diesel trucks showed that electric trucks offered a 20% lower total cost under baseline energy price conditions ($0.20/kilowatt-hour (kWh)), largely due to lower energy and maintenance costs. However, at higher energy prices, such as $0.38/kWh, 300-mile electric trucks with 250 kW chargers experienced cost convergence with diesel trucks, highlighting the need for stable energy pricing to maximize competitiveness.

The model also demonstrated resilience under dynamic conditions, such as grid disruptions and fluctuating energy prices. It adapted dynamically to changes in infrastructure availability and energy costs, maintaining near-optimal cost efficiency with minimal operational impact. For instance, when a CS was unavailable due to a simulated grid failure, the model successfully reconfigured routes, leading to only a 1.5% increase in costs. This flexibility highlights the importance of robust optimization (RO) frameworks for real-time decision-making and handling unexpected logistical challenges.

This research highlights the need for investments in ultra-fast charging infrastructure, extended-range electric trucks, and backup charging networks to support long-distance electric freight operations. The findings provide a scalable solution for decarbonizing freight systems beyond California, offering practical insights for policymakers and industry leaders seeking to expand electric truck adoption. By demonstrating that optimized electric truck operations can be both cost-effective and environmentally beneficial, this project supports future infrastructure planning, fleet expansion strategies, and public policies promoting sustainable freight transport globally. Future expansions should consider region-specific variables and dynamic factors, including charging infrastructure, road conditions, weather, driver behaviors, evolving battery technologies, and local regulations, to enhance the model.

In addition, the platooning of multiple electric trucks (two-truck platoon) has been proposed as a strategy to reduce aerodynamic drag for both the leading and trailing vehicles. Electric trucks, known for their energy efficiency compared to diesel trucks, can further enhance transportation efficiency through platooning. However, maintaining close spacing between multiple trucks raises safety concerns due to their high inertia. In this report we propose a provably safe controller for electric truck platooning that enables the trailing truck to maintain a short following distance without compromising safety. The controller guarantees safety even without vehicle-to-vehicle (V2V) communication. With V2V communication, the trailing truck can more closely follow the lead truck while keeping a close distance without compromising the safety of the two-truck platoon, resulting in higher energy efficiency. Replacing two drivers with one in a two-truck platoon in addition to fuel savings due to reduced aerodynamic drag also reduces the cost of labor and is an attractive solution if safety and operational issues can be effectively addressed.

Use of electric trucks in short-haul trucking

To support the deployment of battery electric vehicle (BEV) fleets in short-haul operations, Chapter 3 introduces a new dispatching problem: the electric vehicle routing problem with backhauls and time windows under travel time and service time uncertainty (EVRPBTW-USUT). This study incorporates a backhauling strategy in which linehaul customers (requiring deliveries) are served first, followed by backhaul customers (requiring pickups). Additionally, this formulation accounts for uncertainty in travel times and customer service times, making it more applicable to real-world urban freight logistics.

To efficiently solve this complex problem, we develop a two-phase metaheuristic algorithm that combines metaheuristic techniques with a RO framework. A key innovation in this study is the introduction of a memorized buffer within the robust model, which significantly reduces computational complexity, cutting computation time by up to 85% compared to the classic RO model. This enhancement improves the scalability and efficiency of solving the RO problem.

Extensive experiments were conducted to evaluate the algorithm's performance, including tests on a newly developed EVRPBTW benchmark dataset and a real-world case study from a full-service supply chain company in San Bernardino County, California. Results from Monte Carlo (MC) simulations demonstrate that the proposed model can reduce total delay time by up to 74%. Additionally, a comprehensive sensitivity analysis of uncertainty factors reveals that service time variability has a greater impact on overall performance compared to travel time uncertainty. This research advances sustainable urban freight logistics and provides valuable insights for decision-makers involved in scheduling BEV fleets.

Chapter 4 presents an integrated approach to optimizing microgrid (MG) management and electric truck operations, particularly in the context of power grid disruptions. This study aims to demonstrate how the synchronized optimization of a MG control algorithm and a battery electric truck (BET) routing algorithm can reduce overall system costs.

Instead of assuming that BEV fleets always start with a fully charged battery, we consider a scenario in which fleet operations begin with a limited SOC due to grid disruptions. The experimental setup includes a 100-kW solar photovoltaic (PV) system, a 500-kWh battery energy storage system (BESS), the electricity demand of a commercial building, and a heavy-duty vehicle charging system.

The MG management system is designed to align with the constraints and requirements of a commercial electric truck charging scheduler. Unlike previous approaches, this integrated framework utilizes the scheduler's outputs—such as time windows and energy demands—as constraints for MG management. The truck scheduling algorithm iteratively optimizes charging times, ensuring that charging occurs during low-cost periods or when renewable energy is available. Additionally, the EV scheduler dynamically adjusts truck arrival times based on the availability of clean energy sources, creating a feedback loop that continuously enhances cost efficiency.

Results indicate that the proposed co-optimization framework can significantly reduce both operational and recharging costs—by up to 71%—compared to a baseline scenario without co-optimization. These findings suggest that integrating MG management with electric truck logistics can effectively lower charging costs and improve the resilience of MGs, making them a viable solution for sustaining fleet operations during power disruptions.

Introduction

California has set aggressive targets and timelines for the sales and adoption of zero-emission trucks in the state. However, developing a charging infrastructure network for medium- and heavy-duty electric trucks is challenging and will take time. In addition, there has also been much debate about whether the electric grid capacity expansion can keep pace with this anticipated mass adoption of electric vehicles (EVs). The goal of this research is to simultaneously address the issues of freight decarbonization and supply chain resiliency by designing electric truck fleet management strategies that: 1) consider the limited availability of charging infrastructure for medium- and heavy-duty electric trucks, at least in the near future; 2) can respond to various uncertainties including those associated with electric grid service interruption or disruption; and 3) analyze the requirements and constraints associated with long-haul and short-haul trucking with respect to electric trucks.

This research builds on previous work by the research team. Specifically, this research extends the work of (Boriboonsomsin et al., 2022) and (Wu et al., 2024) by accounting for various uncertainties in the scheduling and routing of short-haul electric trucks. It also extends the work of routing fleets of long-haul trucks under the constraints of parking availability and Hours of Service (HOS) as well as routing of mixed fleets of trucks (Vital et al., 2020; Vital & Ioannou, 2019, 2021b, 2021a; Chen et al., 2022). In addition, this research develops strategies for operating electric truck fleets under grid service disruption.

Challenges of electric trucks in long-haul trucking

Freight transportation is a cornerstone of California's economy, with the Long Beach to San Francisco corridor serving as a critical route for transportation of goods. Together, the Ports of Los Angeles and Long Beach handle over 40% of all containers entering the United States, emphasizing the national importance of this corridor (Freightquote, n.d.). This route not only connects these major ports to key destinations across the state but also supports the broader logistics network essential for California's economic activity. However, the state's environmental goals demand a transition from diesel-powered trucks to EVs to reduce greenhouse gas emissions and combat climate change.

California leads the nation in EV adoption, accounting for 37% of U.S. registered light-duty EVs as of 2022 (U.S. Energy Information Administration, 2023). Despite this progress in the light-duty sector, the electrification of medium- and heavy-duty vehicles, such as freight trucks, lags behind. Challenges include limited charging infrastructure capable of accommodating large trucks, range limitations of current EV technology, and the higher upfront costs associated with electric trucks compared to their diesel counterparts (California Energy Commission, 2023).

These challenges are particularly pronounced along the approximately 400-mile Long Beach to San Francisco corridor. Limited charging stations (CSs), lengthy recharging times, and regulatory requirements such as mandated driver rest periods create a complex planning environment for electric truck operations (Federal Motor Carrier Safety Administration, n.d.). These issues increase delays and costs, making it harder to efficiently operate electric trucks along this route. In addition, unpredictable power supply cut offs may influence planned charging and last-minute adjustments are necessary.

To address these issues, researchers have explored strategies such as optimizing CS placement and advanced battery technologies to improve range. For example, recent studies have used discrete choice models to identify optimal CS locations based on user behavior and station usage (Lamontagne et al., 2023), while adaptive battery reconfiguration has been proposed to enhance energy efficiency in long-haul electric trucks (Li et al., 2023). However, these solutions often rely on static data, failing to account for dynamic factors like real-time traffic conditions and energy usage and unpredicted disruptions, which limit their applicability (McKinsey & Company, 2024; X. Zhang & Li, 2021). Although promising innovations such as solid-state batteries and ultra-fast charging technologies are emerging, their integration into commercial fleets remains in the early stages (Markus, 2024).

Advances in data analytics and real-time monitoring now offer new opportunities to enhance electric truck operations. By leveraging tools like predictive analytics, Global Positioning System (GPS)-based fleet management systems, and energy optimization algorithms, more precise and adaptive planning can be achieved. This study focuses on utilizing real-world data from trucking operations along the Long Beach to San Francisco corridor to develop dynamic optimization models that account for changing conditions. These models aim to provide actionable insights into energy consumption, charging schedules, and route efficiency, addressing both logistical and regulatory challenges.

Chapters 1 and 2 aim to develop an integrated optimization framework to address the challenges of electrifying freight transport along the Long Beach to San Francisco corridor. By leveraging real-world data, the framework will consider key variables such as battery state of charge (SOC), CS availability, driver rest requirements, and traffic conditions. The objective is to minimize total operational costs while ensuring regulatory compliance and maintaining efficiency. This research not only supports the transition to sustainable freight transportation but also provides a scalable solution that can be adapted to other critical freight corridors.

Challenges of electric trucks in short-haul trucking

In addition to long-haul electric trucking operations along the Long Beach to San Francisco corridor, this study also examines short-haul electric trucking, specifically last-mile delivery services. For this application, the primary objective of freight transportation providers is to maintain high-quality service that meets customers' level of service (LOS) expectations in a timely manner. However, uncertainty in travel and service times can lead to delays that not only degrade LOS but also increase labor costs for drivers. As urban freight dispatching systems transition to fully electric truck fleets, operators must carefully consider three critical factors: customer service times, travel times, and potential recharging times. Most existing studies assume that service and travel times are deterministic during the route planning stage (e.g., Peng, Zhao, et al., 2023; Yang et al., 2022a; Yu, Aloina, et al., 2023). However, failing to account for uncertainties in these variables can result in fragile route plans, leading to significant delays in real-world urban dispatching scenarios.

In Chapter 3, we address the challenges of freight decarbonization and supply chain resiliency by developing commercial electric truck fleet management strategies that (1) account for the limited availability of charging infrastructure for electric trucks and (2) incorporate uncertainties in travel and service times during last-mile delivery. This chapter formulates and solves an optimization model for a practical urban freight delivery service in which an electric truck fleet transports commercial products to suppliers and consignees. To address uncertainties, we introduce a new robust dispatching problem known as the electric vehicle routing problem with backhauls and time windows under uncertain service and travel times (EVRPBTW-USUT).

In addition, as truck fleets transition to EVs in the coming decades, they will increasingly rely on the electrical grid for power. However, grid service has become more vulnerable to interruptions due to various factors, including extreme heat waves (Andreoni, 2023), wildfire prevention measures (*Public Safety Power Shutoffs*, n.d.), and grid attacks (Morehouse, 2022). Fleet operators will likely encounter energy supply limitations that could significantly impact their planning and operations. Therefore, it is essential for fleet operators to develop strategies that account for potential power constraints when planning truck fleet operations.

In Chapter 4, we introduce an integrated approach to optimizing microgrid (MG) management and electric truck logistics, particularly in the context of power grid disruptions. This study demonstrates how the synchronized optimization of a MG control algorithm and a battery electric truck (BET) routing algorithm can reduce overall system costs.

As more electric trucks enter service, electricity demand will naturally rise, leading to increased peak loads—especially when multiple trucks charge simultaneously during high-demand periods. The existing electrical grid may require upgrades to accommodate this additional demand, both in terms of capacity and its ability to handle fluctuations caused by EV charging. To address these challenges, utilities may need to expand demand response (DR) programs that encourage truck operators to charge during off-peak hours or adopt intelligent charging technologies that dynamically adjust schedules based on grid conditions.

Integrating MGs with electric truck CSs offers several key benefits, particularly in energy management and sustainable transportation. Unlike light-duty passenger vehicle charging, heavy-duty electric truck charging requires significantly more power. The concentrated demand from multiple trucks charging simultaneously can strain the local electricity grid, potentially causing instability and increasing peak demand charges. MGs help mitigate these issues by providing localized power generation and storage, reducing reliance on the main grid.

Furthermore, MGs enhance the resilience of electric truck charging infrastructure during grid outages. By integrating renewable energy sources such as solar or wind with energy storage systems (ESS), MGs can ensure continuous operation of CSs, even during power disruptions. This is especially critical for commercial vehicle fleets that support essential services and logistics operations.

Chapter 1 - Routing Long-haul Trucks Under the Constraints of Parking Availability, CS Locations, Charging Times, and Hours of Operation & Reconfiguration of Routes to Accommodate Grid Service Disruption

1.1 Introduction

This section presents the mathematical formulation of the optimization model used to minimize operational costs for electric trucks traveling along the Long Beach–San Francisco corridor. The model integrates variables such as battery SOC, charging times, and driving schedules while ensuring compliance with regulatory requirements, including HOS constraints. The objective is to identify cost-effective routes that balance energy consumption, charging costs, and driver rest periods. The problem is formulated in a way that power disruptions can be taken into account once the information becomes available so the modified optimization problem with a smaller number of stations can be exercised to generate modified routes. The following assumptions are made:

- Trucks have similar characteristics and travel at a constant average speed.
- The location of CSs is known in advance and CSs are always available, and free of queues.
- Partial charging is allowed at any stop.
- Charging time is modeled using four SOC intervals, each with a constant rate to approximate real-world tapering behavior. The penalty on arrival SOC shortfall is used to account for the cost of the initial battery energy, which is otherwise unpriced at the trip's starting point.
- SOC is constrained to remain strictly positive throughout the trip to avoid vehicle breakdown.
- Rest is enforced when the projected driving time exceeds eight hours and is only permitted at stops with at least 0.5 hours rest time.

While the base model assumes static conditions, it can be changed dynamically in response to charging failures or station unavailability, enabling adaptive routing and energy planning.

1.1.1 Relate notations and parameters

Table 1-1. Parameters

Parameters	Meaning
N	Total number of CSs
C_i	Charging cost at station i (currency/1% SOC)
L_i	Location of CS i along the route (miles)
d_i	Distance from station i to station $i+1$, where $d_i = L_{i+1} - L_i$
V	Average driving speed (kilometers per hour)
E	Vehicle energy consumption rate (kilometers per 1% charge)
W	Driver's wage rate (currency units per hour)
$C_{penalty}$	Cost for SOC deficit at the destination (currency/1% SOC)
s_k	Charging speed for SOC interval k (hours/1% SOC)
$\mathrm{k} = 1$	$0\% \leq \mathrm{SOC} < 20\%$
$\mathrm{k} = 2$	$20\% \leq \mathrm{SOC} < 40\%$
$\mathrm{k} = 3$	$40\% \leq \mathrm{SOC} < 80\%$
$\mathrm{k} = 4$	$80\% \leq \mathrm{SOC} \leq 100\%$
M	A large constant used for linearization (big-M method)
ε	A small positive constant used for constraint activation

Table 1-2. Decision Variables

Decision Variables	Meaning
x_i	Amount of charge at a CS
SOC_i	SOC of the vehicle upon leaving CS i
$SOC_{start,i}$	SOC of the vehicle upon arriving at station i, before charging begins
t_i	Total charging time at CS i (hours)
$x_{i,k}$	Amount of charge in SOC interval k at CS i (percentage points)
$t_{onduty,i}$	On-duty time at CS i (hours)
$T_{drive,i}$	Cumulative driving time before arriving at CS i (hours)
R_i	Binary variable indicating whether a 30-minute rest is taken at CS i
δ_i	Binary indicator variable, where δ_i=1 if the charging time $t_i \geq 0.5$ hours, and δ_i=0 otherwise
S_i	Auxiliary binary variable ensuring rest is only scheduled when both $R_i = 1$ and $\delta_i = 1$

1.1.2 Objective function

Minimize the total cost, including the driver's on-duty wage and charging cost:

$$\text{mininize } \mathrm{Z} = \mathrm{W} \times (\mathrm{t}_{\text{drive\_total}} + \sum_{\mathrm{i}=1}^{\mathrm{N}} \mathrm{t}_{\text{onduty,i}}) + \sum_{\mathrm{i}=1}^{\mathrm{N}} \mathrm{C}_{\mathrm{i}} \times \mathrm{x}_{\mathrm{i}} + C_{penalty} \times (100 - SOC_{N+1}) \quad 1.1$$

1.1.3 Constraints

Battery:

$$SOC_0 = SOC_{initial} \quad 1.2$$

SOC upon leaving CS i:

$$SOC_i = SOC_{i-1} - \frac{d_{i-1}}{E} + \mathrm{x}_{\mathrm{i}} \quad 1.3$$

Charging amount cannot be negative or cause SOC to exceed 100%:

$$0 \leq \mathrm{x}_{\mathrm{i}} \leq 100 - (\mathrm{SOC}_{\mathrm{i}-1} - \frac{\mathrm{d}_{\mathrm{i}-1}}{\mathrm{E}}) \quad 1.4$$

After leaving CS i, SOC must be sufficient to reach the next station:

$$SOC_i \geq \frac{d_i}{E} \quad 1.5$$

Decomposition of charging amount across SOC intervals:

$$x_i = \sum_{k=1}^{4} x_{i,k} \quad 1.6$$

Total charging time at station i:

$$t_i = \sum_{k=1}^{4} s_k \times x_{i,k} \quad 1.7$$

(non-linear)

Starting SOC before charging at station i:

$$SOC_{start,i} = SOC_{i-1} - \frac{d_{i-1}}{E} \quad 1.8$$

For each interval k:

0 to 20% 1.9

$$x_{i,1} = \begin{cases} min(20 - SOC_{start,i}, x_i), if\ SOC_{start,i} < 20 \\ 0\ otherwise \end{cases}$$

20 to 40% 1.10

$$x_{i,2} = \begin{cases} min(40 - (SOC_{start,i} + x_{i,1}), x_i - x_{i,1}), if\ SOC_{start,i} + x_{i,1} < 40 \\ 0\ otherwise \end{cases}$$

40 to 80% 1.11

$$x_{i,3} = \begin{cases} min(80 - (SOC_{start,i} + x_{i,1} + x_{i,2}), x_i - x_{i,1} - x_{i,2}), if\ SOC_{start,i} + x_{i,1} + x_2 < 80 \\ 0\ otherwise \end{cases}$$

80 to 100% 1.12

$$x_{i,4} = x_i - x_{i,1} - x_{i,2} - x_{i,3}$$

Driving time between stations:

$$t_{drive,i} = \frac{d_i}{V} \tag{1.13}$$

Total driving time:

$$t_{drive\_total} = \sum_{i=0}^{N} t_{drive,i} \tag{1.14}$$

Initial cumulative driving time:

$$T_{drive,0} = 0 \tag{1.15}$$

To comply with HOS regulations, if the projected cumulative driving time for the next segment exceeds eight hours, the driver must rest at the current CS before departure. When the cumulative driving time reaches or exceeds eight hours, the driver must take at least a 30-minute rest at the next CS.

1.1.4 Solution approach

The problem was solved using the Gurobi Optimizer, a state-of-the-art mixed-integer programming (MIP) solver. The MIP approach handles binary variables and continuous variables effectively, ensuring optimal solutions for complex routing and scheduling problems.

Since the problem contains several nonlinear constraints, several linearization methods are introduced to the formulation. For each CS i and SOC interval k:

$$x_{i,k} \geq 0 \tag{1.16}$$

$$x_{i,k} \leq U_{i,k} \tag{1.17}$$

$$x_{i,k} \leq x_i - \sum_{j=1}^{k-1} x_{i,j} \tag{1.18}$$

Where $U_{i,k}$ is the maximum allowable charge in interval k at station i, computed based on SOC limit

$$U_{i,k} = max(0, Upper\_limit_k - max(SOC_{start,i}, Lower\_Limit_k) \tag{1.19}$$

Where $\mathrm{Upper/Lower\_Limit}_k$ is the upper and lower bounds of SOC interval k.

Cumulative driving time update:

$$T_{drive,i} \geq T_{drive,i-1} + t_{drive,i-1} - MR_{i-1} \tag{1.20}$$

$$T_{drive,i} \leq T_{drive,i-1} + t_{drive,i-1} + MR_{i-1} \tag{1.21}$$

$$T_{drive,i} \leq M(1 - R_{i-1}) \tag{1.22}$$

Where M is a sufficiently large constant.

Rest requirement:

To enforce HOS regulations, the model introduces a binary variable R_i that triggers a rest break before driving from station i if the cumulative driving time exceeds eight hours. However, not all stations are suitable for resting—e.g., a minimum dwell time is required. To capture this, a binary variable δ_i is used to indicate whether the charging time at station i is at least 0.5 hours. An auxiliary variable S_i is defined to be 1 if and only if both $R_i = 1$, and δ_i = 1, using standard linearization (Eq 1.23–1.28). This structure ensures that rest breaks are only scheduled at operationally feasible locations.

Define binary variable S_i:

$$T_{drive,i} - 8 + M(1 - S_i) \geq 0 \tag{1.23}$$

$$T_{drive,i} - 8 - \varepsilon - MS_i \leq 0 \tag{1.24}$$

Where ε is a small positive number

Rest scheduling:

The rest scheduling decision at station i is made by forecasting the cumulative driving time required to reach station $i+1$. If the cumulative time exceeds eight hours, a rest must be scheduled at station i, prior to departure. This forward-looking logic ensures compliance with HOS regulations and avoids violations mid-trip.

$$R_i \geq S_i - S_{i-1} \tag{1.25}$$

Rest can only be taken at a CS where $t_i \geq 0.5$ hours

Definition of δ_i:

$$t_i - 0.5 + M(1 - \delta_i) \geq 0 \tag{1.26}$$

$$t_i - 0.5 - M\delta_i \leq 0 \tag{1.27}$$

$$R_i \leq \delta_i \tag{1.28}$$

1.1.5 Real-world adaptations

To reflect real-world complexities, the model incorporates:

1. Dynamic Input Data: Traffic-adjusted travel times and distances.
2. Charging Availability: Station-specific charging capacities and time-varying costs.
3. HOS Compliance: Explicit constraints aligning with federal regulations.

1.2 Results and discussion

This section presents the outcomes of the optimization model applied to the Long Beach–San Francisco corridor (Figure 1-1) for electric truck routing and charging. The analysis includes a baseline scenario, sensitivity analyses for charging speed and truck range, and a cost comparison between electric and diesel trucks. The findings highlight the effectiveness of the optimization framework in reducing operational costs while ensuring compliance with HOS constraints and logistical feasibility.

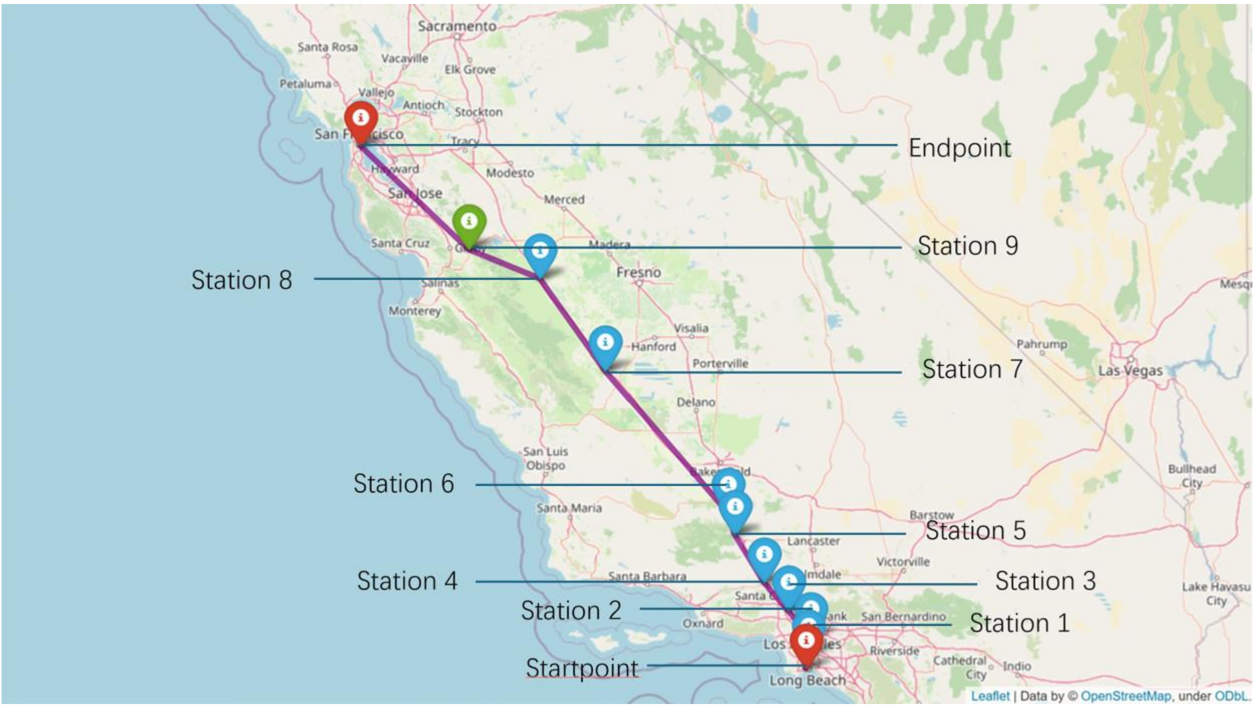

Figure 1-1. The location of CSs along the route.

1.2.1 Baseline scenario

The baseline scenario examines the performance of a 300-mile range electric truck operating along the Long Beach to San Francisco corridor with a charging speed of 250 kilowatts (kW). The total operational cost for this configuration was calculated to be $648.44, encompassing driver wages, energy costs, and charging downtime. Over the course of the journey, the truck required three charging stops, strategically distributed to balance energy consumption and minimize overall downtime.

The journey began with a full charge at 100% SOC, which gradually decreased as the truck traveled along the route. The first charging stop occurred at Station 7, where the SOC had dropped to 30.84%. At this stop, the truck recharged 9.16% SOC in just 0.14 hours, reflecting the efficiency of a 250 kW CS. Subsequent charging stops were made at Stations 8 and 9, with 19.93% and 7.70% SOC recharged, requiring 0.31 hours and 0.12 hours, respectively. These stops were strategically planned to align with energy needs while adhering to operational efficiency goals. Notably, the charging stop at Station 9 coincided with a mandatory rest period, ensuring compliance with HOS regulations.

The SOC management strategy proved effective in maintaining sufficient charge levels throughout the journey, avoiding penalties for insufficient SOC at the destination. The cumulative driving time between stops varied, with shorter intervals early in the journey and a maximum driving time of 7.08 hours before the third charging stop. This scheduling pattern minimized idle time and synchronized charging activities with driver rest requirements wherever feasible.

These findings underscore the logistical feasibility of using 300-mile range electric trucks with 250 kW charging infrastructure for long-haul freight routes. However, while operational costs were within acceptable limits, further optimization is possible. Synchronizing charging stops more effectively with mandatory rest periods could improve time efficiency, and reducing the number of stops through extended battery ranges or ultra-fast charging could lower overall costs.

1.2.2 Reconfiguration of routes to accommodate grid service disruption

This section evaluates the impact of a grid service disruption at Station 9, requiring the optimization framework to reconfigure the truck's route and charging schedule. Despite the unavailability of Station 9, the model dynamically adjusted charging activities and ensured sufficient SOC throughout the journey, maintaining operational feasibility and compliance with HOS regulations.

Under this scenario, the total operational cost increased slightly to $658.49, representing a 1.5% rise compared to the baseline scenario. The reconfigured route involved two effective charging stops (Stations 7 and 8) with adjustments to charging amounts and durations to account for the absence of Station 9.

In the updated plan, the truck's first charging stop occurred at Station 7, where the SOC was restored from 30.84% to 49.16%, requiring 0.35 hours. This additional charging ensured enough energy to reach Station 8, where SOC was further increased from 29.22% to 50.78%, taking 0.41 hours. Although Station 9 was skipped, the reconfiguration ensured the truck could continue the journey without penalties for insufficient SOC.

The SOC dynamics illustrate the model's robustness in handling disruptions. The cumulative driving time before each charging stop remained within HOS limits, with Station 8 coinciding with a required rest period. By integrating charging activities with mandatory breaks, the optimization minimized operational inefficiencies while adhering to regulatory requirements.

This reconfiguration highlights the importance of redundancy in charging infrastructure for long-haul freight routes. The inability to use Station 9 increased charging times at preceding stations and slightly raised operational costs. However, the model successfully mitigated the disruption's impact, demonstrating its flexibility and adaptability in real-world scenarios.

In conclusion, while the total cost rose modestly to accommodate the grid disruption, the framework proved effective in dynamically reallocating resources and maintaining route feasibility.

1.2.3 Sensitivity analysis

Impact of Charging Speed

This analysis evaluates how charging speed influences the total operational costs of a 300-mile-range electric truck. Two charging scenarios are compared: 250 kW chargers and 1,000 kW ultra-fast chargers. Results, as shown in the accompanying graph (Figure 1-2), indicate a linear relationship between energy price and total cost, with costs increasing proportionally as energy prices rise. At a baseline energy price of $0.20/kilowatt-hour (kWh), the total cost with 250 kW chargers was approximately $658, while 1,000 kW chargers reduced costs slightly to $648. The steeper slope observed for the 250 kW chargers reflects their higher sensitivity to energy prices, primarily due to longer charging times, which increase downtime and driver wage costs.

Ultra-fast chargers (1,000 kW) offer clear operational advantages by significantly reducing charging times and aligning with mandatory rest periods required under HOS regulations. While 250 kW chargers remain a viable alternative in areas without ultra-fast infrastructure or where installation costs are prohibitive, their higher operational costs make them less competitive. The benefits of 1,000 kW chargers are most pronounced in regions with low to moderate energy prices. As energy prices increase, the cost differential between the two scenarios diminishes, reducing the advantages of ultra-fast charging.

In summary, 1,000 kW ultra-fast chargers enhance operational efficiency and reduce costs for 300-mile trucks, but their cost-effectiveness depends on regional energy prices and infrastructure investments. Decisions on adopting this technology should balance these factors with long-term scalability.

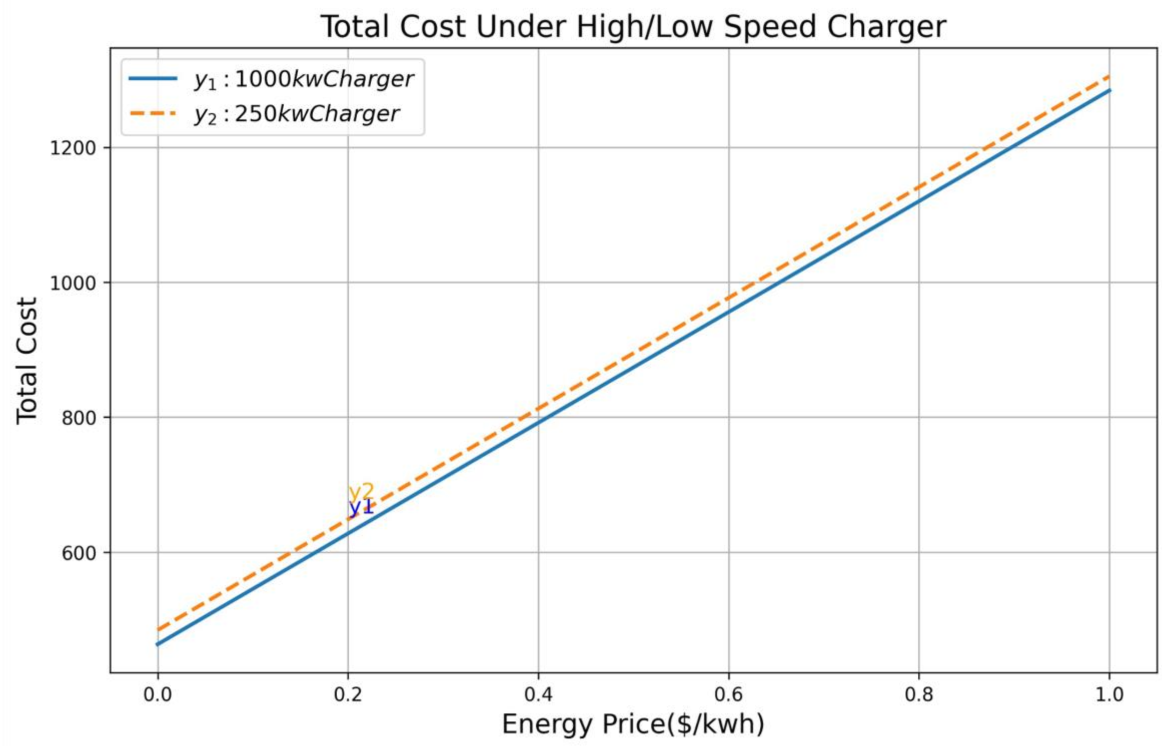

Figure 1-2. Total Cost Comparison Under High/Low Speed Charge.

Impact of Truck Range

This section explores the influence of truck range on total operational costs under two charging scenarios: 250 kW chargers and 1,000 kW ultra-fast chargers. The analysis compares 300-mile and 600-mile range trucks to assess the cost implications of extended-range battery configuration. Two graphs, Figure 1-3 and

Figure 1-4, illustrate the findings for the respective charging scenarios.

Figure 1-3 shows the relationship between energy price and total operational costs for 300-mile and 600-mile range trucks using 250 kW chargers. The results reveal a linear trend, with costs increasing as energy prices rise. At a baseline energy price of $0.20/kWh, the 300-mile truck incurred a total cost of approximately $658, while the 600-mile truck reduced costs to about $600, representing a 9% cost savings. The advantage of the 600-mile truck becomes more pronounced as energy prices increase, primarily because fewer charging stops reduce downtime and associated wage costs.

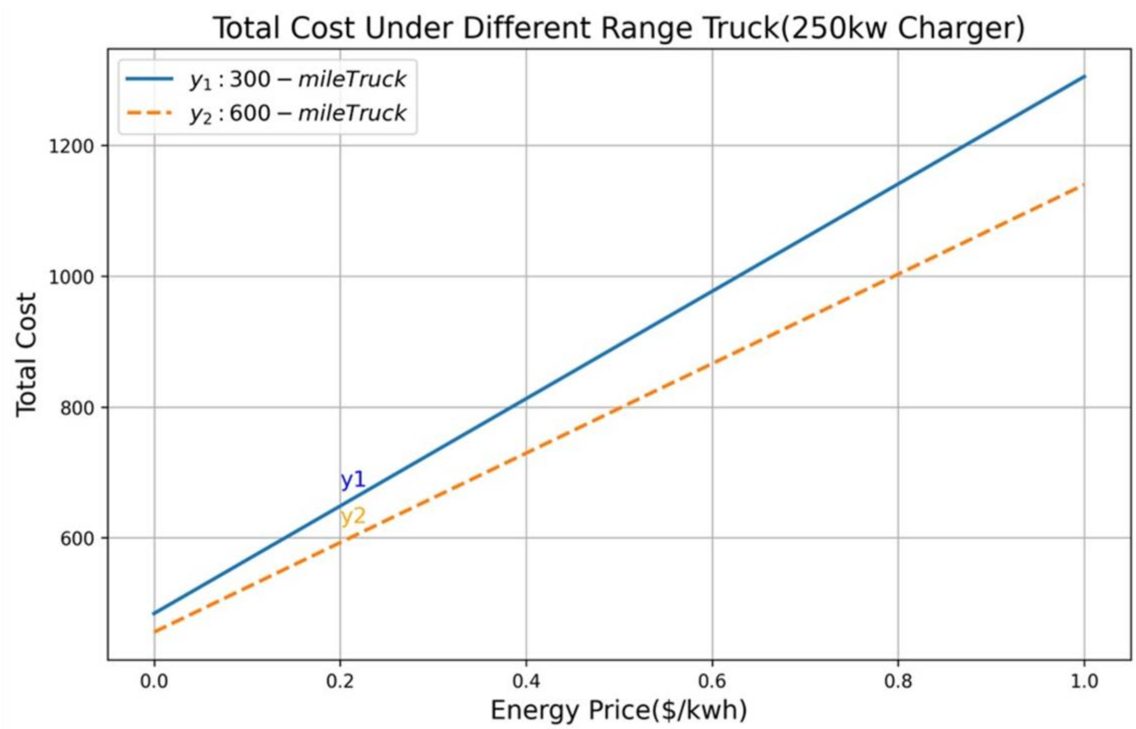

Figure 1-3. Total Cost Comparison Under Different Range Truck (250kw Charger)

Figure 1-4 presents a similar comparison for 300-mile and 600-mile range trucks but under the 1,000 kW ultra-fast charging scenario. The linear relationship between energy price and total costs is also evident here. At $0.20/kWh, the 300-mile truck's total cost was approximately $648, while the 600-mile truck reduced costs further to around $590, achieving a comparable percentage of savings as in the 250 kW scenario. The cost difference between the two truck configurations widens as energy prices increase, underscoring the scalability of longer-range trucks under higher price conditions.

When comparing the two charging scenarios, it is clear that ultra-fast chargers (1,000 kW) reduce operational costs for both truck configurations compared to 250 kW chargers. However, the cost advantages of the 600-mile truck are consistent across both scenarios. Regardless of charging speed, the extended range minimizes the number of stops required, reducing downtime and improving route efficiency. For instance, at $0.20/kWh, the 600-mile truck saves approximately $50 compared to the 300-mile truck in both scenarios, reinforcing the economic value of longer-range configurations.

The analysis highlights the operational and cost benefits of 600-mile range trucks, especially when paired with ultra-fast chargers. While 300-mile trucks remain viable, particularly in regions with robust charging infrastructure, the findings suggest that extended-range trucks offer significant scalability and efficiency for long-haul routes. By reducing charging stops and associated costs, 600-mile trucks present a compelling choice for operators aiming to optimize freight operations under varying energy price conditions.

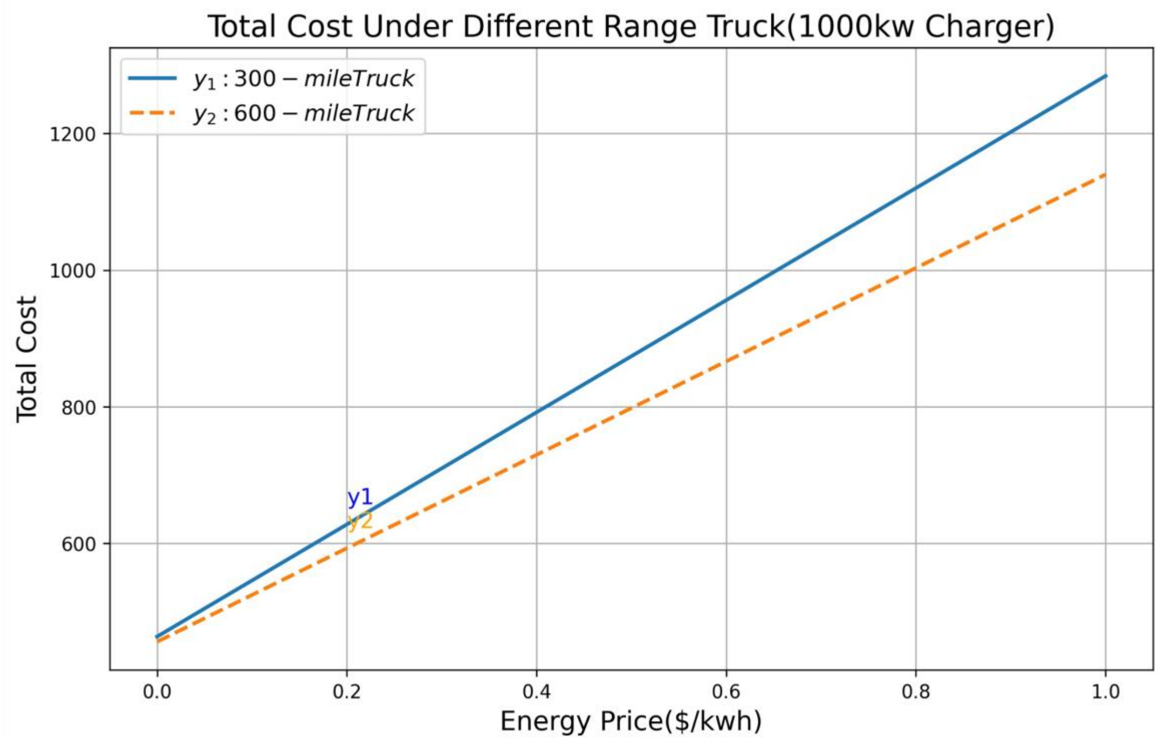

Figure 1-4. Total Cost Comparison Under Different Range Truck (1000kw Charger)

Comparison with Diesel Trucks

This section compares the total operational costs of electric trucks, with 300-mile and 600-mile ranges, to diesel trucks. The analysis accounts for varying electricity prices ($0.20/kWh to $0.38/kWh) and a fixed diesel price of $5 per gallon. The findings, presented in Figure 1-5, highlight the cost differences across these configurations and explore the impact of energy pricing on the competitiveness of electric trucks.

Figure 1-5 illustrates the total costs for four configurations: 300-mile and 600-mile electric trucks using 250 kW and 1,000 kW chargers, and diesel trucks. At an energy price of $0.20/kWh, the 600-mile electric truck demonstrated the lowest operational cost, approximately $600, outperforming both the diesel truck, at $700, and the 300-mile electric trucks, which incurred higher costs due to more frequent charging stops. Specifically, the 300-mile truck using 250 kW chargers cost about $658, while the same truck with 1000 kW chargers cost slightly less at $648.

As energy prices increase, the cost advantage of electric trucks narrows. At $0.38/kWh, the operational cost for 300-mile electric trucks using 250 kW chargers converged with that of diesel trucks, both at approximately $780. In contrast, the 600-mile truck maintained its relative advantage, though its total cost also rose, highlighting the sensitivity of electric trucks to electricity pricing.

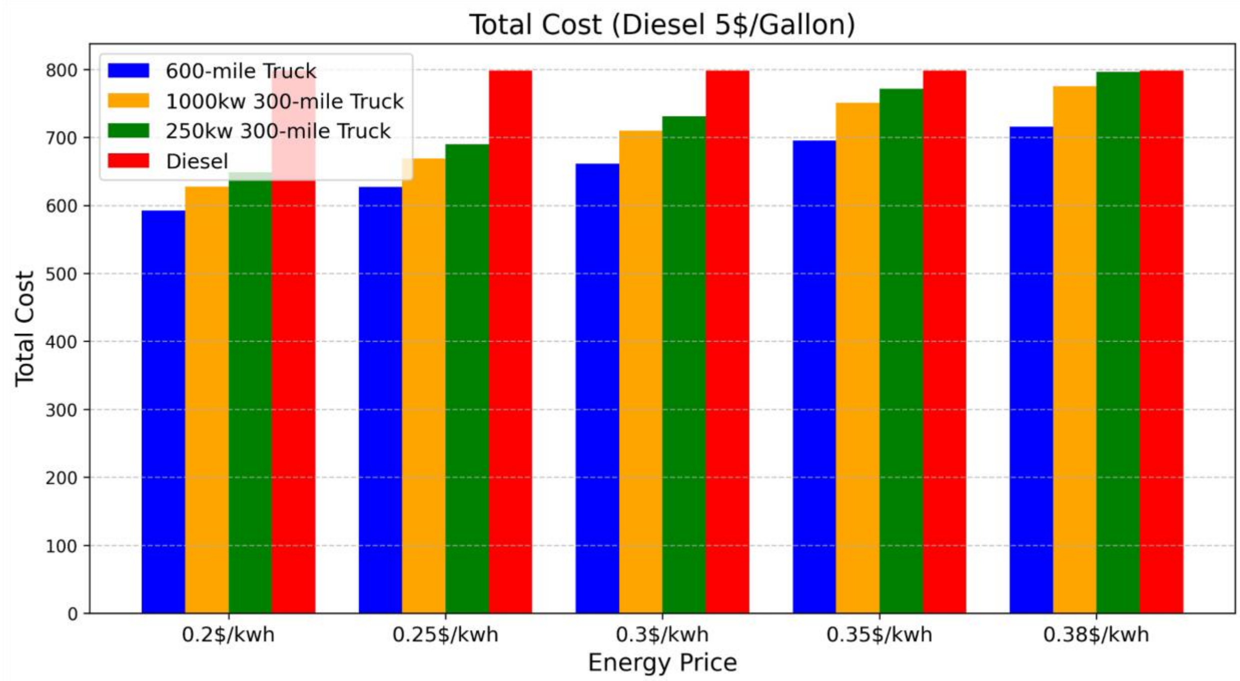

Figure 1-5. Total Cost Comparison between Electric Truck and Diesel Truck

The analysis demonstrates that 600-mile range electric trucks consistently outperform 300-mile range electric trucks in terms of cost efficiency across all energy price levels, regardless of charging speed. This is due to the reduced need for charging stops, which lowers downtime and associated driver wages. Additionally, the use of 1,000 kW chargers improves the competitiveness of 300-mile electric trucks compared to 250 kW chargers, particularly at lower energy prices. However, even with ultra-fast charging, the operational costs of 300-mile trucks remain higher than those of 600-mile trucks.

Diesel trucks, while more stable in cost due to fixed fuel pricing, are less competitive than electric trucks at lower electricity prices. However, their relative stability makes them more predictable and less sensitive to energy price fluctuations. This stability can appeal to operators concerned about the volatility of electricity prices, though it comes at the expense of higher greenhouse gas emissions and reduced alignment with environmental goals.

The findings in Figure 1-5 highlight the economic advantages of 600-mile electric trucks, which consistently achieve the lowest operational costs across most scenarios. While 300-mile electric trucks remain viable, their cost efficiency heavily depends on charging speed and electricity pricing. At higher electricity prices, their costs converge with those of diesel trucks, underscoring the importance of stable and affordable energy pricing to maximize the competitiveness of electric freight options. These results reinforce the value of extended-range configurations and high-speed charging infrastructure for enabling cost-effective and sustainable freight transport.

1.3 Conclusion

This study presents an optimization framework designed to address the specific challenges of electric truck routing and charging along the Long Beach–San Francisco corridor. By incorporating real-world constraints such as CS availability, battery SOC, and HOS regulations, the framework successfully minimizes operational costs while maintaining logistical feasibility.

In the baseline analysis, driver wages emerged as the dominant cost factor, heavily influenced by the time required for charging and mandated rest periods. The placement of charging stops proved to be a critical factor in balancing energy needs and compliance with regulations. These findings highlight the importance of carefully integrating charging schedules with rest requirements to improve efficiency and reduce delays.

The sensitivity analyses further underscored the potential of faster charging infrastructure and extended-range trucks to reduce costs and improve operational flexibility. For instance, ultra-fast chargers (1,000 kW) significantly lowered total costs by reducing downtime, while extended-range trucks minimized the need for charging stops, leading to a 10% reduction in overall costs. These results provide strong evidence for prioritizing investments in high-speed charging networks and advanced battery technology.

When compared to diesel trucks, electric trucks demonstrated a clear economic advantage, with 20% lower total costs under baseline energy pricing. Beyond financial benefits, the environmental impact of transitioning to electric trucks is substantial, aligning with California's climate and sustainability goals. However, the study also highlighted the vulnerability of electric freight operations to fluctuations in energy prices, particularly for trucks with shorter ranges relying on slower chargers. This underscores the need for stable energy pricing policies and targeted infrastructure improvements.

Despite its strengths, the model has several limitations. It assumes a fixed route between origin and destination to control computational complexity and does not account for alternative routing options. While this simplification enables tractable optimization, it may overlook potential cost savings from dynamic route selection in some cases. For long haul, however, especially in California, the truck routes are more or less fixed and there are limited options for alternative routes. Additionally, the model assumes static driving conditions and guaranteed charger availability, and it excludes capital costs such as vehicle purchase, charger installation, and battery degradation. Auxiliary energy consumption (e.g., Heating, Ventilation, and Air Conditioning (HVAC) or idling) and traffic variability are also not considered. These limitations present opportunities for future research to extend the framework into a more comprehensive and dynamic decision-support tool.

Chapter 2 - Use of Two-Truck Platoons

In this chapter, we address the feasibility of using a two-truck platoon where the lead truck is manually driven and the following one is automated. Such configuration reduces the number of drivers from two to one and in addition the charging can be also coordinated to be for two trucks at the same time. The main challenges of using two truck platoons are safety and energy efficiency. Provably safe and energy efficient platooning is essential for broader adoption of electric truck platooning in modern transportation networks. This chapter addresses the challenge of ensuring safe and energy efficient platooning of electric trucks using provably safe automatic longitudinal control based on control barrier functions (CBFs). Platooning, where trucks drive closely together in a coordinated manner, offers substantial benefits in terms of energy efficiency due to reduction of air drag. However, safety remains a critical concern, especially given the safety-critical nature of electric trucks. Through theoretical analysis and simulation, we demonstrate the effectiveness of CBFs in handling safety constraints ensuring robust platooning control. The results indicate that our approach improves energy efficiency by keeping a close inter-vehicular distance without compromising the safety.

The demand for the transportation of goods is rapidly increasing with the growing human population. A significant portion of the demand for transportation is fulfilled by trucks on highway. The trucks face higher aerodynamic drag than passenger vehicles because of their large frontal cross-sectional area. At high speeds, the resistance due to aerodynamic forces is the most dominate portion of total energy expenditure of the trucks. About 65% of total energy consumption is used to overcome the aerodynamic drag at the speed of 70 miles per hour (mph) for heavy-duty trucks (McCallen et al., 1999; Norrby, 2014).

Platooning of two or more trucks has been proposed as a way to reduce the aerodynamic drag on both leading truck and the trailing trucks (Vegendla et al., 2015). For the leading trucks, the decrease in aerodynamic drag is about 8% at close spacing. This effect quickly vanishes for greater distances. However, the effect of platooning is more pronounced for the trailing truck. The aerodynamic drag reduces to 20% to 50% when the spacing between lead vehicle and the following vehicle is equal to 30 feet. Electric trucks are highly energy efficient as compared to diesel trucks. Therefore, platoon formulation of electric trucks can further enhance the overall efficiency of transportation systems.

Since trucks have high inertia, platooning of two or more trucks with small spacing could potentially cause safety issues. Therefore, we need fully verified vehicle following controller than can ensure safety while keeping a small distance from the lead vehicle. We address this issue by proposing a provably safe controller for platooning of electric trucks that allows the trailing truck maintains a close gap without compromising the safety of the platoon. The controller will guarantee safety regardless the availability of vehicle-to-vehicle (V2V) communication.

2.1 Formulation

First, we consider the problem formulation. We refer to the following truck as a trailing truck. We present a non-linear dynamical model for the longitudinal motion of electric trucks.

2.1.1 Longitudinal model

Let X_f, and X_l be the longitudinal positions, and V_f, and V_l be the longitudinal speed of the trailing truck and the lead truck respectively. Let X_r be the inter-vehicular distance or relative distance, i.e., $X_r = X_l - X_f$. Let V_r be the relative speed, i.e., $V_r = V_l - V_f$. Let $\mathbf{x} \in \mathrm{R}^{4\times 1}$ be the state vector such that

$$\boldsymbol{x} = \left[X_l \; V_l \; X_f \; V_f\right]^T \tag{2.1}$$

Let m be the mass of the truck, F_w be the input force applied by wheels, F_{air} be the air drag force, F_{roll} be the rolling friction force, and F_{g} be the gravitational force. Let F_r be the sum of aerodynamic air drag, rolling friction and gravitational forces, i.e., $F_r = F_{\mathrm{air}} + F_{\mathrm{roll}} + F_{\mathrm{g}}$. We use the subscript f and l to differentiate between the corresponding forces of the lead truck and the trailing truck respectively. The system dynamics are given by

$$\dot{x} = \begin{bmatrix} \dot{X}_l \\ \dot{V}_l \\ \dot{X}_f \\ \dot{V}_f \end{bmatrix} = \begin{bmatrix} V_l \\ \dfrac{1}{m_l}\left(F_{w,l} - F_{r,l}\right) \\ V_f \\ \dfrac{1}{m_f}\left(F_{w,f} - F_{r,f}\right) \end{bmatrix} \tag{2.2}$$

The sum of frictional, gravitational and aerodynamic drag forces on the lead and the following vehicles are given by

$$F_{r,l} = F_{air,l} + F_{roll,l} + F_{g,l} \tag{2.3}$$

$$F_{r,f} = F_{air,f} + F_{roll,f} + F_{g,f} \tag{2.4}$$

Let c_d be the air drag coefficient, A_l be the maximum cross-sectional area of the lead truck, A_f be the maximum cross-sectional area of the trailing truck, ρ be the air density. Let $\phi_l(X_r) \in (0,1]$ and $\phi_f(X_r) \in (0,1]$ be the air drag ratios of the lead truck and the trailing truck as functions of X_r. When there is no platooning, then $\phi_l(\infty) = 1$, and $\phi_f(\infty) = 1$ otherwise $0 < \phi_l(X_r), \phi_l(X_f) < 1$ hold. The platoon formation reduces the aerodynamic drag on both trucks. This effect is more pronounced on the trailing truck than on the lead truck. The air drag ratios for different values of X_r are given in Table 2-1 (Vegendla et al., 2015).

The aerodynamic drag forces on lead vehicle and the following vehicle are given by

$$F_{air,l} = \frac{1}{2} c_d A_l p V_l^2 \phi_l(X_r) \qquad 2.5$$

$$F_{air,f} = \frac{1}{2} c_d A_l p V_f^2 \phi_f(X_r) \qquad 2.6$$

Let c_r be the coefficient of friction of the road, g = 9.8 m/s^2 be the gravitational constant, m_l be the mass of the lead truck and m_f be the mass of the trailing truck. The rolling frictional forces on the vehicles are given by

$$F_{roll,l} = c_r m_l g cos(\theta) \qquad 2.7$$

$$F_{roll,f} = c_r m_f g cos(\theta) \qquad 2.8$$

The gravitational forces on the lead vehicle and the following vehicle are given by

$$F_{g,l} = m_l g sin(\theta) \qquad 2.9$$

$$F_{g,f} = m_f g sin(\theta) \qquad 2.10$$

2.1.2 Air drag reduction

The air drag reduction has been studied extensively in the literature (Hussein & Rakha, 2021; McCallen et al., 1999). We use the following values of air drag ratio. We use linear interpolation to estimate the values of air drag for other relative distances.

Table 2-1. Air Drag Ratio of Lead and trailing trucks (Vegendla et al., 2015)

Type	**Relative Distance (feet)**			
	30	60	90	150
Lead Truck	0.92	0.984	0.993	0.99
trailing truck	0.506	0.606	0.67	0.704

2.1.3 V2V communication

We consider two scenarios: (1) with V2V communication and (2) without V2V communication. Let ψ_{v2v} be the binary variable that represents the availability of V2V communication such that ψ_{v2v} = 1 when we have V2V communication and ψ_{v2v} = 0 when we don't have V2V communication.

2.1.4 Safety constraints

We impose the following safety constraints on the platoon.

1. Both trucks must follow a safe speed, i.e., $V_l \leq V_{max}$ and $V_f \leq V_{max}$ must hold where V_{max} is the maximum speed limit.
2. The following vehicle should maintain a safe distance. Let $\underline{a}_f$ and $\underline{a}_l$ be the maximum braking deceleration of trailing truck and the lead truck. Let $X_0 > 0$ be the required relative distance between the lead truck and the trailing truck when they are at rest position. Let β be the constant time headway. The distance between lead vehicle and following vehicle must fulfill the following criteria.

$$h_1(x) = X_r - \beta V_f - \frac{1}{2}\left(\frac{V_f^2}{\underline{a}_f} - \frac{V_l^2}{\underline{a}_l}\right) - X_0 \tag{2.11}$$

   When $h_1(x) \geq 0$ then the trailing truck is at a safe distance from the lead truck. When $V_f = V_l$ snd $\underline{a}_f < \underline{a}_l$ hold then $h_1(x) = 0$ holds and the following vehicle maintains a minimum relative distance greater than X_0, i.e., $X_r > X_0$. On the other hand, when $V_f = V_l$ and $\underline{a}_f = \underline{a}_l$ hold then the following vehicle can safely follow the lead vehicle by keeping a safe distance $X_r = X_0$. Moreover, we need strong safety guarantees regardless of the availability of the V2V communication.
3. The electric trucks have limited braking capacity. We want to ensure the safety constraints while using limited braking capacity. Let a_b and a_a be the absolute values of the maximum deceleration and acceleration respectively. The acceleration of both trucks is limited to $-a_b \leq u_f, u_l \leq u_a$ where u_f and u_l denote the acceleration commands of the trailing truck and the lead truck respectively.

2.1.5 Mobility constraints

We impose the following safety constraints on the platoon. We require that $h_1(x) \rightarrow 0$ and $V_l - V_f = V_r \rightarrow 0$ so that the trailing truck tracks the speed of the lead truck while keeping a safe distance.

2.1.6 Energy

We evaluate the performance of platooning in terms of energy savings. The energy can be defined in terms of force applied by wheels in the following manner.

$$E_w(X_0) = \int F_w ds \tag{2.12}$$

Both vehicles benefit from platooning due to air drag reduction. We define the force reduction factor F_w as

$$\mathcal{F}_w = \frac{\Delta F_w}{F_w(\infty)} = \frac{F_w(\infty) - F_w}{F_{w,\infty}} \tag{2.13}$$

where $F_{w,\infty}$ denotes the force applied in the absence of platooning. Similarly, we define energy reduction factor $\mathcal{E}_w$ in the following manner

$$\mathcal{E}_w = \frac{\Delta E_w}{E_w, \infty} = \frac{E_w(\infty) - E_w}{E_{w,\infty}} \tag{2.14}$$

The forces applied by the wheels of lead vehicle and wheels of the following vehicle are denoted by $F_{w,l}$, and $F_{w,f}$ respectively. Similarly, the force reduction factor and the energy reduction factor are denoted by $F_{w,l}$, $F_{w,f}$ and $\mathcal{E}_{w,l}$, $\mathcal{E}_{w,f}$ respectively. The force reduction factor and energy reduction factor can be calculated using 2.13 and 2.14.

2.1.7 Energy efficiency

The $\mathcal{E}_w$ calculated above is the energy reduction factor during platooning regardless of the source of energy. The energy efficiency of the diesel truck is different than the energy efficiency of an electric truck. Assuming constant average efficiency of different parts of the electric truck and diesel truck we can find estimate their overall efficiency. Let $\mathcal{E}_w$ be the energy consumed by the wheels. Let η_d and η_e be the average efficiencies of the diesel truck and the electric truck. Let η_f be the average efficiency of the final drive, β_{gb} is the average efficiency of the gearbox, and let η_c be the average efficiency of the internal combustion engine. The efficiency of the diesel engine is given by

$$\eta_d = \eta_f \eta_{gb} \eta_c \tag{2.15}$$

Similarly, let η_m be the average electric machine efficiency, and η_b be the average battery efficiency and β_{ch} is the average charging efficiency then the average efficiency of the electric truck is given by

$$\eta_e = \eta_f \eta_{gb} \eta_m \eta_b \eta_{ch} \tag{2.16}$$

Using the values of these parameters from (Verbruggen et al., 2018), we get η_e = 0.71 and η_d = 0.33. Given energy required by the wheels E_w we can estimate the energy required by electric truck and diesel truck. Let E_e be the energy supplied by the grid and E_d be the energy supplied by the fuel then we have

$$E_e = \frac{E_w}{\eta_e}, \quad E_d = \frac{E_w}{\eta_d}. \tag{2.17}$$

Now we propose a provably safe automatic vehicle following controller for electric trucks.

2.2 Control and barrier functions

Since our approach is based on CBFs, we give a brief review of CBFs (Ames et al., 2019) in this section.

Let $x \in D \subseteq R^n$ be the state vector, $u \in U \subseteq R^m$ be the input vector, $f : R^n \rightarrow R^n$ and $g : R^n \rightarrow R^n$ be Lipschitz continuous functions. Let us consider a control affine nonlinear system

$$\dot{x} = f(x) + g(x)u \quad 2.18$$

Let C be the superlevel set of a continuously differentiable function $h(x)$ and it is defined by $C = \{x : h(x) \geq 0\}$. A continuously differentiable function $h(x) : D \rightarrow R$ is called a CBF if $\forall x \in D \subseteq R^n$ the following holds

$$\sup_{u \in U}\left[L_f h(x) + L_g h(x)u\right] \geq -\alpha\big(h(x)\big) \quad 2.19$$

where $\alpha(\cdot)$ is a K_∞ function. The superlevel set C is called the safe set. If the system starts within the safe set, i.e., $x(t_0) = x_0 \in C$ then any piecewise continuous controller $u \in U_{safe}$ would guarantee that the system remains within the safe set C where $U_{safe} \subseteq U \subseteq R^m$ is given by

$$U_{safe} = \{u \in U : L_f h(x) + L_g h(x)u + \alpha(h(x)) \geq 0\} \quad 2.20$$

This property is called forward-invariance and the set U_{safe} is called the set of safe inputs. In our previous work (Waqas et al., 2024), we proposed a provably safe automatic longitudinal control for autonomous vehicles under safety, comfort, and regulatory constraints such as traffic signals regardless of the availability of V2V and vehicle to infrastructure (V2I) communication. In this paper, we only consider safety, and comfort constraints for platooning of electric trucks.

2.3 Control design

Let $u_l = F_{w,l} - F_{r,l}$ and $u_f = F_{w,f} - F_{r,f}$ be the feedback linearized inputs of the lead vehicle and the following vehicle. The new system dynamics are given by

$$\begin{bmatrix} \dot{X}_l \\ \dot{V}_l \\ \dot{X}_f \\ \dot{V}_f \end{bmatrix} = \begin{bmatrix} V_l \\ \frac{1}{m} u_l \\ V_f \\ \frac{1}{m} u_f \end{bmatrix}$$

We represent the safety constraints as CBFs.

$$h_1(x) = X_r - \beta V_f - \frac{V_f^2 - V_1^2}{2u} - X_0 \qquad 2.21$$

$$h_2(x) = V_{max} - V_f \qquad 2.22$$

We use the following PID controller as a nominal controller.

$$u_0(t) = k_1 V_r - k_2 \delta + k_3 \int_{t_0}^{t} \delta \, dt \qquad 2.23$$

2.3.1 CBF constraints

Let $\alpha(\cdot)$ be an extended class-K_∞ function. Using $\alpha(c) = c$ as a class-K_∞ function and $h_1(x) \geq \alpha(h_1(x))$ we get

$$\dot{h}_1(x) = V_r - \beta \underline{u}_f - \frac{V_f}{\underline{u}} u_f + \frac{V_l}{\underline{u}} u_l \geq -h_1(x) \qquad 2.24$$

$$\dot{h}_1(x) = V_r - \frac{V_f}{\underline{u}} u_f + \frac{V_l}{\underline{u}} u_l \geq -h_1(x) \qquad 2.25$$

$$\dot{h}_2(x) = -u_f \geq -h_2(x) \qquad 2.26$$

The above relation can be simplified in the following form

$$u_f \leq \frac{\underline{u}}{\underline{u}_f \beta + V_f}\left(V_l - V_f + h_1(x) + \frac{a_l}{\underline{u}} V_l\right) \qquad 2.27$$

$$u_f \leq h_2(x) \qquad 2.28$$

In other words, the system is safe when the controller satisfies the following constraints.

$$-u \leq u_f \leq \min\left\{h_2(x), \frac{u}{u_f \beta + V_f}\left(V_l - V_f + h_1(x) + \frac{a_l}{u} V_l\right)\right\} \qquad 2.29$$

When we have V2V communication then the following vehicle knows the acceleration command of the lead vehicle. When there is no V2V communication, then we assume that $a_l = -\underline{u}$. The set of safe inputs that guarantees the safety of the system is given below

$$U = \begin{cases} U_{v2v}, & if\ \varphi_{v2v} = 1 \\ U_{nov2v}, & if\ \varphi_{v2v} = 0 \end{cases} \qquad 2.30$$

where U_{v2v} is the set of safe inputs when we have V2V communication and U_{nov2v} is the set of safe inputs when we don't have V2V communication. These sets are given below

$$U_{v2v} = \{u: -\underline{u} \leq u_f \leq u_{v2v}\}, \quad 2.31$$

$$U_{nov2v} = \{u: -\underline{u} \leq u_f \leq u_{nov2v}\}, \quad 2.32$$

$$u_{nov2v} = \min\{h_2(x), \frac{\underline{u}}{\underline{u}_f\beta + V_f}(h_1(x) - V_f)\} \quad 2.33$$

The provably safe controller is given by

$$u_l = \max\{-\underline{u}, \min\{u_0, u_{v2v}, u_{nov2v}, \overline{u}\}\} \quad 2.34$$

2.4 Simulation and results

We run the simulations in the traffic scenario where both vehicles start from rest position with X_r = 100 meters = 328.084 feet. We considered two communication scenarios: (1) V2V (2) without V2V. We studied the effects of air drag reduction on energy using our fully verified controller. We studied the effects under four different desired relative distance $X_0 \in$ {30 feet,60 feet,90 feet,150 feet}.

Consider Figure 2-1. The lead vehicle first accelerates and achieves the maximum speed 55 mph = 24.5872 meters/second (m/s) = 88.5 kilometers/hour (km/hr) and it then maintains its speed. The speed of both trucks is always less than the maximum speed limit V_{max}, i.e., $h_2(x) = V_{max} - V_f \geq 0$ holds.

Figure 2-1 shows that the trailing truck always maintains a safe distance from the lead truck, i.e., $h_1(x) \geq 0$. When we have a V2V communication then the trailing truck maintains a closer distance with $h_1(x) = 0$. However, when there is no V2V communication, the trailing truck adopts a more conservative approach. This is shown in Figure 2-2 and Figure 2-3. The minimum desired relative spacing is achieved only with V2V communication. When we have no V2V communication, the final relative spacing is slightly greater than 9.1 m.

Since the proposed controller makes sure that the trailing truck maintains a close but safe distance from the lead truck, the aerodynamic forces on the trailing truck are reduced significantly. Figure 2-4 shows the relative reduction in wheel force, i.e., force reduction factor F_w for the lead truck as well as the trailing truck. It also compares the values of F_w for both communication scenarios: with V2V and without V2V.

We conducted the same experiment for four different values of desired relative spacing X_0, i.e., $X_0 \in$ {30 feet,60 feet,90 feet,150 feet}. We calculated the energy consumption of each vehicle with and without platooning as well as with and without V2V communication. Then we calculated energy reduction factor E_w for both lead vehicle and the following vehicle to measure the percentage reduction in energy exerted by the wheels. This comparison is shown in Table 2-2. The energy savings for the following vehicle are higher than that of the lead vehicle. Moreover, energy benefits are greater at shorter inter-vehicular spacing than that of longer inter-vehicular spacing. The availability of V2V communications slightly improves the energy efficiency of the vehicles. At large distances such as $X_r \geq 90$ feet, the availability of V2V communication has negligible effect on energy savings.

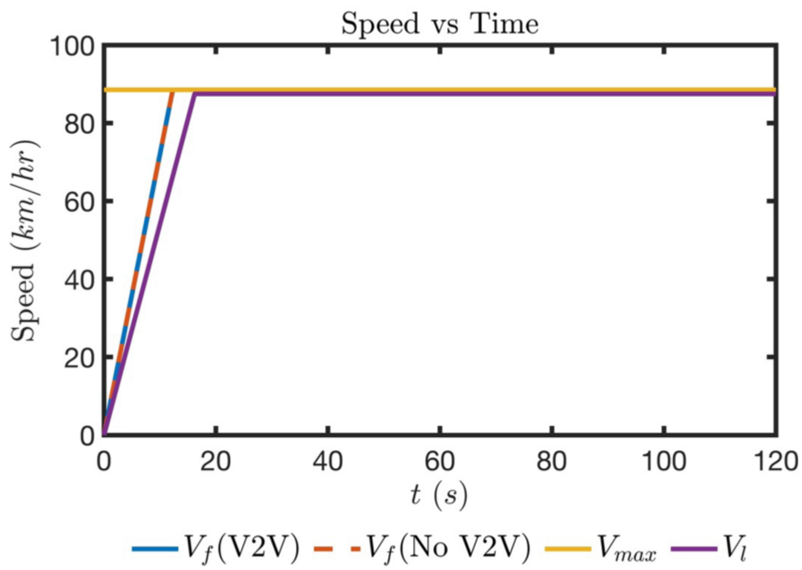

Figure 2-1. The speed profile of the lead truck and the trailing truck. This figure shows speed of the trailing truck while keeping a safe distance from the lead truck. This also shows speed profile with and without V2V communication between trucks. The provably safe controller never violates the maximum speed limit.

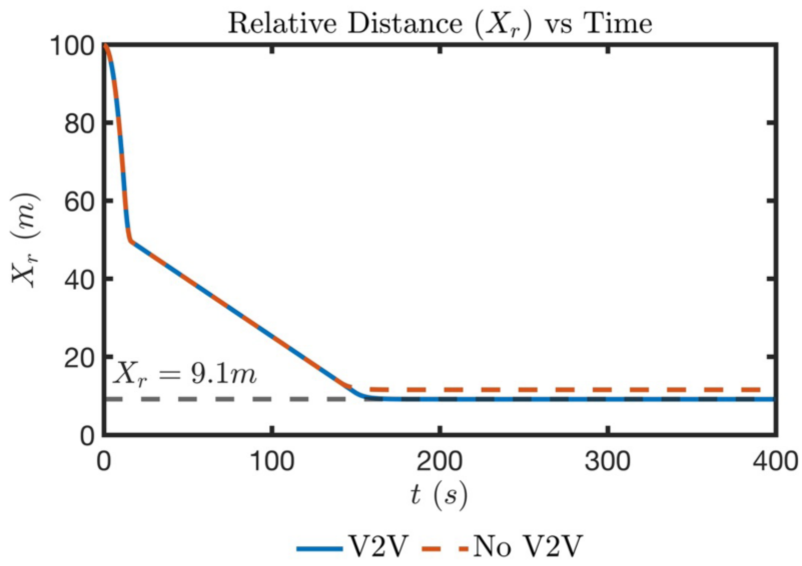

Figure 2-2. The comparison of relative spacing vs time for two scenarios: with V2V communication and without V2V communication. When there is V2V communication between lead and trailing trucks, the trailing truck keeps a smaller relative spacing than the scenario when there is no V2V communication.

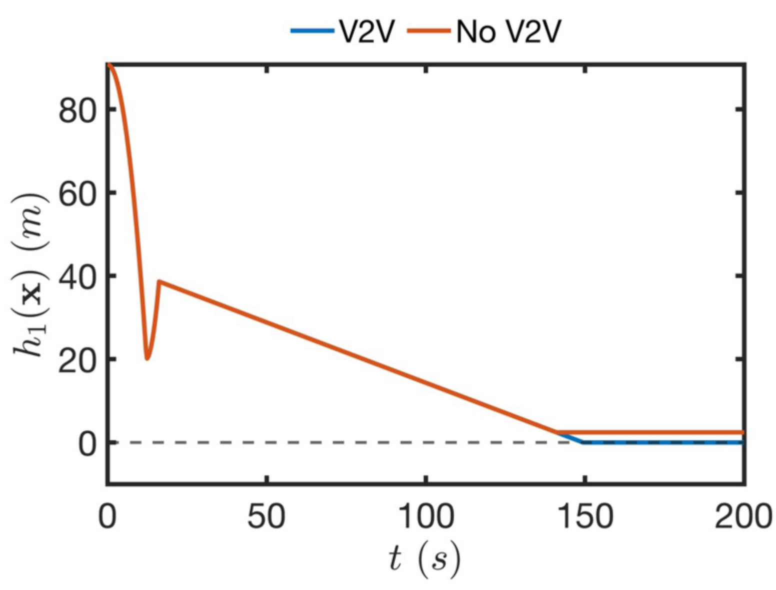

Figure 2-3. The trailing truck maintains a safe distance from the lead truck, i.e., $h_1(x) = X_r - \beta V_f - \frac{V_f^2 - V_1^2}{2u} - X_0 \geq 0$ regardless of the availability of the V2V communication. When there is V2V communication then the following truck keeps a shorter relative distance from the lead truck than the scenario when there is no V2V communication.

Table 2-2. Energy Reduction at Different Desired Relative Spacing

	30	60	90	150
$E_{w,f}$ (V2V)	22.67	18.23	15.21	13.64
$E_{w,f}$ (No V2V)	21.53	17.39	15	13.20
$E_{w,l}$ (V2V)	3.53	0.74	0.28	0.46
$E_{w,l}$ (No V2V)	2.81	0.62	0.30	0.45

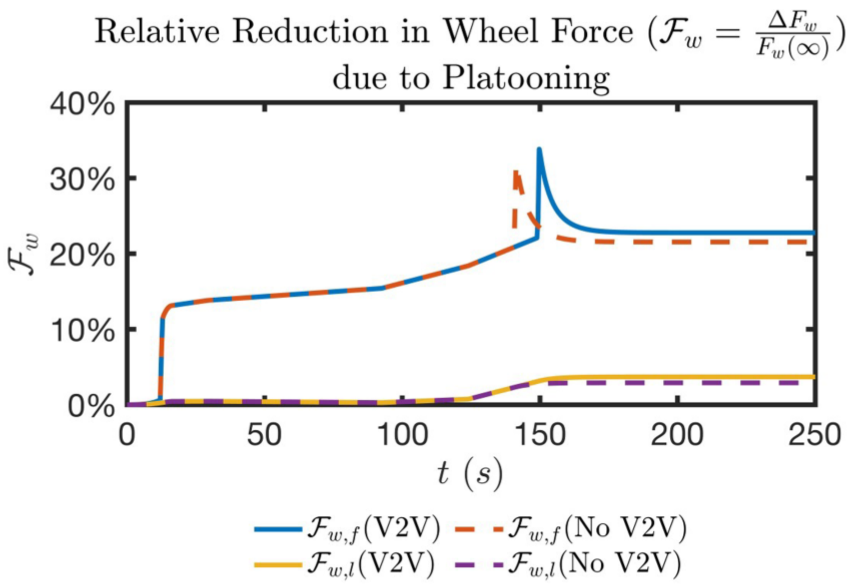

Figure 2-4. The relative reduction in wheel force, i.e., force reduction factor F_w for the lead truck as well as the trailing truck.

2.5 Conclusion

Electric trucks in a two-platoon formation can provide significant savings. The energy benefits of the platooning are considerable when the following vehicle maintains a close distance because the air drag reduction is significant at shorter distances. However, closely following a lead truck gives rise to potential safety concerns. We propose a provably safe controller that guarantees safety while maintaining a desired safety gap to reduce aerodynamic drag. In addition to energy savings the use of one driver less adds additional savings.

Chapter 3 - Routing Short-haul Trucks Under the Uncertainties of Travel Time and Service Time

To support the use of battery electric vehicle (BEV) fleets in last-mile freight logistics, this section introduces a new dispatching problem, the electric vehicle routing problem with backhauls and time windows under uncertain service and travel times (EVRPBTW-USUT). Extending the previous study (Wu et al., 2024), this study incorporates a backhauling strategy, where linehaul customers (requiring deliveries) are visited first, followed by backhaul customers (requiring pickups). Additionally, this formulation accounts for uncertain travel and customer service times, enhancing its applicability to real-world urban freight logistics. To efficiently solve this complex problem, we develop a two-phase metaheuristics algorithm that combines metaheuristics with the robust optimization (RO) method. Another key innovation is the introduction of a memorized buffer within the robust model, which reduces computational complexity and cuts down the computational time significantly compared to the classic RO model. This enhancement improves the scalability and efficiency of solving the RO problem. Extensive experiments were conducted to evaluate the algorithm's performance, including a new hypothetical EVRPBTW benchmark dataset and a real-world case from a full-service supply chain company in San Bernardino County, California. Results from Monte Carlo (MC) simulations demonstrate the introduced model can significantly reduce the total delay time by up to 73.87%. Additionally, a comprehensive sensitivity analysis of the uncertain factors reveals that the uncertain service times have a greater impact compared to the uncertain travel times. This research contributes to advancing sustainable urban freight logistics and provides valuable insights for decision-makers in scheduling BEV fleets.

3.1. Introduction

Over the last decade, there has been an increase in new incentives and regulations aimed at reducing vehicle emissions and promoting alternative fuel choices in the transportation sector. For example, in January 2022, the U.S. developed the National Blueprint for transportation (*The U.S. National Blueprint for Transportation Decarbonization*, n.d.) to addressing the climate crisis and will promote net-zero carbon emissions by 2050. This policy accelerates the adoption of clean energy vehicles in the transportation sector. Similarly, the European Commission sets targets for progressively cutting emissions by adoption of all zero-emission vehicles from 2035 (*Clean Vehicles Directive - European Commission*, n.d.). These factors, along with the increasing awareness of environmental and climate concerns, have prompted many freight logistics companies to transition to cleaner options by adopting BEVs and implementing innovative dispatching strategies to enhance transportation efficiency.

However, despite the benefits of transitioning to BEV fleets in logistics systems, there are still significant limitations in utilizing BEV fleets for last-mile deliveries in urban freight transportation. One major challenge is the limited driving range of BEVs compared to traditional internal combustion engine vehicles. Additionally, the scarcity of recharging stations and the extended time required for recharging present further obstacles. Consequently, commercial fleet operators require more careful dispatch planning to effectively manage recharging schedules.

Commercial urban freight operations involve complex route planning, often characterized by frequent deliveries and pickups. Freight transportation companies must provide daily delivery services to consignees (e.g., warehouses or retailers) and pickup services for senders (e.g., manufacturers or suppliers). To reduce loading and unloading times during service, freight providers typically perform deliveries on linehaul trips with commercial products. Once the truck trailer is empty, pickups are conducted on the return, or backhaul, trips. This first-out, last-in strategy is known as the vehicle routing problem with backhauls (VRPB), which has been demonstrated to be a sustainable approach within urban freight logistics systems (Santos et al., 2020; Toth & Vigo, 1997).

In addition to the specific backhauling service pattern, the most critical objective for freight transportation service providers is to conduct high-quality services that satisfy the LOS for their customers in a timely manner. Such potential uncertain delay risks not only reduce the LOS of customers but also increase the potential labor costs for the drivers. When transiting to the entire EV fleet in urban freight dispatching systems, the freight operators should consider three perspectives regarding customer service times, travel times, and potential recharging times. Most existing studies assume service and travel times are deterministic values during the route planning stage (e.g., Peng, Zhao, et al., 2023; Yang et al., 2022a; Yu, Aloina, et al., 2023). However, suppose the freight operators neglect the uncertain travel and service times. In that case, the route plan for BEVs is fragile, resulting in high potential delay risks in real-world urban dispatching scenarios.

This study aims to formulate and solve an optimization model for a practical delivery service in urban freight transport in which an EV fleet is used for transporting commercial products to the suppliers and consignees. To deal with such uncertain factors, we introduce a new robust dispatching problem, which is a so-called EVRPBTW-USUT. To deal with the uncertainties, we incorporate a route-dependent approach (Agra et al., 2013; Hu et al., 2018a) with an RO framework (Ben-Tal et al., 2009). It extends the traditional EV routing problem with time windows, backhauls and partial recharging proposed by (Peng, Wu, et al., n.d.) considering uncertain service times and travel times.

Major contributions of this section to the research field are summarized as follows:

- *Formulation of a new robust EV routing problem*: This study proposes a new problem, EVRPBTW-USUT, which introduces key considerations such as backhauling, en route partial recharging, limited vehicle range and capacity, and time window constraints. The model extends the classic EVRPTW by incorporating uncertain travel times and customer service times, addressing real-world challenges in urban freight logistics. This formulation captures the complexity of BEV operations while ensuring adaptability to uncertainties in service and travel conditions.
- *Development of an efficient dispatching strategy*: To address the proposed robust routing problem, we developed a two-phase metaheuristics algorithm. The framework combines an adaptive large neighborhood search (ALNS) with simulated annealing (SA) in the first phase and an iterative local search (ILS) metaheuristics algorithm in the second. A notable innovation in our approach is the introduction of a memorized buffer within the robust model, which significantly reduces computational complexity. This buffer mechanism decreases the computational time for the robust model by up to 84.82% compared to the version without the buffer, thus greatly improving the efficiency of solving the RO problem.
- *Validation with benchmark and real-world fleet dispatching data*: To evaluate the performance of the proposed dispatching algorithm in terms of both solution quality and robustness, we apply it to a VRPB benchmark dataset and compare its results with those of other metaheuristics algorithms. Additionally, we generate a new EVRPBTW benchmark dataset, based on the widely recognized EVRPTW dataset, and assess the solution under both deterministic and uncertain dispatching scenarios. To further validate the effectiveness of the method, real-world fleet dispatching data from a full-service logistics company in Southern California, U.S., is used. Extensive experiments reveal the trade-off between minimizing total travel costs and maintaining robustness in solution quality.

The remainder of this section is organized as follows. Section 3.2 reviews the literature regarding the EV routing problems (EVRP) and its variations. Section 3.3 presents a mixed-integer linear programming (MILP) model of the EVRPBTW-USUT. Section 3.4 introduces the calculation of the potential delay time and the memorized buffer into the RO model. Section 3.5 presents the proposed two-phase metaheuristics algorithm. Section 3.6 presents extensive computational experiments. Section 3.7 concludes the key findings and discusses the future research directions.

3.2. Literature review

There are two classes of EVRP that are mostly related to the EVRPBTW-USUT. First, section 3.2.1 briefly reviews the literature on the EV routing problems, mainly focusing on the EVRP with different recharging policies and EVRP with pickup and delivery. Second, section 3.2.2

reviews the RO model of uncertain vehicle routing problems. We summarize the main research gaps and the contributions in section 3.2.3.

3.2.1 Related literature on EV routing problems (EVRP)

The EVRP aim to find a set of routes for an EV fleet, particularly considering en route recharging visits due to limited battery capacity. Erdoğan and Miller-Hooks (Erdoğan & Miller-Hooks, 2012) considered a green energy vehicle fleet into the routing problem and introduced a green vehicle routing problem (GVRP). A potential en route recharging visit is taken into consideration. Schneider et al. (Schneider et al., 2014) introduced the EVRP with time windows (EVRP-TW), which incorporated payload capacity and the possibility of recharging on electric commercial vehicles. The EV fleet is fully recharged when visiting the recharging station during the dispatching. Also, the customer time windows should be satisfied. Regarding different recharging policies of EVRP, Desaulniers et al. (Desaulniers et al., 2016) considered different recharging policies thoroughly, including a set of combinations of fully/partially en route recharging and multiple/single recharging times. An exact branch-price-and-cut algorithm was presented to solve the EVRPTW. Furthermore, Keskin and Çatay (Keskin & Çatay, 2016a) investigated the partial recharging strategies for the EVRPTW, demonstrating the efficiency of the partial recharging option. Montoya et al. (Montoya et al., 2017a) extended the classic EVRP models and considered non-linear charging functions. Recently, Lin et al. (B. Lin et al., 2021) considered the vehicle-to-grid (V2G) technology and introduced an EVRP with a charging/discharging problem. Bezzi et al. (Bezzi et al., 2023) proposed a route-based algorithm to solve the EVRP with multiple partial recharging technologies. Yu et al. (Yu et al., 2021) studied an EVRP with a mixed fleet and considered realistic energy consumption and partial recharging policy.

Another related variant of EVRP is EVRP with pickup and delivery, which is one of the common transportation patterns for urban freight logistics (Peng, Zhao, et al., 2023), meal delivery (H. Liu et al., 2024), and dial-a-ride systems (Bongiovanni et al., 2019). This problem extends the traditional VRPB, where the customers are partitioned into deliveries and pickups, and has been demonstrated as an efficient dispatching method in the logistics systems (e.g., Brandão, 2016; Mingozzi et al., 1999; Palhazi Cuervo et al., 2014; Ropke & Pisinger, 2006c, 2006a). For more comprehensive classifications of VRPB, we refer to the recent reviews (Koç & Laporte, 2018; Parragh et al., 2008; Santos et al., 2020). Recently, many scholars have focused on solving different freight pickup and delivery tasks by considering the EV fleet. Yang et al. (Yang et al., 2022b) investigated an integrated electric logistics vehicle recharging station location and routing problem with backhauls. The problem aimed to determine the selection of a recharging station considering the EV routing plan and other realistic constraints. The mixed pickup and delivery requests and time windows are considered in this study. Xiao et al. (Xiao et al., 2023) proposed an EVRP with time windows and mixed backhauls and designed a new diversity-enhanced memetic algorithm to solve the problem. Recently, Peng et al. (Peng, Wu, et al., 2023a) focused on the energy-efficient BET dispatching problem in urban logistics systems, considering the backhaul strategies, customer time windows, and partial recharging policy. A real-world case study in Southern California, U.S., is conducted to assess the effectiveness of the proposed model.

3.2.2 Uncertainty EV routing problem

The above studies consider deterministic scenarios, where information such as traffic conditions, service times, energy consumption rate, customer demands, and time windows are determined and known before the dispatching strategy is implemented. However, in real-life urban freight logistics, the deterministic dispatching solution might be fragile when those parameters change. Also, many studies have been mainly focused on solving robust dispatching problems for conventional internal combustion vehicles, such as mitigating potential customer delays (Agra et al., 2013; Hu et al., 2018a; Kuo et al., 2016; Shi et al., 2019) and cargo capacity violations (Gounaris et al., 2013; Hu et al., 2018a; Shen et al., 2022), (Yu, Anh, et al., 2023). When transitioning to a greener vehicle fleet, considering such characteristics plays a vital role in the adoption of a BEV fleet to conduct urban freight dispatching tasks.

A few existing papers have considered uncertain factors for the EV fleet. Keskin et al. (Keskin et al., 2021) and (Keskin et al., 2019) studied the EVRPTW with stochastic waiting times at the recharging stations. Specifically in (Keskin et al., 2021), a simulation-based heuristic based on an ALNS is used to address the potential uncertain waiting times. Considering the uncertainty energy consumption rate of the EV fleet, Pelletier et al. (Pelletier et al., 2019) used a RO method (Ben-Tal & Nemirovski, 1998) to address the EVRP under energy consumption uncertainty. A set of uncertain sets is used to describe the uncertain levels of energy consumption. Moreover, considering an uncertain energy consumption rate, Basso et al. (Basso et al., 2021) applied a probabilistic energy consumption model with machine learning to expect energy consumption for EV routes. A two-stage routing model incorporating energy consumption prediction is introduced to solve the EV routing problem. Amiri et al. (Amiri et al., 2023) introduced a robust multi-objective routing problem for heavy-duty electric trucks, considering uncertain energy consumption. Jeong et al. (Jeong et al., 2024) proposed a two-stage adaptive RO framework for the EVRP under energy consumption uncertainty.

It is necessary to consider additional uncertain factors rather than just energy consumption uncertainty. Recently, Shen et al. (Shen et al., 2022) introduced a robust EVRPTW under demand uncertainty. They considered the cargo weight-dependent energy consumption of EVs using a microscopic energy consumption model. Those uncertainties are described in the uncertainty polytopes within the RO model. The authors developed an ALNS metaheuristics algorithm to solve the introduced RO model. Additionally, Liu et al. (X. Liu et al., 2023) introduced a robust EV pickup and delivery problem with time windows under demand uncertainty. The authors devised an exact two-phase decomposition method to find robust dispatching solutions.

3.2.3 Summary of research gaps

To support the adoption of BEV fleets in urban freight logistics, this study introduces a robust EV routing problem with backhauls and time windows, considering uncertainties in both service times and travel times. Beyond deterministic dispatching scenarios, accounting for these uncertainties can significantly enhance the robustness of dispatching solutions. A two-phase metaheuristic framework is developed to solve the problem effectively. Additionally, to improve the scalability of the RO model, we introduce an intermediate memory buffer, significantly reducing solution time. To our knowledge, no prior research has incorporated a memory buffer into the RO model to improve algorithm efficiency. Table 3-1 summarizes related works on EVRP, highlighting the key differences in assumptions and methods between this study and existing literature.

Table 3-1. Comparison of this study with the recent literature on EVRPTW

Research	Time windows	Backhauls	Recharging strategy	Recharging policy	Source of uncertainty	Case study	Modelling approach
Schneider et al. (2014)	•		Full	Linear function	/	Hypothetical	Deterministic MILP model
Desaulniers et al. (2016)	•		Full & Partial	Linear function	/	Hypothetical	Deterministic MILP model
Keskin and Çatay (2016)	•		Partial	Linear function	/	Hypothetical	Deterministic MILP model
Keskin and Çatay (2019)	•		Partial	Linear function	Queueing time	Hypothetical	MILP model
Montoya et al. (2017)	•		Partial	Multiple techniques	/	Hypothetical	Deterministic MILP model
Pelletier et al. (2019)			Partial	Linear function	Energy consumption	Hypothetical	RO model
Yu et al. (2021)	•		Partial	Linear function	/	Real-world	Deterministic MILP model
Lin et al. (2021)	•		Partial	Linear function	Electricity prices	Hypothetical and real-world	MILP model
Basso et al. (2021)			Partial	Linear function	Energy consumption	Real-world	MILP model
Yang et al. (2022)	•	•	Partial	Linear function	/	Real-world	Deterministic MILP model
Shen et al.	•		Partial	Linear function	Energy consumption & Customer demand	Real-world	RO model
Xiao et al. (2023)	•	•	Full	Linear function	/	Hypothetical and real-world	Deterministic MILP model
Peng et al. (2023)	•	•	Partial	Linear function	/	Real-world	Deterministic MILP model
Amiri et al. (2023)	•		Partial	Linear function	Energy consumption	Hypothetical and real-world	RO model

Research	Time windows	Backhauls	Recharging strategy	Recharging policy	Source of uncertainty	Case study	Modelling approach
Liu at al. (2023)	•	•	Battery swapping	/	Customer demand	Hypothetical	RO model
Jeong et al. (2024)	•		Partial	Linear function	Energy consumption	Hypothetical	Two-stage adaptive RO model
This research	•	•	Partial	Linear function	Travel time & service time	Hypothetical and real-world	RO model with memorized buffer

3.3 Problem description and formulation

Section 3.3.1 briefly describes the proposed EVRPBTW-USUT. In Section 3.3.2, we formally introduce the mixed integer linear programming (MILP) model of the deterministic version of EVRPBTW. Section 3.3.3 describes the uncertain polytopes for travel times and customer service times. Section 3.3.4 presents a robust version of the proposed dispatching problem.

3.3.1 Problem assumptions

The assumption of EVRPBTW-USUT is described as the following.

- Each EV starts a journey from a single depot and ends the trip at the same depot. We assume that the BEV fleet is fully recharged at night before starting their journey.
- Each vehicle performs exactly one route.
- Each vehicle is fully or partially loaded at the depot before departure and visits linehaul customers first, followed by the backhaul customers.
- A trip only containing the backhaul customers is not allowed, which is the same as the backhaul policy (Ropke & Pisinger, 2006a).
- The time windows of each customer are known and should be satisfied.
- The service time of each customer is heterogeneous and uncertain.
- The travel time between every two nodes is heterogeneous and uncertain.

Figure 3-1 shows an example of the proposed EVRPBTW-USUT. It considers a set of homogenous fleets of BEVs that are available at a single depot. All the BEVs start from a depot and must return to the same depot before the due date. The customer’s demands are known before dispatching. The delivery orders (e.g., D1-D5) are loaded in the vehicle before departure at the depot, where those linehaul customers are served first, followed by the backhaul customers (P1-P3). During the trips, the BEVs can visit the CSs and recharge partially if the current SOC is too low not to continue the rest of the journey.

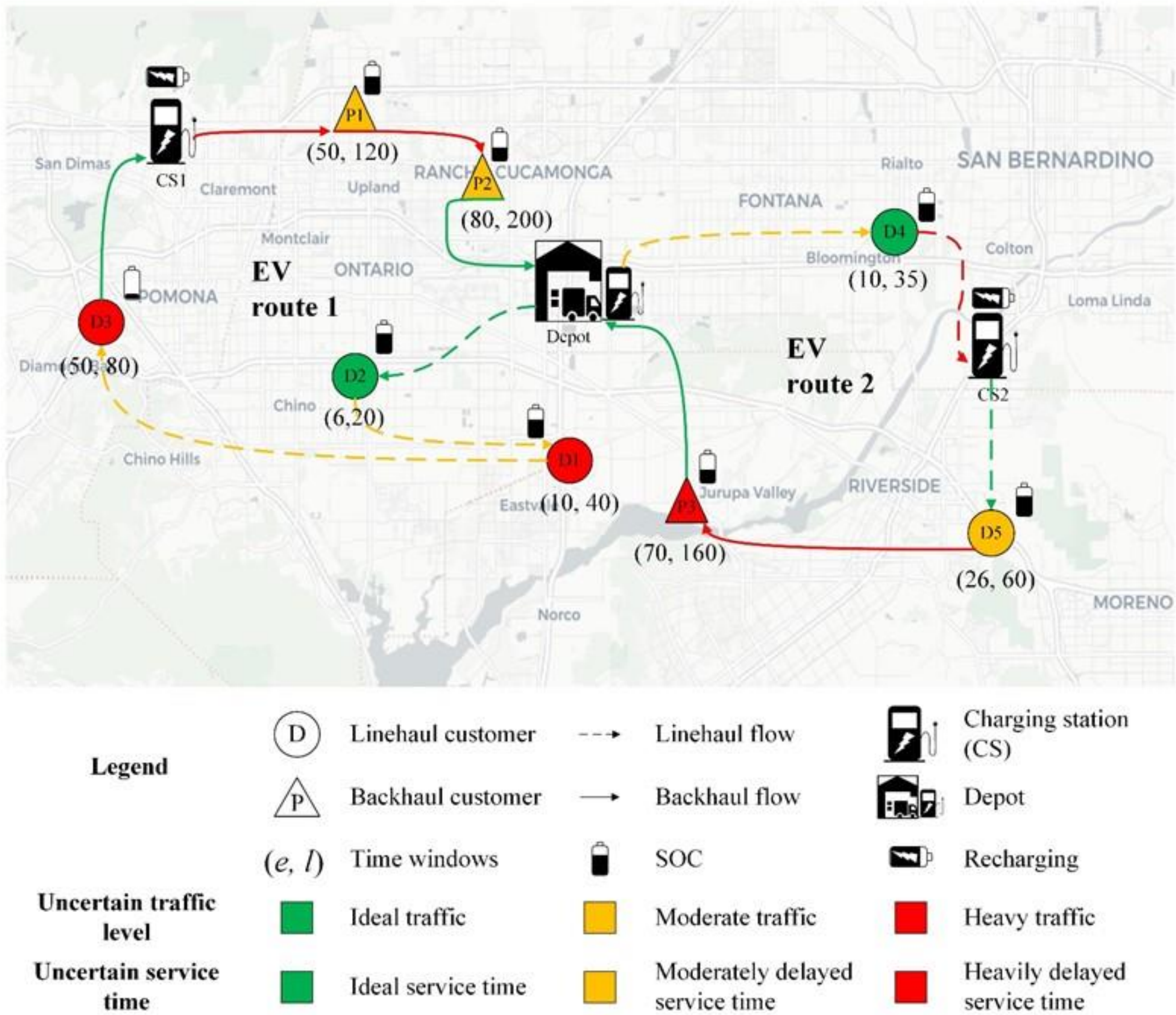

Figure 3-1. An example solution of the EVRPBTW-USUT. By considering uncertain traffic and service time, the EV_1 may detour to visit customer D2 first, which has a narrow time window, and visit D1 later, even though the total travel distance is increased.

When the traffic conditions and customer service times are uncertain, some customers may have priority to visit since their time windows are narrow, and such uncertain traffic or service time may cause potential delays. For example, although customer D1 is closer to the depot than D2, customer D2 is preferred to visit first because its due time is shorter than D1. Customer D2 has a potential delay risk when considering uncertain travel times and uncertain service times.

3.3.2 Mixed integer programming model for the deterministic EVRPBTW

The sets and indices, parameters, and decision variables are introduced in Table 3-2.

Table 3-2. The notations and parameters of the mathematical model

Notation	Description
Sets and indices	
O, D	Depot notation (original and destination)
K	Set of homogeneous EVs (operating)
$\mathcal{N}$	Set of customer vertices
L	Set of linehaul customer vertices
B	Set of backhaul customer vertices
$\mathcal{R}$	CSs
$\mathcal{A}$	Set of arcs
$i, j = 0, 1, \dots, n, n+1$	Index of the nodes. Especially, 0 indicates the start index of depot, $n+1$ represents destination index of depot.
k	Index of the vehicles, $k \in K$
r	Index of recharging stations, $r \in \mathcal{R}$
Parameters	
d_{ij}	Distance between vertices *i* to *j*
t_{ij}	Travel time between vertices *i* to *j*
q_i	Demand at vertex (positive if pick-up, negative if drop-off)
e_i	Earliest start of service time at vertex *i*
l_i	Latest start of service time at vertex *i*
s_i	Service time at vertex *i*
h_i	Recharging time at vertex $i, i \in \mathcal{R}$
c	Energy consumption rate
g	Inverse refueling rate
C	Cargo payload capacity of the vehicles
Q	Battery capacity of the vehicles

Notation	Description
Decision variables	
τ_i	Service start time of the vehicle at vertex *i*
k_i	Decision variable specifying the visit to recharging station vertex *i*. 0 if customer, 1 if CS.
u_i	Nonnegative continuous decision variable specifying the remain cargo on arrival at vertex *i*
y_i	Nonnegative continuous decision variable for current SOC for the vehicle$k$ when arrive at vertex *i*
Y_i	Nonnegative continuous decision variable of finishing charging SOC for the vehicle k at vertex *i*
x_{ij}	Binary decision variable. 0 if the route from *i* to *j* is not visited by the vehicle k, 1 otherwise

To formulate the deterministic EVRPBTW, we define it on a complete directed graph $\mathcal{G} = (\mathcal{N}'_{O,D} \cup \mathcal{R}, \mathcal{A})$, where $\mathcal{N}'_{O,D}$ is the set of nodes include customer nodes $\mathcal{N}$, depot node (O, D), and $\mathcal{R}$ represents a set of recharging stations. The customers $\mathcal{N}$ can be partitioned into two sets, i.e., $N = \{L, B\}$, where the sets $L = (1, 2, \dots, n)$ and $B = (n+1, n+2, \dots, n+m)$ represent the linehaul customers and the backhaul customers, respectively. The arc set is defined by $\mathcal{A} = A_1 \cup A_2 \cup A_3$, followed by the integer programing model in Toth and Vigo (1997) (Toth & Vigo, 1997). Specifically, set $A_1 = \{(i,j) \in \mathcal{A}: i \in L \cup O, j \in L \cup \mathcal{R}\}$ to connect all forward flows, $A_2 = \{(i,j) \in \mathcal{A}: i \in B \cup \mathcal{R}, j \in B \cup D\}$ to represent the backward flows, and the interface arc is represented by $A_3 = \{(i,j) \in \mathcal{A}: i \in L \cup \mathcal{R}, j \in B \cup D\}$. To simplify the flow degrees in the mathematical formulation, we define $\Delta_i^+ = \{j: (i,j) \in \mathcal{A}, i \in \mathcal{N}'_{O,D}\}$ which denotes the forward of i, and $\Delta_i^- = \{j: (j,i) \in \mathcal{A}, i \in \mathcal{N}'_{O,D}\}$ which denotes the backward of i.

Each customer $i \in \mathcal{N}$ has a specific service type, an unknown service time s_i, a time window $[e_i, l_i]$, and a demand q_i (negative if delivery and positive if pickup). Traveling from a node i (i.e., the depot, a customer, or a recharging station) to another node j can be denoted as an arc (i,j), which has an associated travel distance d_{ij} and travel time t_{ij}. We assume the energy consumption rate is constant and linearly related to travel distance d_{ij}.

A vehicle can arrive at a customer before the opening of its time window and wait for service to start. We assume unlimited homogenous BEVs are available at the depot with a trailer capacity of Q and battery capacity B.

The EV fleet can be recharged en route at a set of predetermined recharging stations $\mathcal{R}$. Same as the assumption in (Desaulniers et al., 2016), we assume that the recharging rate is constant and the EV can visit a recharging station en route at most once. Additionally, each vehicle can be partially recharged, where the finished SOC can complete the remaining visit and return to the depot. The partial en route recharging policy has been introduced in (Desaulniers et al., 2016) and (Keskin & Çatay, 2016b), demonstrating its efficiency compared to the fully recharging policy.

The objective function of the deterministic model $f^{DM}(S)$ aims to minimize the total travel distance (Eq. **3.1**a), where the MILP model can be formulated as:

$$f^{DM}(S) = min \sum_{i \in \mathcal{N}'_0 \cup \mathcal{R}, j \in \mathcal{N}'_D \cup \mathcal{R}, i \neq j} d_{ij} x_{ij} \qquad 3.1a$$

Subject to:

Demand and flow balance constraints:

$$\sum_{i\in\Delta_i^-} x_{ij} = 1,\ j \in \mathcal{N} \cup \mathcal{R} \quad 3.1b$$

$$\sum_{j\in\Delta_j^+} x_{ij} = 1,\ \ i \in \mathcal{N} \cup \mathcal{R} \quad 3.1c$$

$$\sum_{j\in \mathcal{N'}_D\cup\mathcal{R},\mathrm{i}\neq j} x_{ij} - x_{ji} = 0, \forall i \in \mathcal{N'}_O \cup \mathcal{R} \quad 3.1d$$

$$\sum_{i\in\Delta_O^-} \sum_{j\in\Delta_O^-} x_{ij} \leq K \quad 3.1e$$

$$\sum_{i\in\Delta_O^+} \sum_{j\in\Delta_O^+} x_{ij} \leq K \quad 3.1f$$

Vehicle constraints:

$$y_O = Q,\ \forall j \in\ \mathcal{N} \cup \mathcal{R} \quad 3.1g$$

Recharging and SOC constraints:

$$\tau_i + t_{ij}x_{ij} + g(Q - y_i) - (l_0 + gQ)\left(1 - x_{ij}\right) \leq \tau_j \quad 3.1h$$
$$\forall i \in O \cup \mathcal{N} \cup \mathcal{R}, \forall j \in (D \cup \mathcal{N} \cup \mathcal{R}), i \neq j$$

$$0 \leq y_j \leq y_i\ - \left(h \cdot d_{ij}\right)x_{ij} + Q(1 - x_{ij}), \forall i \in\ \mathcal{N'}_O \cup \mathcal{R}, j \in\ \mathcal{N'}_D \cup \mathcal{R}, i\ \neq j \quad 3.1i$$

$$0 \leq y_j \leq Q\ - \left(h \cdot d_{ij}\right)x_{ij}, \forall i \in\ O \cup \mathcal{R}, j \in\ \mathcal{N'}_D \cup \mathcal{R}, i\ \neq j \quad 3.1j$$

Time window constraints:

$$\tau_i + \left(s_i + t_{ij}\right)x_{ij} - l_0\left(1 - x_{ij}\right) \leq \tau_j \quad 3.1k$$
$$\forall i \in O \cup \mathcal{N} \cup \mathcal{R}, \forall j \in j \in (D \cup \mathcal{N} \cup \mathcal{R}), i \neq j$$

$$e_i \leq \tau_i \leq l_i,\ \forall i \in \mathcal{N'}_{O,D} \quad 3.1l$$

Demand constraints:

$$0 \leq u_o \leq C \quad 3.1m$$

$$0 \leq u_j \leq (u_i - q_i)x_{ij} + C\left(1 - x_{ij}\right) \quad 3.1n$$
$$\forall i \in O \cup \mathcal{N} \cup \mathcal{R}, \forall j \in D \cup \mathcal{N} \cup \mathcal{R}, i \neq j$$

Binary decision variable:

$$x_{ij} \in \{0,1\},\ \forall i,j \in \mathcal{N'}_{O,D}\ , i \neq j$$ $x_{ij} \in \{0,1\},\ \forall i,j \in \mathcal{N}$

Constraints (3.1b)-(3.1d) define the forward and backward flow conservation constraints. Constraints (3.1e) and (3.1f) ensure that the number of routes equals the number of operating BEVs. Constraint (3.1g) defines the BEV fleet as fully recharged with battery capacity Q when departing at the depot. Constraint (3.1h) guarantees satisfaction of the time windows when the EV charges at the CSs. Constraints (3.1i)-(3.1j) state the SOC of a BEV should not be exceeded to the maximum battery capacity and larger than zero during the operation. Constraints (3.1k) and (3.1l) force the vehicle to visit the customers within the scheduled time windows. Constraints (3.1m) and (3.1n) guarantee the cargo load does not exceed the payload capacity of either linehauls or backhauls. Finally, condition (3.1o) defines the binary decision variables.

3.3.3 Incorporating uncertain service time and travel times

Real-world last-mile delivery operations face numerous uncertainties, as highlighted in Section 3.1. In this study, we specifically address the uncertainties in service times and traffic conditions, with the goal of identifying a robust dispatching solution for the BEV fleet. To achieve this, the BEV fleet dispatching problem has been reformulated using the RO method (Ben-Tal et al., 2009). Since reliable historical data on service and travel times may not always be available during the planning horizon, the RO method proves to be an effective approach for deriving robust dispatching solutions that can handle uncertain scenarios.

Similar to (Shi et al., 2019) and (Hu et al., 2018b), we define the uncertain travel time $\tilde{t}_{ij}$ $((i,j) \in \mathcal{A})$ and uncertain service time $\tilde{s}_i$ $(i \in N)$ can be varying in the predetermined polytopes U_t^k and U_s^k, respectively for a BEV trip k.

$$U_t = \times_{k \in K} U_t^k \qquad 3.2$$

$$U_t^k = \left\{ \begin{matrix} \tilde{t}_{ij} \in R^{|A^k|} \,|\tilde{t}_{ij} = \bar{t}_{ij} + \sigma_{ij}\hat{t}_{ij}, \\ \sum_{(i,j)\in A^k} |\sigma_{ij}| \leq \Gamma_t^k, 0 \leq \sigma_{ij} \leq 1, \Gamma_t^k = \lceil \theta_t |A^k| \rceil, \forall (i,j) \in A^k \end{matrix} \right\} \qquad 3.3$$

In equation 3.2, U_t is the Cartesian product of the travel time uncertainty set U_t^k for each BET $k \in K$. In 3.3, A^k represents the set of arcs on a route traveled by vehicle k. The uncertain travel time $\tilde{t}_{ij}$ of an arc $(i,j) \in A^k$ can take any value from its interval $[\bar{t}_{ij}, \bar{t}_{ij} + \hat{t}_{ij}]$. $\bar{t}_{ij}$ denotes the nominal value of uncertain travel time in an arc $(i,j) \in A^k$, and $\hat{t}_{ij} = \alpha^t \bar{t}_{ij}$ represents the maximum deviation from the nominal value $\bar{t}_{ij}$, where $\alpha^t \in [0,1]$. σ_{ij} is an auxiliary variable, and Γ_t^k denotes the uncertain travel time budget for a trip. Specifically, Γ_t^k controls the number of arcs with high travel time uncertainty, which is calculated by $\lceil \theta_t |A^k| \rceil$, where $\theta_t \in [0,1]$ is the travel time uncertainty budget coefficient and $|A^k|$ is the number of arcs in route k. For example, if $\theta_t = 0$, then $\Gamma_t^k = 0$, which means the uncertainty degree is zero, so the uncertain travel time $\tilde{t}_{ij}$ equals $\bar{t}_{ij}$ for all arcs in route k. If $\theta_t = 1$ and $\Gamma_t^k = |A^k|$, all the arcs in route k can take any value in the interval $[\bar{t}_{ij}, \bar{t}_{ij} + \hat{t}_{ij}]$. Thus, the larger value of Γ_t^k provides greater route robustness as it takes into account a higher degree of travel time uncertainty.

$$U_s = \times_{k \in K} U_s^k \,, \qquad 3.4$$

$$U_s^k = \left\{ \begin{array}{c} \tilde{s}_i \in R^{|N^k|} \mid \tilde{s}_i = \bar{s}_i + \tau_i \hat{s}_i, \\ \sum_{i \in N^k} |\tau_i| \leq \Gamma_s^k, 0 \leq \tau_i \leq 1, \Gamma_s^k = \lceil \theta_s |N^k| \rceil, \forall i \in N^k \end{array} \right\} \quad 3.5$$

Extending the uncertain travel time, we also consider an uncertain service time. In equation 3.4, U_s is the Cartesian product of the service time uncertainty set U_s^k for each vehicle $k \in K$. In 3.5, N^k represents the set of customers visited by vehicle k. The uncertain service time $\tilde{s}_i$ for customer $i \in N^k$ can be described within its uncertainty set U_s^k. Like the function 3.3, the maximum deviation of uncertain service time $\hat{s}_i$ can be calculated by $\hat{s}_i = \alpha^s \bar{s}_i$, where $\alpha^s \in [0,1]$. τ_i is an auxiliary variable. Γ_s^k denotes the uncertainty budge of the customers, which is controlled by budget coefficient θ_s.

3.3.4 RO version

In this section, we propose an RO model for EVRPBTW that accounts for uncertainties in both travel times and service times. We assume that the uncertain travel time $\tilde{t}_{ij}$ ($(i,j) \in \mathcal{A}$) and uncertain service time $\tilde{s}_i$ ($i \in N$) can vary in the predetermined polytopes U_t^k and U_s^k, respectively. Consequently, rather than using a deterministic model, we acknowledge that the decision variable τ_i is affected by these uncertainties. This necessitates optimizing for robustness, ensuring that the solution remains feasible and effective across the range of possible scenarios defined by these uncertain factors.

To account for uncertainties, we extend the deterministic model into the RO model by revising both the objective function and the time window constraints. The objective function of the RO model $f^{RO}(S)$ is to minimize the total travel distance considering the uncertainty polytopes $t \in ext(U_t)$ and $s \in ext(U_t)$, which can be expressed as equation 3.6.

$$f^{RO}(S) = min_{t \in ext(U_t), s \in ext(U_t)}^{sup} \sum_{i \in \mathcal{N}_0' \cup \mathcal{R}, j \in \mathcal{N}_D' \cup \mathcal{R}, i \neq j} d_{ij} x_{ij}(s,t) \quad 3.6a$$

Time window constraints:

$$\tau_i(s,t) + (\tilde{s}_i + \tilde{t}_{ij}) x_{ij} - l_0(1 - x_{ij}) \leq \tau_j(s,t) \quad 3.6b$$
$$i \in O \cup \mathcal{N} \cup \mathcal{R}, \forall j \in j \in (D \cup \mathcal{N} \cup \mathcal{R}), i \neq j, t \in ext(U_t), s \in ext(U_t)$$

$$e_i \leq \tau_i(s,t) \leq l_i, \ \forall i \in \mathcal{N}'_{O,D} \quad 3.6c$$

In constraint (3.6b), decision variable $\tau(s,t)$ denotes the service start time by considering uncertain travel times and service times. Constraint (3.6c) ensures that the starting service time for a customer is within its time windows.

3.4 Calculating the latest arrival time and a memorized buffer

We first incorporate the RO method and reformulate the cost function in Section 3.4.1 to find a robust solution based on the predetermined uncertain polytopes. To address scalability issues and enhance the efficiency of the RO model, Section 3.4.2 introduces a memorized buffer mechanism, which optimizes computational performance within the RO model.

3.4.1 Calculating the latest possible arrival time for customers

To calculate the latest possible arrival time for the customers on the vehicle k (sometimes we may say route k), we first consider a given solution S that consists of several routes $\{\mathfrak{s}_1, \mathfrak{s}_2, \mathfrak{s}_3, \dots, \mathfrak{s}_k\}$, where $k \in K$ and $\mathfrak{s}_k \in S$. For a route $\mathfrak{s}_k$, the start node and the end node are represented by p_1^k and $p_{|\mathfrak{s}_k|}^k$, respectively. Also, the customers' nodes or a recharging station visit are included in $\{p_2^k, \cdots, p_{|\mathfrak{s}_k|-1}^k\}$. Considering an uncertainty degree of travel time Γ_t^k for a route traveled by BET k, we denote the latest arrival time for node i in this route as $\Lambda(i, \Gamma_t^k)$.

For a complete route, the vehicle can visit the recharging station to charge an amount of energy if needed. Therefore, the recharging time $h_{p_i^k}$ should be considered when calculating the latest possible arrival time for the customer. Equation (7) Inspired by a calculation of the latest arrival time in (Agra et al., 2013) and (Hu et al., 2018a), we take recharging time $h_{p_i^k}$ into account during the route. Therefore, the latest arrival time function $\Lambda(i, \Gamma_t^k, \Gamma_s^k)$ is formulated as follows.

Equation 3.7

(1) 0	, if $i = 1$
(2) $\Lambda(i-1, \Gamma_t^k, \Gamma_s^k) + \bar{s}_{p_{i-1}^k} + \bar{t}_{p_{i-1}^k p_i^k}$	, if $p_i^k \in \mathcal{R}, \Gamma_t^k = 0$ and $\Gamma_s^k = 0$
(3) $\Lambda(i-1, \Gamma_t^k, \Gamma_s^k - 1) + \bar{s}_{p_{i-1}^k} + \tilde{s}_{p_{i-1}^k} + \bar{t}_{p_{i-1}^k p_i^k}$	, if $p_i^k \in \mathcal{R}, \Gamma_t^k = 0$ and $1 \leq \Gamma_s^k \leq i-1$
(4) $\Lambda(i-1, \Gamma_t^k - 1, \Gamma_s^k) + +\tilde{s}_{p_{i-1}^k} + \bar{s}_{p_{i-1}^k} + \bar{t}_{p_{i-1}^k p_i^k} + \tilde{t}_{p_{i-1}^k p_i^k}$	, if $p_i^k \in \mathcal{R}, \Gamma_s^k = 0$ and $1 \leq \Gamma_t^k \leq i-1$
(5) $\Lambda(i-1, \Gamma_t^k - 1, \Gamma_s^k - 1) + \bar{s}_{p_{i-1}^k} + \tilde{s}_{p_{i-1}^k} + \bar{t}_{p_{i-1}^k p_i^k} + \tilde{t}_{p_{i-1}^k p_i^k}$,	, if $p_i^k \in \mathcal{R}, 1 \leq \Gamma_s^k \leq i-1$ and $1 \leq \Gamma_t^k \leq i-1$
(6) $\max\begin{pmatrix} e_{p_{i-1}^k} \\ ,\Lambda(i-1, \Gamma_t^k, \Gamma_s^k) + h_{p_{i-1}^k} + \bar{t}_{p_{i-1}^k p_i^k} \end{pmatrix}$	, if $p_{i-1}^k \in \mathcal{R}$ and $\Gamma_t^k = 0$

Equation 3.7

$$
\Lambda(i, \Gamma_t^k, \Gamma_s^k) =
\begin{cases}
(7)\ \max\begin{pmatrix} e_{p_{i-1}^k}, \\ \Lambda(i-1, \Gamma_t^k - 1, \Gamma_s^k) + h^k_{p_{i-1}^k} + \bar{t}_{p_{i-1}^k p_i^k} + \tilde{t}_{p_{i-1}^k p_i^k}, \\ \Lambda(i-1, \Gamma_t^k, \Gamma_s^k) + h_{p_{i-1}^k} + \bar{t}_{p_{i-1}^k p_i^k} \end{pmatrix} & \text{, if } p_{i-1}^k \in \mathcal{R} \text{ and } 1 \le \Gamma_t^k \le i - 1 \\
(8)\ \max\begin{pmatrix} e_{p_{i-1}^k} \\ , \Lambda(i-1, \Gamma_t^k, \Gamma_s^k) + \bar{s}_{p_{i-1}^k} + \bar{t}_{p_{i-1}^k p_i^k} \end{pmatrix}, & \text{, if } \Gamma_t^k = 0 \text{ and } \Gamma_s^k = 0 \\
(9)\ \max\begin{pmatrix} e_{p_{i-1}^k}, \\ \Lambda(i-1, \Gamma_t^k, \Gamma_s^k - 1) + \bar{s}_{p_{i-1}^k} + \tilde{s}_{p_{i-1}^k} + \bar{t}_{p_{i-1}^k p_i^k}, \\ \Lambda(i-1, \Gamma_t^k, \Gamma_s^k) + \bar{s}_{p_{i-1}^k} + \bar{t}_{p_{i-1}^k p_i^k} \end{pmatrix} & \text{, if } \Gamma_t^k = 0 \text{ and } 1 \le \Gamma_s^k \le i - 1 \\
(10)\ \max\begin{pmatrix} e_{p_{i-1}^k}, \\ \Lambda(i-1, \Gamma_t^k - 1, \Gamma_s^k) + \bar{s}_{p_{i-1}^k} + \bar{t}_{p_{i-1}^k p_2^k} + \tilde{t}_{p_{i-1}^k p_i^k}, \\ \Lambda(i-1, \Gamma_t^k, \Gamma_s^k) + \bar{s}_{p_{i-1}^k} + \bar{t}_{p_{i-1}^k p_i^k} \end{pmatrix} & \text{, if } \Gamma_s^k = 0 \text{ and } 1 \le \Gamma_t^k \le i - 1 \\
(11)\ \max\begin{pmatrix} e_{p_{i-1}^k}, \\ \Lambda(i-1, \Gamma_t^k - 1, \Gamma_s^k - 1) + \\ \bar{s}_{p_{i-1}^k} + \tilde{s}_{p_{i-1}^k} + \bar{t}_{p_{i-1}^k p_i^k} + \tilde{t}_{p_{i-1}^k p_i^k}, \\ \Lambda(i-1, \Gamma_t^k, \Gamma_s^k - 1) + \bar{s}^k_{p_{i-1}^k} + \tilde{s}_{p_{i-1}^k} + \bar{t}_{p_{i-1}^k p} \\ \Lambda(i-1, \Gamma_t^k, \Gamma_s^k - 1) + \bar{s}^k_{p_{i-1}^k} + \tilde{s}_{p_{i-1}^k} + \bar{t}_{p_{i-1}^k p} \\ \Lambda(i-1, \Gamma_t^k, \Gamma_s^k) + \bar{s}_{p_{i-1}^k} + \bar{t}_{p_{i-1}^k p_i^k} \end{pmatrix} & \text{, if } 1 \le \Gamma_s^k \le i - 1 \text{ and } 1 \le \Gamma_t^k \le i - 1 \\
(12)\ \Lambda(i, \Gamma_t^k - 1, \Gamma_s^k) & \text{, if } 2 \le i \le \Gamma_t^k - 1 \\
(13)\ \Lambda(i, \Gamma_t^k, \Gamma_s^k - 1) & \text{, if } 2 \le i \le \Gamma_s^k - 1
\end{cases}
\quad 3.7
$$

Equation (3.7) shows the calculation of latest possible vehicle arrival time at each vertex on route $\mathfrak{s}_k$, including the customer node or recharging station. Function $\Lambda(i, \Gamma_t^k, \Gamma_s^k)$ is a recursive function of the sequence of the nodes on the route and the parameters Γ_t^k and Γ_s^k are defined in the uncertain sets U_s^k and U_t^k, respectively.

As illustrated at the beginning of Section 3.4.1, infeasible solutions, such as time windows violations due to the uncertainties, can be accepted to avoid the searching process getting trapped in local optimality. We then design a surrogate objective function $f^{RO}(S)$ (see equation (3.6a)) and add a penalty for the possible delay $f^{DC}(S)$ for the customers by using the recursive function (3.7).

$$f^{SRO}(S) = f^{RO}(S) + f^{DC}(S) \quad 3.8$$

$$f^{DC}(S) = \gamma_t \sum_{k \in K} ^{m} \sum_{i=1}^{|s_k|} \max\left(0, \Lambda(i, \Gamma_t^k, \Gamma_s^k) - l_i\right) \quad 3.9$$

In equation (3.8), the surrogate objective is represented by $f^{SRO}(S)$. The first term $f^{RO}(S)$ represents the total travel distance for a given solution S which can be calculated by equation (3.6). The second term calculates the total delay penalty $f^{DC}(S)$ for current solution S, where a penalty score is denoted by γ_t. By leveraging this surrogate function, we can simultaneously minimize the total travel distance and mitigate potential delays.

3.4.2 Memorized buffer

Based on the observation in (Pelletier et al., 2019), computing the robustness for a solution is a time-consuming process. It is not a trivial task to evaluate the robustness of every generated solution during the search, especially when the problem size is larger and complex. Unlike most of the existing literature in solving uncertain vehicle routing problem (VRP) (e.g., Hu et al. (Hu et al., 2018b) and Shi et al. (Shi et al., 2019)), we create a memorized buffer mechanism to mitigate the scalability issue for the RO model, which can reduce unnecessary computation and enhance the efficiency of the algorithm.

In the RO model, computing the latest possible vehicle arrival time at each vertex is necessary to evaluate the potential delay cost, as described in equation (8). However, it should be noted that the recursive function $\Lambda(i, \Gamma_t^k, \Gamma_s^k)$ in equation (7) is computationally intensive, especially when the length of a BEV route increases, and the uncertainty parameters become larger. The time complexity of the recursive function $\Lambda(i, \Gamma_t^k, \Gamma_s^k)$ is $O(n^3)$ in the worst case.

To effectively handle the computational demands of the calculation for the latest arrival time $\Lambda(i, \Gamma_t^k, \Gamma_s^k)$, a memorized buffer is to store intermediate results that are already computed values. The memorized buffer is a tensor $\mathcal{M} = [p_i^k, \Gamma_t^k, \Gamma_s^k\ ] \in \mathbb{R}^3$. p_i^k denotes the index of EV route k. Γ_t^k and Γ_s^k represent the uncertain degree of uncertain travel time and service time, respectively. During the computation of the latest arrival times at each node, the memory buffer records the calculated results to prevent redundant calculations. Therefore, all the possible latest arrival times can be calculated and stored in the memorized buffer. Those values can be retrieved when calculating the delay cost $f^{DC}(S)$.

The structure of the memorized buffer is illustrated in Figure 3-2. The memorized buffer is used to record all potential lateness for each visit (represented by the colored points) under different levels of uncertainty. The red-doted lines and black dashed lines connect the intermediate data points needed to compute the potential latest arrival times for node p_2^k and p_3^k, respectively. Note that not all connection lines are shown in the figure for simplicity.

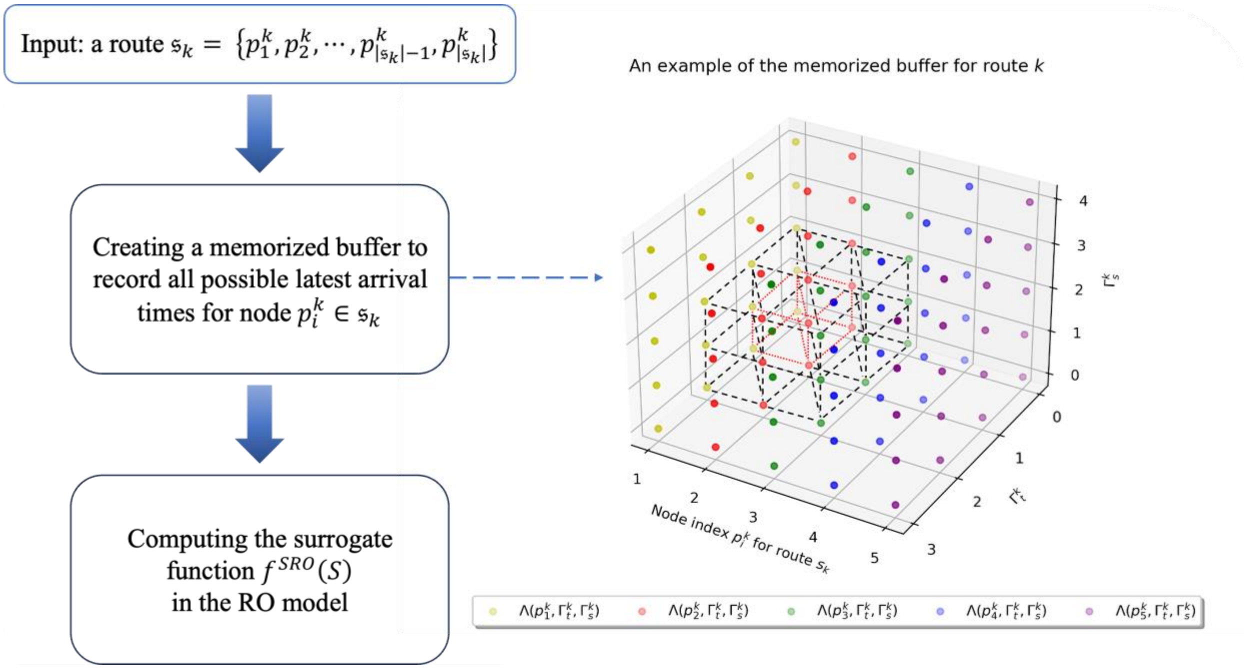

Figure 3-2. An illustration example for the memorized buffer.

Take a BEV route $\mathfrak{s}_k = \{p_1^k,\ p_2^k, \cdots, p_{|\mathfrak{s}_k|-1}^k, p_{|\mathfrak{s}_k|}^k\}$ in a solution as an example. When computing the latest arrival time for the first node on a given route, $\Lambda(1, \Gamma_t^k, \Gamma_s^k)$, this value is stored in the buffer. When calculating the arrival time for subsequent nodes, such as $\Lambda(2, \Gamma_t^k, \Gamma_s^k)$, the previously stored result is retrieved from the memory buffer. This allows the computation to proceed directly without recalculating previous steps. By storing all intermediate arrival times, the memory buffer not only reduces computational redundancy but also accelerates the estimation of costs in later steps.

This mechanism significantly reduces the overall computational time by storing the computed results in the buffer. This strategic use of memory buffer addresses the scalability issue of the proposed RO model, making it feasible to handle larger BEV networks by considering uncertain service times and travel times.

3.5 Solution methodology: two-phase metaheuristics

We first incorporate the RO method and reformulate the cost function in Section 3.4.1 to find a robust solution The developed MIP model extends the classic EVRPTW (Schneider et al., 2014), which is also NP-hard. The number of decision variables grows exponentially as the number of customers increases. Additionally, the problem incorporates several hard constraints typically in urban freight logistics, such as backhauling strategies (last-in, first-out), customer time windows, BEV driving range, and the location of en route recharging stations. In the robust version (see Section 3.4), travel times and service times are considered uncertain variables, adding further to the computational complexity of the problem. These constraints and uncertainties make it difficult to obtain an exact solution using existing commercial solvers, especially for large-scale instances. To address this, we propose a two-phase metaheuristics algorithm that generates high-quality robust solutions within a reasonable computation time.

Two-phase methods have been shown to be quite successful in both deterministic and stochastic routing problems (see e.g., (Pelletier et al., 2019), (Bongiovanni et al., 2022), and (Alkaabneh & Diabat, 2023)). Unlike the two-phase metaheuristics developed in (Pelletier et al., 2019), we combine an ALNS with SA in the first phase and an ILS metaheuristics algorithm in the second. The goal of the ALNS metaheuristics (Phase I) is to find a high-quality deterministic solution efficiently. Phase II then focuses on enhancing robustness by making targeted adjustments to the deterministic solution using ILS. This phase leverages ILS's strengths, allowing for incremental improvements through local search (LS) operators, requiring only a few iterations. An overview of the two-phase framework is presented in Figure 3-3, with the detailed algorithm provided in Appendix Algorithm A.1.

The remainder of this section is structured as follows: In Section 3.5.1, we first construct an initial feasible solution for a BEV fleet using a construction heuristic algorithm, and we discuss the solution representation. Section 3.5.2 details our ALNS framework, covering a variety of customer-oriented destroy operators and several repair operators. Finally, Section 3.5.3 presents Phase II, where we utilize ILS metaheuristics to identify a robust solution.

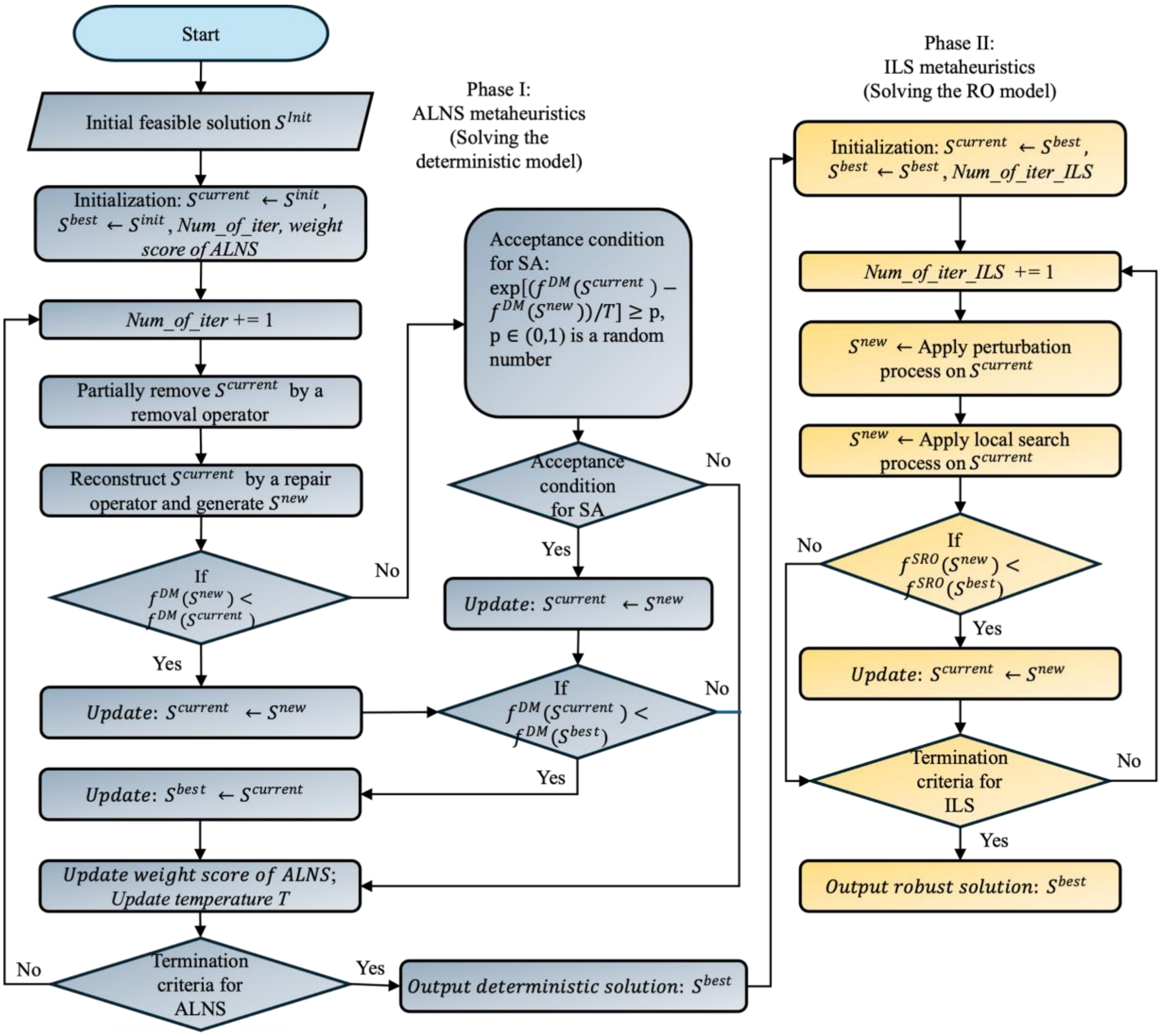

Figure 3-3. An overview of the two-stage metaheuristics framework.

3.5.1 Solution generation and solution representation

The initial solution for the BEV fleet is generated by a greedy constructive heuristic, which is similar in (Peng, Wu, et al., n.d.). The procedure for generating the initial solution is illustrated in Figure 3-4. Before generating the initial solution, all the unvisited customers are stored in the unvisited customer pool $N^{unvisited}$, including for both the linehaul customers and backhaul customers. Also, a list of CSs $\mathcal{R}$ is available to be visited if the recharging process is necessary.

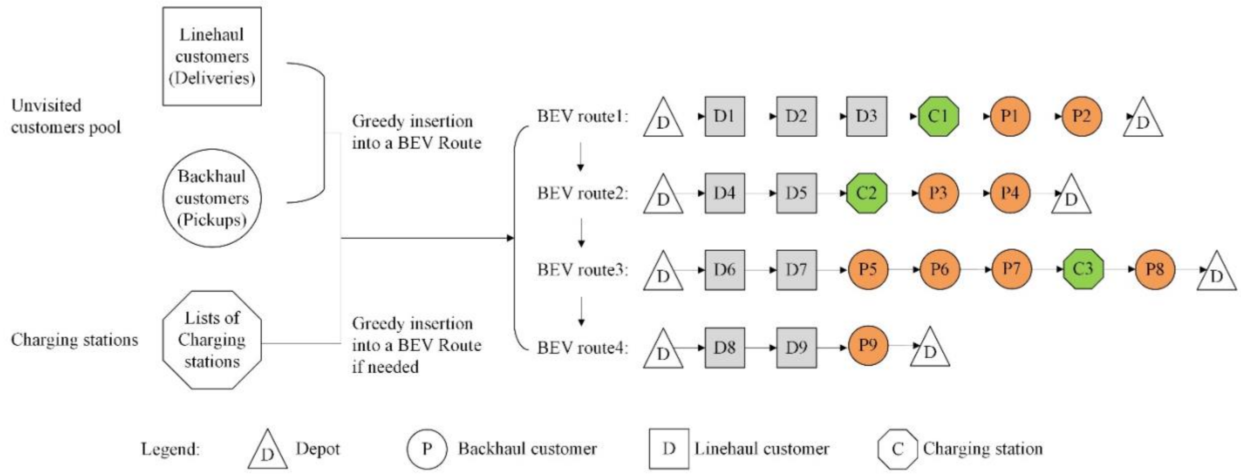

Figure 3-4. The procedure of generating an initial solution.

Algorithm A.2 (in Appendix) outlines the pseudocode for constructing initial solutions. When constructing the initial solution of the BEV fleet, we begin with the first journey, represented by BEV route_1. At the beginning of construction, a customer $i \in N^{unvisited}$ is randomly selected and inserted into BEV route_1. Then, a greedy heuristic algorithm is used to determine a favorable customer i and its preferred insertion location x from unvisited customer pool $N^{unvisited}$, which leading a minimum increasing in the total cost, i.e., $\Delta cost = f^{DM}(S^{init}) - f^{DM}(S^{init}_{-i,x})$, where S^{init} and $S^{init}_{-i,x}$ is the solution with and without the candidate customer i, respectively.

This greedy insertion process iteratively selects candidates and adds them to the current BEV journey. Importantly, during each insertion, feasibility checks are conducted to ensure: (1) backhaul customers are inserted only after linehaul customers, and (2) the BEV route adheres to constraints such as driving range, cargo load capacity, and time windows after each customer is added.

When no preferred customers can be added to the current route due to battery capacity constraints, an en route recharging visit is considered. A potential recharging station is greedily selected from the list of available stations, with the insertion cost being the minimal increase compared to the total travel cost before the insertion. Once a recharging visit has been accommodated, more unvisited customers may be added to the route using the greedy heuristic algorithm. If no additional customers can be added due to constraint violations, a new BEV route is initiated to visit the remaining unvisited customers, following the same process.

Based on our observation, the total number of BEVs in the constructed initial solution can vary due to the problem's hard constraints. In some cases, more vehicles may be necessary because certain customers cannot be scheduled appropriately. To address this, Algorithm A.2 (in Appendix) is executed ς times, and the solution with the minimal number of vehicles is chosen as the preferred initial solution, which can later be refined using the ALNS framework.

As illustrated in Figure 3-4, the initial solution is represented by $S^{init} = \{1: \mathrm{O} - \mathrm{D1} - \mathrm{D2} - \mathrm{D3} - \mathrm{C1} - \mathrm{P1} - \mathrm{P2} - \mathrm{O}; 2: \mathrm{O} - \mathrm{D4} - \mathrm{D5} - \mathrm{C2} - \mathrm{P3} - \mathrm{P4} - \mathrm{O}; 3: \mathrm{O} - \mathrm{D6} - \mathrm{D7} - \mathrm{P5} - \mathrm{P6} - \mathrm{O}\}$. The depot node is represented by O. The linehaul and backhaul customers are represented by D and P with different integer numbers. The en route recharging schedules are represented by C.

3.5.2 Phase I: ALNS search algorithm

The initial solution for the BEV Extending the most popular ALNS removal and repair operation built in (Goeke & Schneider, 2015; Ropke & Pisinger, 2006c), we have developed several customer-oriented operators to address the proposed routing problem efficiently. Specifically, we design two new removal operators, the worst linehaul customer demand removal (R8) and the StationPathRe removal (R9) operators. These operators strategically remove components of the solution based on customer service types and the locations of CSs, thereby diversifying the solution space and enabling the ALNS to efficiently identify high-quality solutions.

Additionally, our ALNS framework incorporates nine destroy operators and four repair operators to iteratively reconstruct new solutions by modifying the visit sequences of customers and recharging stops. This framework also facilitates the development of a promising en route partial recharging schedule.

Removal operators

In the developed ALNS framework, one of the following removal operators is selected to remove n vertices (including customers and recharging stations) from the current solution and put the removed customers into an unvisited list. For each route $\mathfrak{s}_k$, the number of customers/vertices $n = \lceil \epsilon \cdot |\mathfrak{s}_k| \rceil$ is computed by the destroy rate ϵ, where ϵ is randomly sampled from the range [0.30, 0.45] when implement the removal operators. The removal heuristics are detailed as follows.

- **Random removal (R1)** randomly removes n customers/vertices from the BEV routes. It can randomly remove customers or recharging schedule.
- **Random path removal (R2)** destroys an entire consecutive sub-path with n vertices.
- **Simplified Shaw removal (R3)** identifies and removes customers according to their geographical positions. First, we randomly choose a customer from the route and find the closest customer which has not been chosen to remove. This pair of customers are identified and removed to subset $L_{removal}$. Next, the new request is selected from this route which has not been touched by the removal operator, and a new pair is identified by their distance. This process continues several times until the desired number of customers has been removed to the subset $L_{removal}$.

- **Shaw removal (R4)** (Shaw, 1998) removes a set of n similar customers. A relatedness function is used to check the similarity for the customer i and j, which can be calculated by $\Lambda(i,j) = \phi_1 \frac{d_{ij}}{\max\limits_{i,j\in\mathcal{N}}(d_{ij})} + \phi_2 \frac{|e_i - e_j|}{\max\limits_{i\in\mathcal{N}}(e_i) - \min\limits_{i\in\mathcal{N}}(e_i)} + \phi_3 \frac{|q_i - q_j|}{\max\limits_{i\in\mathcal{N}}(q_i) - \min\limits_{i\in\mathcal{N}}(q_i)}$. The weight vector $\phi = (\phi_1, \phi_2, \phi_3)$ is applied to normalize the relatedness function. At the beginning, a customer $i \in \mathcal{N}$ is randomly selected as a candidate customer who needs to be removed. Next, the most related customer $j \in \mathcal{N}\backslash i$ is chosen by calculating the similarity function with the smallest value $\Lambda(i,j)$. The operator continues to remove the related customer with j. Finally, the Shaw removal operator terminates once n customers have been removed.
- **Shaw time removal (R5)** iteratively removes n customers who have similar time windows. The relatedness for the time windows between customers i and j can be calculated by $\Lambda_{time}(i,j) = \frac{|e_i - e_j|}{\max\limits_{i\in\mathcal{N}}(e_i) - \min\limits_{i\in\mathcal{N}}(e_i)}$. Like the Shaw removal operator, the Shaw time removal operator starts with a customer $i \in \mathcal{N}$, with random selection, and destroys current solution iteratively until n customers have been removed.
- **Worst removal (R6)** iteratively removes n vertices that contribute the most considerable insertion cost. It first sorts the insertion cost of all vertices in a descending order by calculating $c_i = f^{DM}(s) - f^{DM}(s_{-i})$, where s and s_{-i} denote the route with and without customer i, respectively. Then, the worst removal operator iteratively removes a customer with the highest insertion cost.
- **Worst demand removal (R7)** iteratively removes n customers who contribute the largest payload in the current route. The operator first sorts the insertion demand cost of all customers in descending order by calculating $c_i^{demand} = \sum_{i\in s} d_i - \sum_{j\in s\backslash i} d_j$. This process repeats until the number of removal customers reaches to n. The purpose of this operator is to identify a customer who has the heaviest payload and allocate it to different vehicles, aligning with the specific objective of minimizing the overall fleet size embedded within the proposed optimization problem.
- **Worst linehaul customer demand removal (R8)** iteratively removes n linehaul customers who contribute heavier payload in the vehicle. This operator is a variant of the worst demand removal operator. However, since the number of linehaul customers is mostly larger than backhaul customers in the backhaul dispatching scenarios. Therefore, the potential removal of a linehaul customer can be estimated $c_i^{L\_demand} = \sum_{i\in s} d_i - \sum_{j\in s\backslash i} d_j, \forall i \in L$. The purpose of this operator is to remove an unfavorable linehaul customer whose demand is much higher than others.
- **StationPathRe removal (R9)** is a variant of station vicinity removal, as presented in (Goeke & Schneider, 2015) and specifically designed for a route with a recharging visit. For a route $\mathfrak{s}_k$, the purpose of the StationPathRe operator is to reconstruct part of a route in the vicinity of recharging stations. Figure 3-5 shows an example of the removal process by using the developed operator. To define the vicinity of a recharging station, we define the recharging station as the central node. Next, the

operator removes a path where contains n vertices including the recharging station and customers from the current vehicle route. The beginning index of the removed path is $p^k_{start} = p^k_{\max(i-\lceil 0.5n \rceil,1)}$, where the position of recharging station is p^k_i. The end index of the path is defined by $p^k_{end} = p^k_{\min(start+n,|\mathfrak{s}_k|)}$. Finally, a path from p^k_{start} to p^k_{end} can be removed from the current route $\mathfrak{s}_k$. The removal operator is implemented for all BEV routes that have a recharging visit during a search. The purpose is to find an improved recharging schedule.

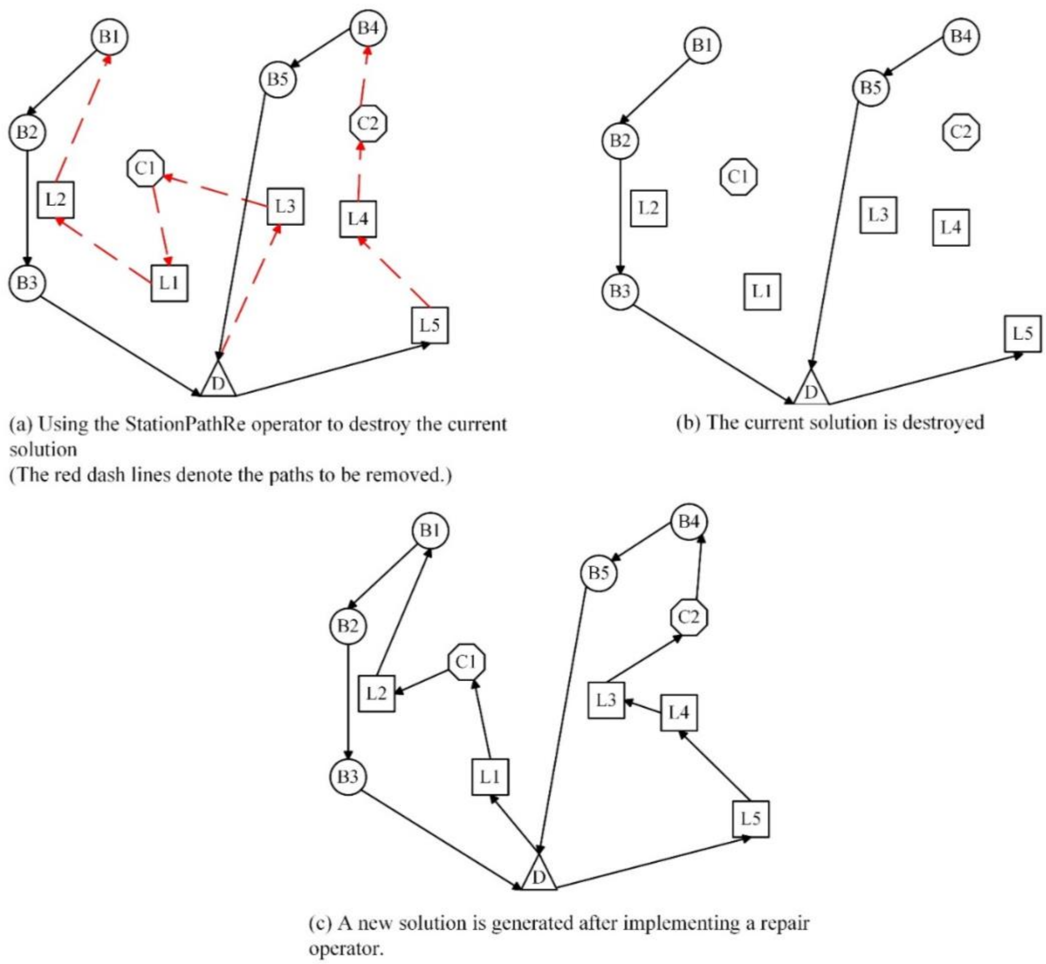

(a) Using the StationPathRe operator to destroy the current solution
(The red dash lines denote the paths to be removed.)

(b) The current solution is destroyed

(c) A new solution is generated after implementing a repair operator.

Figure 3-5. An example of StationPathRe removal operator and an example of repairing process.

Repair operators

The ALNS framework incorporates four repair operators designed to enhance solution quality by reinserting all unvisited customers and favorable recharging visits into the current routing configuration. These operators aim to optimize the routing of the BEV fleet while adhering to various constraints. All the repair operators are detailed in the following.

- **Greedy insertion (I1)** iteratively reinserts unvisited customers to construct a route by selecting the feasible cost-minimizing position for each customer. For every insertion, the increase of the cost function $f^{DM}(S)$ for each possible insertion position is evaluated. The insertion position that results in the minimal cost increase is then selected.
- **Regret insertion (I2)** has been applied in (Ropke & Pisinger, 2006b) and (Goeke & Schneider, 2015), which aims to estimate the future effect of an insertion operation. It identifies the insertion position that maximizes the difference between the best insertion position and the k^{th} best insertion position. The regret value $reg_{i,k}$ can be calculated by $reg_{i,k} = \Delta f^{DM}(i, pos_{i,1}) - \Delta f^{DM}(i, pos_{i,k})$, where $\Delta f^{DM}(i, pos_{i,1})$ indicates the cost improvement with the best insertion and $\Delta f^{DM}(i, pos_{i,k})$ denotes the cost improvement generated by the k^{th} best insertion. In this study, we use the Regret-2 insertion method.
- **Greedy insertion with CSs (I3)** is employed to construct routes and determine a recharging schedule. For the insertion of customers, it follows the greedy insertion process. If a BEV route is found to be energy infeasible, an appropriate recharging station visit is inserted, taking into account the detour cost and recharging constraints. If the current BEV route has a possible en route recharging visit, more customers are allowed to visit. When no more customers can be inserted into the current route due to the constraints, a new BEV route should be started. However, there is an exception: once a recharging visit has been assigned, no additional customers can be inserted. In this case, the recharging visit will be removed since recharging is unnecessary.

3.5.3 Phase II: ILS metaheuristics to find a robust solution

In phase II, a customized ILS metaheuristics algorithm is applied to slightly modify the near-optimal solution obtained from stage I, aiming to identify a robust solution without significantly increasing computational time. As noticed in (Pelletier et al., 2019), checking the robustness for a solution is computational intensively. To mitigate this, we only use the surrogate function $f^{SRO}(S)$ as the objective function in the ILS metaheuristic algorithm while the designed memorized buffer is embedded as introduced in Section 3.4. This approach helps streamline the process of finding robust solutions by leveraging the strengths of both the surrogate function and the customized ILS framework.

The devised ILS metaheuristics follow a best-improvement strategy, employing a composite neighborhood of a list of operators to refine the best solution S^{best} obtained from the ALNS metaheuristics. The pseudocode of the ILS metaheuristics is illustrated in Appendix A Algorithm I (lines 17-23). It consists of three steps: 1) perturbating the current solution, 2) finding a new robust solution by local search (LS) procedures, and 3) accepting a new solution. The detailed description of those steps is elaborated in the following.

The main drawback of the iterative improvement is that the search process may easily fall into local optima solutions that are significantly worse than the global optimum (Lourenço et al., n.d.). Therefore, applying a perturbation process is necessary to diversify the solution, which can be improved further by the LS step. To perturb the solution, we randomly choose one operator from the neighborhood structure to reconstruct the solution. For example, a two-opt move can modify the inner route by changing the visit sequence between two vertices, as Figure 3-6 illustrates. It should be noted that the perturbation does not necessarily generate an improved solution, but the feasibility of the perturbed solution should always be satisfied for the perturbation procedure.

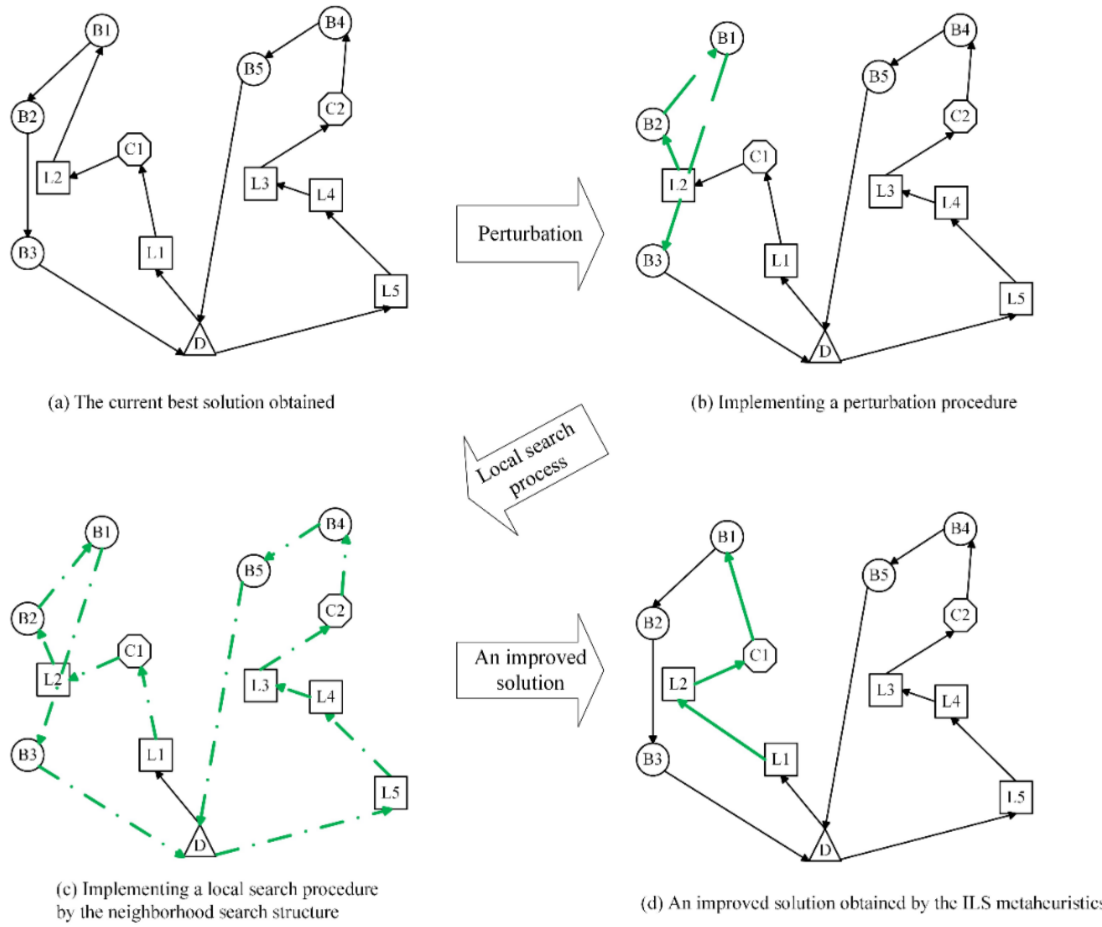

Figure 3-6. An example of one iteration of the ILS metaheuristics.

Next, the ILS follows a best-improvement strategy using the following composite neighborhood structures. We use a list of inner- or intra-route constructive operators to generate new feasible solutions, including 2-opt (S. Lin, 1965), or-opt (OR, n.d.), 2-opt* (Potvin & Rousseau, 1995), relocate and exchange (Savelsbergh, 1992). When implementing those LS operators, each move is evaluated, and a move is superior if a new feasible solution has a lower cost in terms of checking the surrogate cost function $f^{SRO}(S)$.

Based on the above perturbation and the LS procedures, the ILS is applied to iteratively refine the routes and find a favorable solution with lower delay risk and shorter travel distance. The termination criterion of the ILS is when the maximum iteration η_{ILS}^{max} is reached.

3.6 Computational experiments

To evaluate the proposed dispatching strategy, we present extensive computational results assessing the effectiveness of the proposed two-phase metaheuristics across various instances. First, we create a new EVRPBTW benchmark dataset (see Section 3.6.1) to assess the performance of the developed metaheuristics and investigate the influence of using the memorized buffer when solving the RO model. Second, to assess the solution quality and run-time, we conduct tests on available VRPB benchmark instances by the developed metaheuristics and compare them with the best-known solutions (BKS) and a recent well-known metaheuristic, an ILS constructed by (Brandão, 2016). Third, we conduct tests on solving both deterministic and robust models using the newly introduced benchmark dataset. Fourth, we perform a comprehensive examination to investigate the influence of the uncertainty factors on the RO model. Lastly, we conduct a real-world application based on realistic data from a full-service logistics company in Southern California, U.S.

The section is structured as follows. Section 3.6.1 introduces the generated EVRPBTW benchmark instances. Section 3.6.2 describes the experimental setup, the parameter settings, and the framework designed for evaluating the proposed method. In Section 3.6.3, we assess the solution quality of the proposed ALNS metaheuristic algorithm by testing it on the standard VRPB benchmark dataset (Goetschalckx & Jacobs-Blecha, 1989). Section 3.6.4 compares the performance of the proposed metaheuristics to the commercial solver Gurobi on the test instances. Section 3.6.5 analyses the computational results for EVRPBTW-USUT. Section 3.6.6, a comprehensive sensitivity analysis is conducted to further investigate the impact of the key uncertain parameters for the RO model. In section 3.6.7, we conduct a comprehensive sensitivity analysis to further investigate the impact of the uncertain factors for the RO model.

The mathematical models described in our study are programmed in Python 3.9. The tests performed on the benchmark instances are conducted on an online server with 32 gigabytes (GB) of Random Access Memory (RAM).

3.6.1 Introduction of the new EVRPBTW benchmark dataset

To exam the proposed EVRPBTW-USUT, we introduce a new EVRPBTW benchmark data sets based on the well-known EVRPTW benchmark instances introduced by Schneider et al. (Schneider et al., 2014). The classic EVRPTW benchmark dataset has been widely performed on solving the EVRPTW and its variants (e.g., (Desaulniers et al., 2016; Goeke & Schneider, 2015; B. Lin et al., 2021; Montoya et al., 2017b)). Our EVRPBTW benchmark datasets incorporate a backhaul strategy for a BEV fleet, which reflects a practical application in urban logistics and supply chain services. The customers are divided into two groups, i.e., linehaul customers who require deliveries and backhaul customers who require pickups

We selected 10 instances from the EVRPTW benchmark dataset, where the customers are randomly distributed in the hypothesis scenario. For each problem instance, similar to (Toth & Vigo, 1997), we generate two EVRPBTW instances based on one EVRPTW dataset, where each corresponding to an approximate linehaul percentage of 66% and 75%, respectively. Backhaul customers are distributed in groups of every three or four customers.

Other aspects, such as customer locations, time windows, recharging station's locations, and EV characteristics, remain unchanged. Therefore, for each EVRPTW benchmark dataset, we can generate two new EVRPBTW instances. For example, the instance named "r201_C25B3" represents a case with 25 customers, where 13 are linehaul customers and 12 are backhaul customers, accounting for approximately 66% backhaul customers. This instance includes 21 recharging stations. Finally, a total number of 60 instances are generated (see first column in Table 3-7 and Table 3-8).

3.6.2 The experiment setup and parameter settings

The parameters related to problem assumptions—such as recharging rate, EV battery capacity, cargo load capacity, and energy consumption rate—follow the same values as those defined in the EVRPTW benchmark dataset (Schneider et al., 2014). For further details, interested readers are referred to the data summary section and the accompanying dataset.

The proposed two-phase metaheuristic framework comprises the customized ALNS metaheuristics (Phase I) and the ILS metaheuristics (Phase II). Table 3-3 summarizes the final parameter of the devised two-phase metaheuristics. In Phase I, most parameters of our ALNS-based metaheuristics algorithm are adopted from a recent study conducted by Peng et al. (Peng, Wu, et al., n.d.), which has performed well in addressing the EVRPBTW as well as traditional VRPB. In Phase II, based on our investigation, we set the maximum iterations of the ILS process to be 25 for consideration of the complexity of the RO model. The default values used in the RO model is described in Table 3-4.

Table 3-3 Final parameters setting of two-phase metaheuristics used in numerical studies

Notation	Value	Description
ALNS algorithm		
ς	100	Maximum iteration in the construction of initial feasible solution.
ϕ	(0.5, 0.25, 0.25)	Parameter vector in Shaw removal operator.
T_{init}	10	Initial temperature in the SA heuristic.
T_{init}	0.05	The end temperature in the SA heuristic.
δ	0.9998	Cooling rate in the SA heuristic.
λ	0.8	Decay parameter in the ALNS metaheuristics.
η_{ALNS}^{max}	2000	Maximum iterations in the ALNS metaheuristics.
$\eta_{non\_improve}$	750	Non-improved iterations in the ALNS metaheuristics.
ψ	(15, 9, 8, 5)	Score vector in the ALNS metaheuristics.
ILS algorithm		
η_{ILS}^{max}	25	Maximum iterations in the ILS metaheuristics.

Table 3-4 Default parameter setting in the RO model.

Notation	Value	Description
α^t	0.2	Uncertain range of travel time
α^s	0.2	Uncertain range of service time
θ^t	0.3	Uncertain level of travel time
θ^s	0.3	Uncertain LOS time
γ_t	50	Delay penalty score in the RO model

3.6.3 Experiments on standard VRPB instances

To assess the performance of the proposed two-phase metaheuristics in terms of the solution quality and solution time, we implement it on a standard VRPB benchmark dataset introduced by Toth and Vigo (Toth & Vigo, 1997). The TV89 instance set contains a total of 36 problem instances with customer sizes ranging from 21 to 100. The proportion of linehaul customers varies in different instances. The instance set has been used to evaluate the performance of algorithms for solving standard VRPB in (Brandão, 2016; Ropke & Pisinger, 2006b; Toth & Vigo, 1997).

Using the parameter settings in Appendix B Table B-1, the devised ALNS metaheuristics algorithm aims to minimize the total travel distance objective in the standard VRPB instances. Appendix B Table B-2 shows the experiment results. Columns *L* and *B* represent the number of linehaul and backhaul customers, respectively. We compare our results with the BKS and another state-of-the-art metaheuristics method (Brandão, 2016), denoted by ILSA(B16).

Our results show that the ALNS metaheuristics can find 20 optimal solutions among 33 optimal results, surpassing ILSA(B16) by four additional optimal results. Overall, the ALNS approach performed competitively, with an average cost increase of 1.78% compared to the BKS. The algorithm's computational efficiency was also tolerated, with an average solution time of 136.46 seconds across all instances.

3.6.4 Benchmark against with the MILP formulation

This section compares the performance of the proposed two-phase metaheuristic algorithm with the direct solution of the MILP formulation using the commercial solver Gurobi. To evaluate the accuracy and optimality of the proposed metaheuristic, we implement the MILP model described in Section 3.3.2 and solve it using Gurobi with a maximum central processing unit (CPU) time limit of one hour. A range of small-size instances from the EVRPTW benchmark dataset, involving five to 20 customers, is selected for this comparison.

Table 3-5 shows the comparison of numerical results for small-scale instances. The proposed metaheuristics algorithm demonstrates strong performance, consistently achieving optimal solutions. Moreover, its computation time is comparable to or lower than that of Gurobi, particularly as the problem size increases. Notably, when the number of customers reaches 15, Gurobi may exceed the CPU time limit (3,600 seconds). In contrast, the proposed metaheuristic algorithm can still solve these instances in under one minute in most instances.

Table 3-5 Comparison of results for small-scale instances.

	Gurobi		Metaheuristics			
Instance	f^{dist}	***t (s)***	f^{dist}	***t (s)***	$\Delta_{dist}(\%)$	Δ_t
c101_C5	72.68	0.14	72.68	0.51	0.00	0.37
c103_C5	44.41	0.1	44.41	0.48	0.00	0.38
c202_C5	115.58	0.51	115.58	0.76	0.00	0.25
r105_C5	156.8	0.1	156.8	0.75	0.00	0.65
r203_C5	138.87	0.24	138.87	0.65	0.00	0.41
rc108_C5	88.77	0.14	88.77	0.92	0.00	0.78
c101_C10	127.73	0.66	127.73	1.98	0.00	1.32
c103_C10	97.65	0.22	97.65	2.18	0.00	1.96
c202_C10	198.74	1.84	198.74	2.48	0.00	0.64
r105_C10	295.62	0.02	295.62	1.53	0.00	1.51
r203_C10	238.40	10.37	238.40	3.54	0.00	-6.83
c101_C10	127.73	0.66	127.73	1.98	0.00	1.32
c103_C15	214.04	6.68	214.04	5.98	0.00	-0.70
c202_C15	289.98	261.63	289.98	4.84	0.00	-256.79

c203_C15	257.69	3600.19	264.60	8.13	0.03	-3592.06
r104_C15	399.26	50.00	399.26	6.73	0.00	-43.27
r203_C15	336.22	78.49	336.22	13.85	0.00	-64.64
rc108_C10	216.51	3600.13	216.51	7.73	0.00	-3592.40
c103_C20	332.27	1330.91	332.27	25.32	0.00	-1305.59
c109_C20	243.37	3600.00	243.37	8.00	0.00	-3592.00
c202_C20	313.34	874.46	313.34	10.63	0.00	-863.83
r204_C20	330.23	276.57	330.23	80.39	0.00	-196.18
rc204_C20	315.36	3600.21	315.36	39.12	0.00	-3561.09
rc207_C20	387.71	375.02	387.71	20.17	0.00	-354.85

3.6.5 Influence of memorized buffer in the RO model

As described in Section 3.4.2, we introduce a memorized buffer in the RO model as an intermediate storage to record the calculated latest arrival time for each node, which can greatly reduce computational complexity and improve efficiency. To assess the impact of the memorized buffer, this section implements the two-phase metaheuristic algorithm to solve the robust dispatching model, comparing results with and without the buffer.

We use 25-customer size instances as test cases and apply the metaheuristic algorithm to solve the RO model. Table **3-6** presents the computational times. The results indicate that incorporating the memorized buffer significantly reduces computation time, with reductions ranging from 29.49% to 99.66%, depending on the size of instances and customers' requirements. The results indicate that incorporating the memorized buffer significantly reduces computation time, with reductions ranging from 29.49% to 99.66%, depending on the size of instances and customers' requirements.

Notably, solving the RO model without the memorized buffer may result in computation times exceeding 3,600 seconds (see example r207_C25B4). Overall, these findings underscore the effectiveness of the memorized buffer in improving the efficiency of the RO model and enhancing its scalability for solving larger problem instances.

Table 3-6. Comparison of the solution time using the memorized buffer in 25-customer size instances.

	RO model w.o. memory buffer	RO model w. memory buffer	
Instance	Ave. t	Ave. t	Dev_t
c101_21_25b50	70.29	63.79	-9.26%
c101_21_25b66	59.24	55.59	-6.16%
c101_21_25b80	62.15	54.05	-13.05%
c103_21_25b50	96.17	67.57	-29.74%
c103_21_25b66	279.38	85.30	-69.47%
c103_21_25b80	113.34	69.32	-38.84%
c106_21_25b50	81.71	72.03	-11.85%
c106_21_25b66	76.99	62.06	-19.39%
c106_21_25b80	92.89	68.86	-25.87%
c108_21_25b50	78.15	69.71	-10.80%
c108_21_25b66	74.63	73.90	0.98%
c108_21_25b80	83.51	69.08	-17.28%
Ave.	97.37	67.61	
Total	1168.48	811.26	-30.57%

3.6.6 Computational results of the small-size EVRPBTW-USUT benchmark instances

This section presents the experiment results for solving the EVRPBTW-USUT benchmark instances. First, we introduce the evaluation framework and discuss the main indicators describing the robustness of the solution in detail. Subsequently, we report the experimental results obtained from the deterministic model and the robust model for the benchmark instances with 25 customers, 50 customers, and 100 customers. Lastly, a comprehensive sensitivity analysis is conducted to further examine the impact of uncertainty factors in the robust dispatching model.

A MC simulation process and evaluation framework

Figure 3-7 presents the evaluation framework for assessing the robustness of solutions obtained by the deterministic or robust models. In an uncertain dispatching environment, a MC simulation process is commonly performed to assess the robustness of a solution (similar to (Amiri et al., 2023; Hu et al., 2018a; Shi et al., 2019)). When considering uncertain customer service times and travel times, we employ an MC simulation to generate 1,000 heterogeneous uncertain simulation scenarios. In each scenario, a customer's service time $\tilde{s}_i$ $(i \in N)$ is heterogeneity uncertain, which can be uniformly sampled within its interval $[\bar{s}_i, \hat{s}_i]$. The maximum deviation $\hat{s}_i$ in the MC simulation defaults to $\bar{s}_i + 0.2\bar{s}_i$. Additionally, the travel time of each arc $\tilde{t}_{ij}$ $(i, j) \in \mathcal{A}$, can be vary in its range $[\bar{t}_{ij}, \hat{t}_{ij}]$ in a simulation scenario, with the maximum deviation of uncertain travel time set to $\bar{t}_{ij} + 0.2\,\hat{t}_{ij}$. After conducting the MC simulation, we record a set of vital characteristics that describe the robustness of the solution.

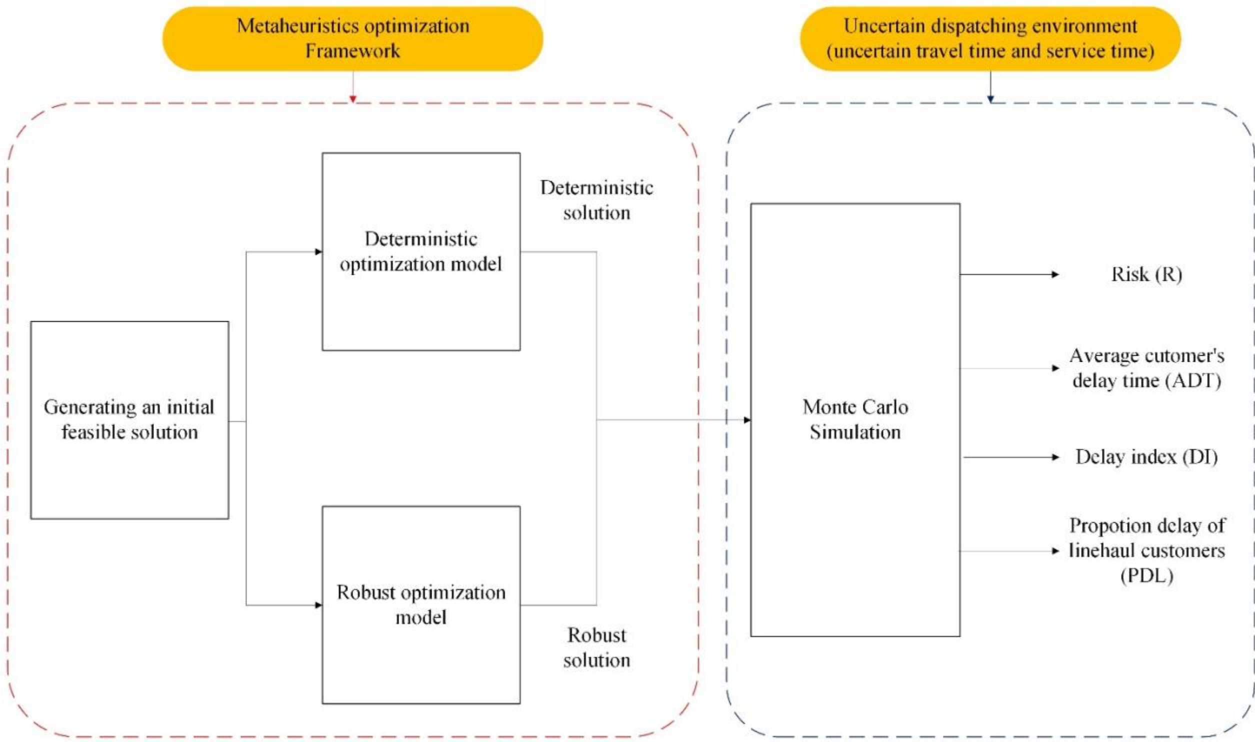

Figure 3-7. An evaluation framework to assess the robustness of a solution (adopted from Shi et al., 2019).

Inspired by Shi et al., 2019, we apply several indicators to further investigate the robustness of a solution. All the indicators are summarized as follows.

Risk (R): The risk value represents the proportion of infeasible solutions among the total number of MC simulations. Risk value can be calculated by $Risk(R) = (\frac{Count\ of\ infeasible\ scenarios}{Total\ numbers\ of\ MC\ scenarios}) \times 100\%$.

Average customers' delay time (ADT): average delay time (ADT) for each customer in the MC simulations, which is estimated by $ADT = \frac{Total\ delay\ time}{Total\ numbers\ of\ delay\ customers}$.

Computational results on instances with 25 customers

The computational results of the deterministic model and the RO model for the EVRPBTW instance with 25 customers are presented in Table 3-7. For each instance, we executed the developed two-phase metaheuristic framework ten times, recording the best solution, which corresponds to the lowest cost. The "m" column indicates the total number of EVs deployed in the best deterministic solution. The column $f^{dist}(S)$ represents the total travel distance, $f^{DC}(S)$* records the total equivalent delay cost. The CPU run-time time (in seconds) for the best solution of each instance is denoted by "t (s)." Additionally, to assess the robustness of the solutions, the abovementioned indicators are recorded in Table 3-7**.**

We observe that the deterministic solutions exhibit fragility. Six deterministic solutions among the twenty instances have delay risks, where the average delay time is 0.85. However, only two robust solutions have potential delay risks during the MC simulation process and the average delay time is significantly reduced to 0.27, representing a reduction of approximately 68.24%. Additionally, although there still existing a customer delay risk in instance r207_C25B3, the average delay time for the delayed customer is reduced by 50.84%.

It is worth noting that our robust solution is merely to increase the total travel distance by 0.41% on average to ensure the robustness of dispatching, the average delay cost is significantly reduced by 43.69%. To reduce the delay cost, the solution of the RO model may slightly detour to visit the customers with tight time windows to mitigate the delay risk under the uncertainty scenario. Therefore, the total travel distance is increased merely, however, the delay time and risk are significantly reduced. Figure 3-8 provides a visualization of the detailed routes for both the deterministic and robust solutions, for an example instance (r201_C25B4), highlighting the differences in routing strategies between the two approaches.

Additionally, the CPU run time of solving the RO model in 25-customer size instance is similar to the deterministic model, with the difference of less than one second. These results demonstrate the efficiency and robustness of the proposed RO model.

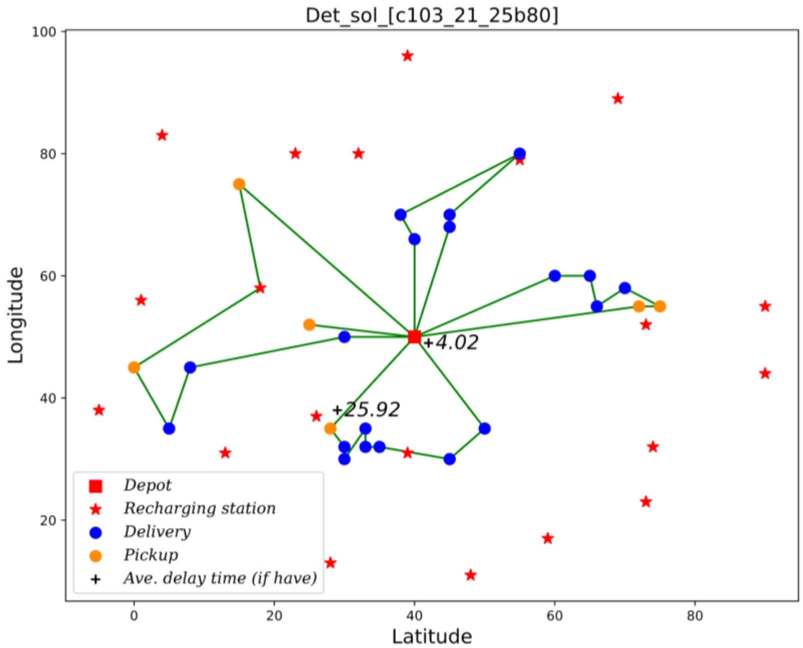

(a) Det_sol_[c103_21_25b80]: total travel distance = 384.05 Risk = 100.00%

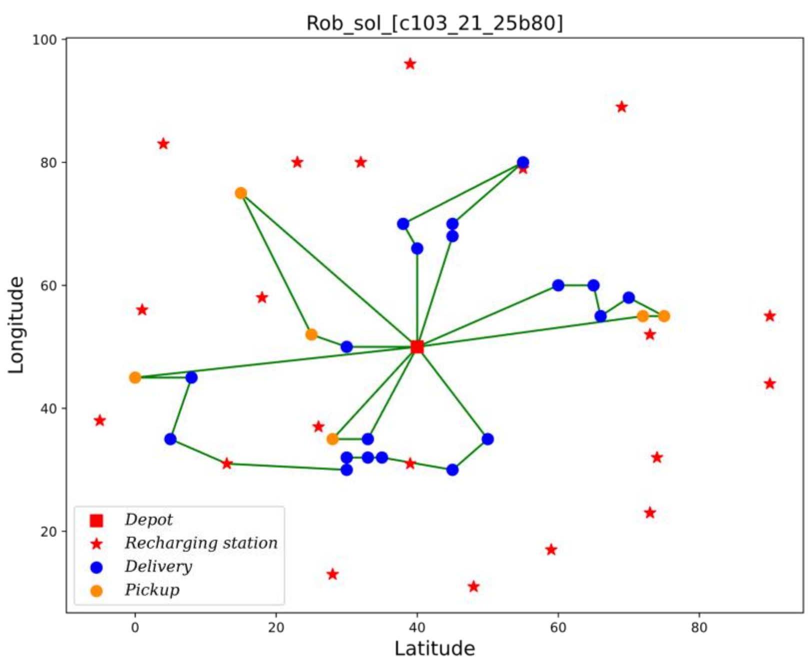

(b) Rob_sol_[c103_21_25b80]: total travel distance = 397.41 Risk = 0.00%

Figure 3-8. The visualization of det_sol (a) and rob_sol (b) of instance r201_C25B4.
Note: The EV routes are shown as green lines. We use "+ (Ave. delay time)" to represent potential average delay times for a delayed node (as shown in Figure 3-8 (a)). Notably, the det_sol has a higher risk value (100.00%), where two nodes have higher risks of encountering potential delays during MC simulation. However, there are no delay customers in rob_sol.

Table 3-7 Comparison of the delay risk on the 25-customer size EVRPBTW instances.

	Deterministic Model						Robust Model										
Instance	***m***	f^{dist}	f^{DC*}	***t (s)***	***Risk (%)***	***ADT***	***m***	f^{dist}	f^{DC*}	***t (s)***	***Risk (%)***	***ADT***	Δ_m	$\Delta_{dist}(\%)$	$\Delta_{DC}(\%)$	Δ_t	Δ_{Risk}
r201_C25B3	4	532.41	0.00	16.61	0.00	0.00	4	532.41	0.00	28.17	0.00	0.00	0	0.00%	—	11.56	0.00
r202_C25B3	3	473.60	0.00	17.42	0.00	0.00	3	473.60	0.00	24.99	0.00	0.00	0	0.00%	—	7.57	0.00
r203_C25B3	3	445.94	0.00	19.50	0.00	0.00	4	438.08	0.00	11.45	0.00	0.00	1	-1.76%	—	-8.06	0.00
r204_C25B3	2	386.21	404.82	26.29	12.10	1.31	2	387.22	0.00	35.34	0.00	0.00	0	0.26%	-100.00%	9.06	-12.10
r205_C25B3	3	476.12	0.00	37.09	0.00	0.00	3	476.12	0.00	15.78	0.00	0.00	0	0.00%	—	-21.31	0.00
r206_C25B3	3	399.90	241.64	18.32	16.30	0.72	3	399.90	241.64	15.34	19.00	0.81	0	0.00%	0.00%	-2.98	2.70
r207_C25B3	2	385.33	2191.11	26.15	99.70	9.52	2	393.54	0.00	28.41	0.00	0.00	0	2.13%	-100.00%	2.26	-99.70
r208_C25B3	2	381.23	0.00	53.72	0.00	0.00	2	381.23	0.00	50.82	0.00	0.00	0	0.00%	—	-2.90	0.00
r209_C25B3	3	457.36	0.00	30.56	0.00	0.00	3	457.36	0.00	32.97	0.00	0.00	0	0.00%	—	2.41	0.00
r210_C25B3	3	453.00	0.00	17.50	0.00	0.00	3	453.00	0.00	29.97	0.00	0.00	0	0.00%	—	12.47	0.00
r201_C25B4	4	584.97	781.90	14.68	100.00	4.70	4	604.46	0.00	10.77	0.00	0.00	0	3.33%	—	-3.91	-100.00
r202_C25B4	3	496.90	0.00	17.39	0.00	0.00	3	496.90	0.00	13.40	0.00	0.00	0	0.00%	—	-3.99	0.00
r203_C25B4	3	461.25	0.00	18.95	0.00	0.00	3	461.30	0.00	31.30	0.00	0.00	0	0.01%	—	12.35	0.00
r204_C25B4	3	433.37	0.00	23.66	0.00	0.00	3	433.37	0.00	15.46	0.00	0.00	0	0.00%	—	-8.20	0.00
r205_C25B4	4	494.39	100.00	23.48	33.90	0.73	4	509.39	0.00	11.96	0.00	0.00	0	3.04%	—	-11.52	-33.90
r206_C25B4	3	475.84	0.00	24.91	0.00	0.00	3	475.84	0.00	51.02	0.00	0.00	0	0.00%	—	26.12	0.00
r207_C25B4	2	428.40	0.00	22.53	0.00	0.00	3	410.08	0.00	16.95	0.00	0.00	1	-4.28%	—	-5.58	0.00
r208_C25B4	2	402.13	0.00	39.26	0.00	0.00	2	405.30	0.00	18.38	0.00	0.00	0	0.79%	—	-20.89	0.00
r209_C25B4	3	485.13	0.00	17.38	0.00	0.00	3	485.08	0.00	16.59	0.00	0.00	0	-0.01%	—	-0.79	0.00
r210_C25B4	3	463.21	0.00	24.72	0.00	0.00	3	463.21	0.00	14.40	0.00	0.00	0	0.00%	—	-10.32	0.00
Avg.		455.84	185.97	24.51	13.10	0.85		456.87	12.08	23.67	0.95	0.04		0.23%	-93.50%	-0.83	-12.15

Notes. ***m*** denotes the EV numbers. f^d and f^{DC*} denote total travel distance and total equivalent delay cost (DC), respectively. ***t (s)*** denotes the CPU run time in seconds. ***Risk (%)*** and ***ADT*** denote risk value in percentage and average delay time (ADT), respectively.

Table 3-8 Comparison of the delay risk on the 50-customer size EVRPBTW instances.

	Deterministic Solution						Robust Solution										
Instance	*m*	f^{dist}	f^{DC*}	*t (s)*	*Risk (%)*	*ADT*	*m*	f^{dist}	f^{DC*}	*t (s)*	*Risk (%)*	*ADT*	Δ_m	$\Delta_{dist}(\%)$	$\Delta_{DC}(\%)$	Δ_t	Δ_{Risk}
r201_C50B3	6	880.55	103.60	108.01	20.30	0.70	6	909.98	0.00	69.68	0.00	0.00	0	3.34%	-100.00%	-38.33	-20.30
r202_C50B3	4	817.02	1479.33	127.28	100.00	4.36	4	861.92	0.00	98.91	0.00	0.00	0	5.50%	-100.00%	-28.36	-100.00
r203_C50B3	4	717.53	0.00	92.50	0.00	0.00	4	742.31	0.00	204.78	0.00	0.00	0	3.45%	—	112.28	0.00
r204_C50B3	3	618.50	2414.11	168.19	100.00	8.36	3	640.77	0.00	207.54	0.00	0.00	0	3.60%	-100.00%	39.35	-100.00
r205_C50B3	4	887.07	0.00	141.34	18.40	1.55	4	889.13	0.00	220.64	0.00	0.00	0	0.23%	—	79.30	-18.40
r206_C50B3	6	766.51	0.00	61.31	0.00	0.00	6	766.51	0.00	99.08	0.00	0.00	0	0.00%	—	37.77	0.00
r207_C50B3	4	663.83	95.17	177.31	0.00	0.00	4	672.11	0.00	168.29	0.00	0.00	0	1.25%	-100.00%	-9.02	0.00
r208_C50B3	4	639.74	0.00	120.06	0.00	0.00	4	639.74	0.00	151.99	0.00	0.00	0	0.00%	—	31.93	0.00
r209_C50B3	4	773.59	121.43	118.67	0.00	0.00	4	813.28	0.00	322.77	0.30	0.17	0	5.13%	-100.00%	204.09	0.30
r210_C50B3	5	733.60	286.29	141.29	28.50	0.94	5	741.74	0.00	135.59	0.00	0.00	0	1.11%	-100.00%	-5.70	-28.50
r201_C50B4	6	873.24	0.00	108.63	0.00	0.00	6	873.24	0.00	107.38	0.00	0.00	0	0.00%	—	-1.24	0.00
r202_C50B4	4	844.33	1878.88	81.62	99.80	6.16	4	862.15	584.17	95.54	87.90	4.50	0	2.11%	-68.91%	13.92	-11.90
r203_C50B4	4	702.46	1677.54	116.25	99.60	3.04	4	696.41	459.82	179.58	93.80	2.72	0	-0.86%	-72.59%	63.33	-5.80
r204_C50B4	3	635.44	0.00	170.70	0.00	0.00	3	635.44	0.00	674.27	0.00	0.00	0	0.00%	—	503.58	0.00
r205_C50B4	5	794.47	0.00	115.25	0.00	0.00	5	799.90	0.00	65.08	0.00	0.00	0	0.68%	—	-50.17	0.00
r206_C50B4	4	733.62	0.00	156.89	0.00	0.00	4	733.62	0.00	197.07	0.00	0.00	0	0.00%	—	40.18	0.00
r207_C50B4	3	678.77	671.03	123.75	92.20	4.72	3	680.71	0.00	210.43	0.00	0.00	0	0.29%	-100.00%	86.68	-92.20
r208_C50B4	3	601.31	0.00	276.67	0.00	0.00	3	605.61	0.00	1022.31	0.00	0.00	0	0.72%	—	745.64	0.00
r209_C50B4	4	714.57	1389.34	169.32	98.10	2.33	4	753.15	0.00	145.17	0.00	0.00	0	5.40%	-100.00%	-24.15	-98.10
r210_C50B4	4	673.74	515.49	122.40	32.10	1.39	4	678.62	0.00	117.66	0.00	0.00	0	0.72%	-100.00%	-4.74	-32.10
Avg.		737.49	531.61	134.87	34.45	1.68		749.82	52.20	224.69	9.10	0.37		1.67%	-90.18%	89.82	-25.35

Table 3-9 Comparison of the delay risk on the 100-customer size EVRPBTW instances.

Instance	Deterministic Solution						Robust Solution										
	m	f^{dist}	f^{DC*}	*t (s)*	*Risk (%)*	*ADT*	*m*	f^{dist}	f^{DC*}	*t (s)*	*Risk (%)*	*ADT*	Δ_m	$\Delta_{dist}(\%)$	$\Delta_{DC}(\%)$	Δ_t	Δ_{Risk}
r201_C100B3	12	1373.03	199.61	699.32	15.70	0.97	12	1392.27	0.00	434.87	0.00	0.00	0	1.40%	-100.00%	-264.45	-15.70
r202_C100B3	9	1208.64	0.00	914.70	0.00	0.00	8	1228.06	0.00	955.21	0.00	0.00	-1	1.61%	—	40.51	0.00
r203_C100B3	8	1075.41	317.89	967.48	36.00	1.12	8	1070.22	123.75	1012.20	3.40	0.31	0	-0.48%	-61.07%	44.72	-32.60
r204_C100B3	5	911.68	5488.83	1559.12	100.00	17.53	5	907.38	0.00	1772.37	0.00	0.00	0	-0.47%	-100.00%	213.25	-100.00
r205_C100B3	8	1232.66	974.53	717.57	100.00	7.59	8	1258.00	482.15	771.45	76.30	1.82	0	2.06%	-50.52%	53.88	-23.70
r206_C100B3	9	1133.49	0.00	953.27	0.00	0.00	8	1147.86	1147.86	960.97	0.00	0.00	-1	1.27%	—	7.71	0.00
r207_C100B3	5	1007.97	3033.73	1725.29	100.00	6.25	8	1040.63	1153.92	5145.55	100.00	4.22	0	3.24%	-61.96%	3420.25	0.00
r208_C100B3	5	900.60	4528.90	2109.33	100.00	15.90	6	922.39	0.00	1448.70	0.00	0.00	1	2.42%	-100.00%	-660.63	-100.00
r209_C100B3	8	1105.13	1337.56	1075.04	100.00	2.28	6	1164.83	2491.35	3702.26	100.00	7.45	-2	5.40%	86.26%	2627.22	0.00
r210_C100B3	7	1098.66	2500.07	1360.18	100.00	10.75	8	1145.30	77.26	661.92	2.60	0.28	1	4.25%	-96.91%	-698.26	-97.40
r201_C100B4	10	1302.59	1469.42	545.06	100.00	3.49	9	1370.12	870.58	907.89	51.70	1.25	-1	5.18%	-40.75%	362.83	-48.30
r202_C100B4	8	1187.15	939.11	883.40	100.00	11.37	8	1190.98	86.88	1179.68	0.00	0.00	0	0.32%	-90.75%	296.28	-100.00
r203_C100B4	7	1017.97	3219.95	1118.21	100.00	6.54	7	1064.70	442.81	1265.51	74.90	1.98	0	4.59%	-86.25%	147.30	-25.10
r204_C100B4	5	881.46	4393.32	1764.12	100.00	5.97	5	899.23	2209.76	1328.75	89.50	3.52	0	2.02%	-49.70%	-435.38	-10.50
r205_C100B4	8	1174.81	531.40	1085.71	94.80	3.14	8	1204.69	311.09	887.44	7.80	0.51	0	2.54%	-41.46%	-198.27	-87.00
r206_C100B4	8	1085.16	713.64	1228.63	96.00	2.87	8	1500.61	1132.87	1190.31	28.50	0.77	0	38.29%	58.75%	-38.33	-67.50
r207_C100B4	5	950.65	2889.69	1653.04	100.00	8.20	6	991.65	991.65	2525.41	0.00	0.00	1	4.31%	-65.68%	872.37	-100.00
r208_C100B4	5	870.37	740.45	2328.43	93.40	2.87	6	866.59	816.66	2249.51	99.60	7.15	1	-0.43%	10.29%	-78.92	6.20
r209_C100B4	8	1054.68	242.44	676.00	88.50	1.96	7	1166.16	172.70	1554.14	8.40	1.69	-1	10.57%	-28.77%	878.14	-80.10
r210_C100B4	7	1046.47	2092.66	783.90	100.00	7.09	7	1078.86	515.46	1285.31	75.60	1.31	0	3.10%	-75.37%	501.41	-24.40
Avg.		1080.93	1780.66	1207.39	81.22	5.79		1120.61	537.53	1338.58	36.86	1.70		3.67%	-69.81%	131.19	-44.36

Computational results on instances with 50 customers

To further investigate the scalability and performance of the algorithm on larger customer instances, we applied it to the EVRPBTW benchmark instances with 50 customers.

Table 3-8 presents a comparison of delay risks for these instances. As the customer size increases, the deterministic solution becomes more fragile, and the number of instances with high delay risks grows. For example, among the 20 instances with 50 customers, 10 deterministic solutions exhibit delay risks. In contrast, only three instances demonstrate delay risks when using the RO solutions.

This demonstrates the necessity of implementing the RO model to identify solutions with reduced delay risk as customer size increases, especially given that the total travel distance increases only slightly. According to the results in Table 3-8, the average total travel distance of the RO solutions increases by just 1.67%, while the total delay cost is significantly reduced—by 90.18%. Additionally, the average delay time in the deterministic solutions is approximately five times greater than that observed in the robust solutions.

The average computation time for solving the RO model is also competitive compared to the deterministic model. Specifically, although the average computation time for the RO model is approximately 224 seconds (about 110 seconds slower than solving the deterministic dispatching model), the delay risk is significantly reduced.

Computational results on instances with 100 customers

When the instance size scales up to 100 customers, the proposed algorithm and RO model remain capable of finding high-quality robust solutions within a moderate computation time. As shown in Table 3-9, 18 instances exhibit delay risks under the deterministic scenario, with 16 of them having delay risks exceeding 85%. In contrast, under the RO solutions, only four instances experience customer delay risks greater than 85%.

Notably, by leveraging the memory buffer mechanism in the proposed RO model, the scalability issue is effectively addressed—especially when compared to traditional RO models (see, e.g., Agra et al., 2013; Peng, Barth, et al., n.d.; Shen et al., 2022). The average computation time for solving the deterministic model is 1,207 seconds, while the RO model requires an average of 1,338 seconds, representing only a 10.85% increase. Furthermore, the average total travel distance increases by just 3.67%, thereby maintaining dispatching efficiency.

In summary, based on the proposed EVRPBTW benchmark dataset, this numerical study not only demonstrates the effectiveness of the two-phase metaheuristics algorithm but also ensures the robustness of the RO solutions. Additionally, the proposed algorithm consistently produces high-quality robust solutions with practical computation times, making it suitable for real-world implementation by industry practitioners.

3.6.7 Sensitivity analysis on the key uncertainty parameters in the RO model

In this section, we conduct a comprehensive sensitivity analysis to evaluate the impact of key uncertainty parameters in the RO model, including the uncertainty range of travel time and service time, as well as the uncertainty budget coefficients associated with these variables. We use instance r207_C50B4 as a representative case for further investigation, as it exhibited high risk levels in previous experiments.

To assess the effect of each uncertainty parameter, we vary one parameter at a time while keeping the others fixed at their default values. The test values for each parameter are selected from the set {0.0, 0.1, 0.2, 0.3, 0.5}. Take the uncertain range of travel time α^t as an example. It is adjusted accordingly in the predetermined set from 0.0 to 0.5, where the larger value of α^t represents the greater deviation of travel time $\hat{t}_{ij}$. All the rest parameters are the same as the default values listed in Table 3-4.

A similar approach is used to investigate the impact of the uncertainty budget coefficient for travel time θ^t, we adjust it accordingly within the predetermined set and remain the rest of uncertainty parameters are the same as the default values. For the rest of the uncertainty parameters, the same strategy is applied. Each configuration is run ten times, and the best solution from each set is recorded for analysis.

Figure 3-9 shows the visualization of the key parameters of the RO model for instance r207_C25B3. Overall, all parameters contribute positively to reducing the risk of customer delays. Notably, incorporating both uncertain travel time and uncertain service time into the RO model yields significantly better performance than considering each independently. For example, when considering uncertain service time only (i.e., $\alpha^t = 0$) or uncertain travel time only (i.e., $\alpha^s = 0$), this instance still encounters high delay risks in those two conditions, reaching 99.8% and100.00%, respectively. However, when both uncertainty factors are simultaneously accounted for, the delay risk drops to zero and remains stable, demonstrating the effectiveness of a combined uncertainty modeling approach in the RO framework.

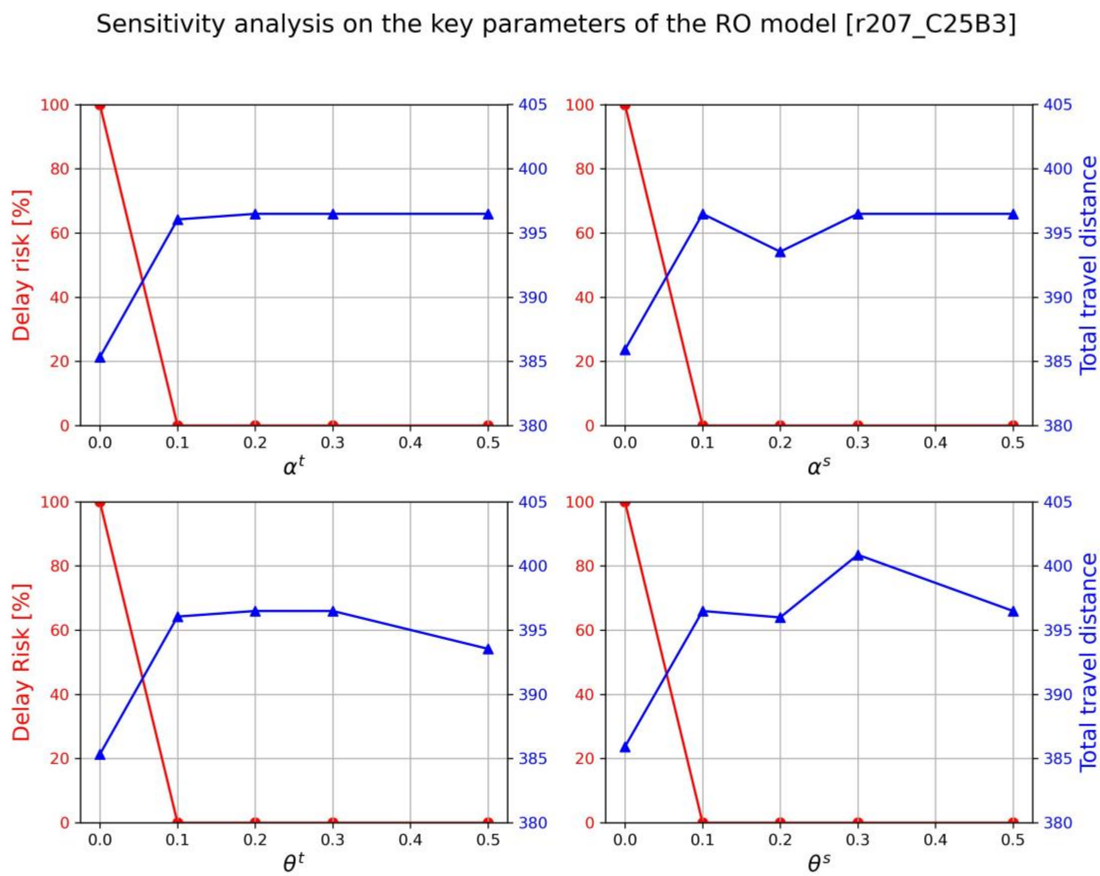

Figure 3-9 Sensitivity analysis on the key parameters of the RO model in instance r207_C25B3.

3.6.8 Sensitivity analysis on the uncertain factors in the RO model

In this section, we perform a comprehensive sensitivity analysis to evaluate the impact of uncertainty factors, uncertain service times and uncertain travel times, on the total cost and robustness in the proposed RO model. The instances with 50 customers and 66% backhaul customer rate are used to conduct sensitivity analysis. Each test is conducted 10 times, and the best solution is recorded.

We compare the dispatching solutions obtained by 1) the deterministic model (EVRPBTW), 2) the RO model with uncertain service times only (EVRPBTW-US), 3) the RO model with uncertain travel times only (EVRPBTW-UT), 4) the RO model with uncertain service times and travel times (EVRPBTW-USUT). The results are summarized in Table 3-9.

Upon comparing the dispatching solutions obtained from the four models, we observe that uncertain service times have a more significant impact on customer delays than uncertain travel times. In Table 3-10, the average delay cost $f^{DC}(S)$ in the EVRPBTW-US model is significantly reduced by 91.78%, compared to the deterministic model, while the average total travel distance is merely increased by 0.65%. The average delay risk is reduced by

87.99% on the EVRPBTW-US model, compared to the deterministic solutions. However, the EVRPBTW-UT model still has high customer delay cost and risk, where the average delay cost is 343.07.

Table 3-10. Sensitivity analysis on different uncertain factors.

Model	$Avg.m$	$Avg.f^{dist}$	$Avg.f^{DC*}$	$Avg.ADT$	$Avg.Risk$	$\Delta_{dist}(\%)$	$\Delta_{DC}(\%)$	$\Delta_{Avg.ADT}(\%)$	Δ_{Risk}(%)
EVRPBTW	4	749.79	449.99	1.59	26.72	-	-	-	-
EVRPBTW-US	4	754.63	38.34	0.20	3.21	0.65%	-91.48%	-87.42%	-87.99%
EVRPBTW-UT	4	750.29	343.07	2.21	25.15	0.07%	-23.76%	38.99%	-5.88%
EVRPBTW-USUT	4	767.75	0.00	0.02	0.03	2.40%	-100.00%	-98.74%	-99.89%

Moreover, it is worth noting that the proposed EVRPBTW-USUT can provide a more robust solution among those four models. The average "Risk" value is significantly reduced by 99.89%. On the other hand, the average travel distance only increases slightly by 2.40%. These results highlight the efficiency and robustness of the proposed RO model, demonstrating its effectiveness in minimizing risks while keeping additional costs minimal.

3.7 Real-world case study in southern California, U.S.

To evaluate the proposed EV fleet dispatching strategy in the real-world scenario, this section presents numerical tests using real data from a full-service supply chain company. The section is structured as follows. Section 3.7.1 presents the characteristics of real-world data used for experiments. Section 3.7.2 discusses the experimental results from applying the proposed EV dispatching strategy to the real-world urban freight dispatching scenario in southern California, U.S.

3.7.1 Case setup

A real-world regional freight dispatching data in Southern California, U.S., is used to evaluate the proposed EVRPBTW-USUT. This dispatching model is representative of typical urban regional freight operations. The problem instance consists of a local distribution center equipped with a fleet of BETs (class-8). The problem instance includes 47 customers, including 33 linehaul and 14 backhaul customers. Customers are associated with their service ID, nominated service time, time windows, required demand, and city name. We randomly selected 12 recharging stations, where the locations of recharging facilities ensure the BET can reach the farthest customer and back to the depot.

In the real-world case study, we set the driving range of the BET as 96 miles to ensure the robustness of the solutions, which is 80% threshold obtained from the estimated driving range 120 miles. The recharging rate is 62.60 meters per second. The cargo load capacity is 66,000 Gross Combined Weight (GCW). The energy consumption rate is assumed to be linear with travel distance. The uncertain parameters are the same as the default values in the previous experiments. To assess the robustness of the solutions, we use the same setting for the MC simulation as described in Section 3.6.5.

3.7.2 Experiments on the real-world case study

Table 3-10 presents the details of solutions obtained from solving the deterministic model and RO model for the real-world case study in Southern California. The visualization of the detailed routes is shown in Figure 3-10. The experimental results indicate that the proposed EVRPBTW-USUT model performs effectively in the urban freight logistics dispatching scenario, significantly reducing potential delays for customers. As illustrated in Table 3-10, the total travel cost of the deterministic solution is 386.51, accompanied by a high delay risk of 100% (when the service times and travel times are uncertain). It can be noted that the DI index is [0, 0, 1000], meaning that there are three or more nodes that have potential delay risks during 1000 MC simulation scenarios. Those nodes are highlighted in Figure 3-10 with varying average delay times. Table 3-11. Comparison of the deterministic and robust solutions in a real-world case study.

Model	NV	$f^{DM}(S)$	$f^{DC}(S)$*	t (s)	Risk (%)	ADT
Det_sol	5	386.51	175206.20	214.77	100.00	1158.76
Rob_sol	6	410.48	410.48	518.36	0	0.00

The results demonstrate that the proposed dispatching model performs effectively on real-world data. The solution time for the RO model is also reasonable, taking less than nine minutes. Furthermore, compared to the deterministic solution, the robust dispatching solution derived from the RO model significantly reduces the delay risk from 100% to 0% during dispatching. In comparison, the total travel cost has increased only slightly by 6.20%, from 386.51 to 410.58.

It is important to note that the deterministic solution may encounter potential delay risks in uncertain scenarios. The average delay time for each node is 1158.76 seconds (approximately 20 minutes) based on the MC simulation. By leveraging the RO model, there are no delayed customers in the robust solution, ensuring a high LOS for all customers.

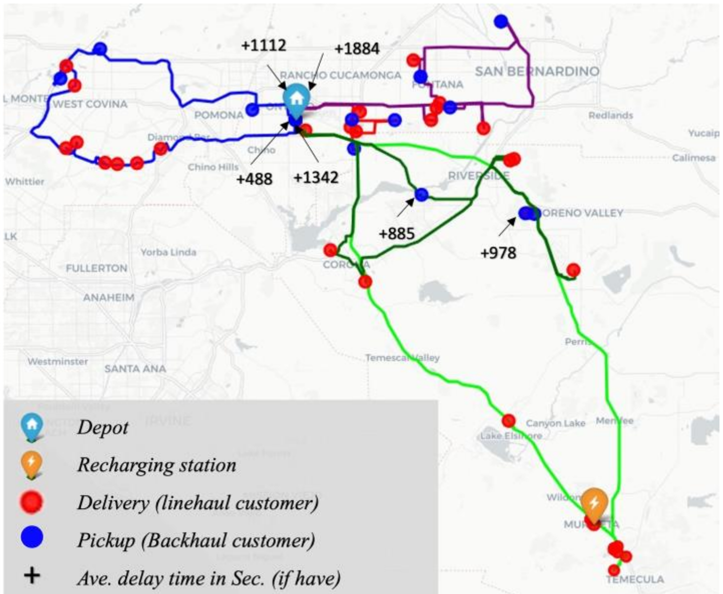

(a) Routes for the deterministic solution.
Total travel cost is 386.51 miles and risk is 100%.

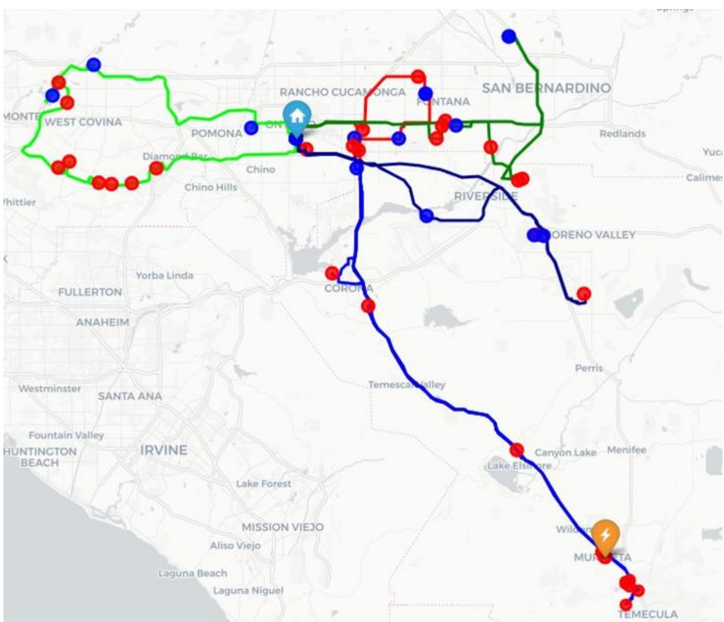

(b) Routes for the robust solution.
Total travel cost is 410.48 miles and risk is 0%.

Figure 3-10. Visualization of the deterministic solution (a) and robust solution (b).

Note: Each colored edge represents a separate BEV route. In the deterministic solution (det_sol), six nodes are identified as having potential delay risks when service times and travel times are uncertain. The average delay times for these nodes during the MC simulation process are displayed in Figure 3-11 (a). By solving the RO model, the delay risk is significantly mitigated, reducing it from 100% to 0%, while the total travel cost increases from 386.51 to 410.48 miles. Both solutions include one charging visit during the dispatch.

3.8 Conclusion and future work

This study introduces a novel EV Routing Problem with Backhauling, Time Windows, and Uncertainty in Service and Travel Times (EVRPBTW-USUT). It addresses several critical factors, including backhauling, an en route partial recharging policy, limited range and capacity, and time window constraints. This problem extends the classic EV Routing Problem with Time Windows (EVRPTW) by incorporating uncertainties in travel and customer service times. The main contributions of this research are summarized below.

Advantage of the two-phase metaheuristics' framework

We have developed a two-phase RO framework to address the EVRPBTW-USUT. In Phase I, the ALNS metaheuristic is employed to find a high-quality dispatching solution for the deterministic scenario. In Phase II, our ILS algorithm is utilized to refine the near-optimal solution obtained from Phase I, resulting in a robust dispatching solution. By leveraging the two-stage metaheuristics framework, the algorithm does not pay excessive attention to searching for robust solutions, which is computationally intensive. Because checking the robustness of a solution may take a long time during each iteration. To this end, in stage II, the ILS metaheuristics relies on LS procedures that modify the BEV routes slightly to obtain a robust dispatching solution. As a result, a high-quality robust solution can be obtained within a reasonable computation time.

Efficient memorized buffer in the RO model

Inspired by the existing literature (Agra et al., 2013; Hu et al., 2018b; Shi et al., 2019), we consider a potential recharging time for a BEV fleet and devise a recursive function to compute the potential latest time for each vertex, as introduced in Section 3.4.1. However, solving the RO model can be computationally intensive. To address this issue, we design a memorized buffer, a 3-D array, to store the computed latest arrival times and avoid unnecessary recursive calculations. Therefore, this approach eliminates the need to recalculate the latest arrival time for each vertex from the starting vertex. Using the memory buffer mechanism can address the scalability issue of RO model. Based on the experiment results, we note that incorporating the memorized buffer can significantly reduce the computation time, ranging from 29.49% to 99.66%, depending on the size and the customer's requirements of the instance. Also, the designed memorized buffer can be generally applied to address similar uncertain vehicle routing problems.

A comprehensive sensitivity analysis is performed, providing marginal insights for the decision-makers

A comprehensive sensitivity analysis is performed to provide valuable insights for decision-makers. The results indicate that uncertain loading and unloading service times of customers contribute to a higher delay risk during dispatching compared to uncertain travel times. This is critical, as service times constitute a significant portion of the total operation time for the vehicle fleet. These observations offer valuable insights for freight owners aiming to mitigate potential delay risks. For instance, employing well-trained crews or drivers can significantly reduce delays during loading and unloading processes. Additionally, decision-makers may consider increasing the robustness of customer service times when developing dispatch strategies, particularly for less experienced crews or customers with specific additional requirements.

Future study

Regarding future study, this work can be extended in various directions. First, a realistic EV energy consumption model can be incorporated into EVRPBTW-USUT. A limitation of this study is that we assume the energy consumption rate is constant and linearly related to the travel distance. The purpose of this study is to investigate the effect of the backhaul strategy and uncertain factors for a BEV fleet by extending the well-known benchmark EVRPTW dataset. Future work could leverage a more realistic energy consumption model. Second, a variant recharging policy can be considered. For instance, future studies could explore multiple en route charging strategies, which would introduce additional complexity to the problem. Third, there may exist an inherent conflict between CS visits and the number of deployed EVs. Multi-objective optimization methods could be utilized in future research to balance the potential dispatching costs associated with charging visits and the required number of EVs. Finally, when historical service data logs become available, data-driven methods can be employed to predict potential service times for customers. Incorporating a forecast stochastic model into the dispatching framework offers a promising avenue for deriving a set of robust dispatching solutions.

Chapter 4 - Method for Co-Optimizing EV Scheduling and Microgrid (MG) Management in Freight Logistics

This section presents an integrated approach to optimizing MG management and electric truck logistics for transportation research when the power grid service disruption. The study aims to demonstrate how synchronized optimization of a MG control algorithm and a BET routing algorithm can reduce overall system costs. Rather than a full SOC battery recharging for the service, we assume that the starting SOC of the fleet is limited due to grid service disruption. The experiment involves a 100 kW solar photovoltaic (PV) system, a 500 kWh BESS, the electric demand of a commercial building, and a heavy-duty vehicle charging system. The MG management system is designed to meet the constraints and requirements of a commercial electric truck charging scheduler. This integrated approach is an improvement over previous systems as it uses the scheduler's outputs—such as time frames and energy requirements—as constraints for MG management. The truck scheduling algorithm iteratively learned to optimize charging times, ensuring that charging occurs during low-cost periods or when renewable energy is available. The EV scheduler adjusted truck arrival times based on the availability of clean energy sources, creating a feedback loop that continuously improves cost efficiency. Results show that the proposed co-optimization can significantly reduce the operation cost and recharging cost by up to 71.09%, compared to the baseline scenario without the co-optimization framework. These findings suggest that the proposed integrated approach can effectively reduce recharging costs and improve the resilience of MGs.

4.1 Introduction

Over the past decade, EV technologies, such as extreme fast charging (XFC), have significantly advanced. Despite this progress, the widespread adoption of EVs faces challenges like the lack of fast CSs. A smart, dynamic pricing scheme is necessary to encourage investment participation, considering the interactions between pricing, demand, and environmental factors to maximize long-term profit.

Transportation is becoming increasingly electrified, and little research has been done on the rate of utility impact from EV truck charging. The impact of EV trucks on utility systems is a growing area of interest, especially as the transportation sector becomes more electrified. Here are some key considerations when assessing the impact of EV truck charging on utilities. As more EV trucks hit the roads, the electricity demand will naturally increase. This can lead to higher peak loads, especially if many trucks charge simultaneously during peak hours. The existing electrical grid may need upgrades to handle the additional load. This includes the capacity to deliver more power and the robustness to handle fluctuations in demand, typical with EV charging. Utilities might need to implement or expand demand response (DR) programs to manage the load more effectively. This could involve incentivizing truck operators to charge during off-peak hours or using intelligent charging technology that automatically adjusts charging times based on grid demand. Utilities could increase their investment in renewable energy sources to mitigate the impact of increased electricity consumption and reduce their carbon footprint associated with EV charging. This also aligns with the broader environmental goals of reducing carbon emissions from the energy and transportation sectors. Utilities may need to reconsider their rate structures to accommodate EV trucks' specific needs and consumption patterns. Special rates could be developed for commercial EV fleets to encourage efficient energy use and grid reliability. Integrating energy storage systems (ESS) can help manage the load by storing excess energy during low-demand periods and releasing it during peak times. This is particularly useful in areas where EV truck charging significantly impacts the grid. More research is needed to understand the specific impacts and to develop.

Integrating MGs with heavy-duty EV CSs provides several key benefits, such as addressing energy management and promoting sustainable transportation. Heavy-duty EVs, such as buses, trucks, and commercial vehicles, require significantly more charging power than light-duty passenger vehicles. The concentrated demand from multiple heavy-duty EVs charging simultaneously can substantially strain the local electricity grid, potentially leading to instability and increased peak demand charges. MGs can help manage this load by providing localized generation and storage resources, smoothing out the main grid's demands. MGs enhance the resilience of charging infrastructure against grid outages. Integrating renewable energy sources, like solar or wind, with ESS (such as batteries), MGs can ensure the continuous operation of EV CSs during power outages or other grid disturbances. This is particularly crucial for commercial vehicles, essential for critical services and logistics.

This study's contributions are as follows:

- Integration of Truck Scheduling in the Optimization of MG Facilities: This research investigates how truck scheduling can be integrated with MG optimization to enhance energy management and reduce costs.
- Truck Scheduling Accounting for Electric Utility from MG Charging: We explore how truck scheduling can be optimized by considering the availability and cost of electricity from MG charging, leading to significant cost savings.
- Feedback Loop Framework for MG and Regional Distribution EV Truck Charging and Truck Dispatching: We propose a feedback loop framework to coordinate MG operations with regional distribution networks for EV truck charging and dispatching, ensuring optimal energy usage and reducing operational costs.

4.2 Literature Review

Related literature on MG systems

A MG consists of various distributed generators (DG), distributed storage (DS), and diverse customer loads. It represents an electric power distribution system segment downstream of the distribution substation to the end user. Emerging technologies like mini wind turbines, PV, micro-turbines, combined heat and power (CHP), fuel cells, and solar energy provide more opportunities for MG generation.

Reference Szilagyi et al., 2023 raised a minimized cost function using intelligent management methods at uncertain weather conditions to reduce the cost of energy the MG produces. We can see that MGs can be cost-optimized. Reference (Uddin et al., 2023) proposed the potential cost benefit of the MGs, including investing in the grid, which can mitigate risks, providing a safeguard against unpredictable and potentially high costs of emergency energy. It also protects against fluctuating electricity bills. Meanwhile, depending on local market regulations and incentives, MGs can reduce peak load prices, participate in DR markets, and offer frequency regulation services to the larger grid. This can generate revenue by lowering peak load costs, engaging in DR markets, and providing frequency management services to the rest of the grid.

MG Energy Management and EV Freight Truck Scheduling

Significant advancements have been made in MG energy management algorithms in recent years. Earlier versions of the algorithm, such as those discussed in references Hasan et al., 2023 and Fernando Enriquez-Contreras et al., 2022, focused on optimizing MG energy but did not consider the management of EV charging loads. These studies highlighted the potential of MGs to manage local energy resources effectively but fell short in integrating EV charging load management.

Dynamic load allocation has been explored in reference (Lee et al., 2018), which thoroughly addresses dynamic load allocation with a large number of passenger EV chargers, and in reference (Luke et al., 2021), where the co-optimization of autonomous vehicle scheduling and EV charging was considered. However, these studies treated the EV charger as an independent system and did not integrate the EV truck charger as part of the MG.

The study by reference Garrido et al., 2022 looked into freight truck scheduling with EV charging, but similar to previous studies; it did not consider the EV charger within the context of the MG's overall energy management. Conversely, reference (Purvins et al., 2018) optimized EV charging with respect to the MG but did not incorporate vehicle scheduling.

This represents a significant gap, as optimizing the energy distribution within a MG that includes EV truck charging can lead to more efficient and cost-effective operations. The dual role of the MG in providing renewable energy at certain times and dealing with the limitation of cheap power availability is largely overlooked. This study aims to bridge this gap by combining freight vehicle scheduling with MG energy management, including the dynamic allocation of EV truck chargers.

For the EV freight truck scheduler, this study builds on methodologies described in (Peng, Wu, et al., 2023b; Wang et al., 2022; S. Zhang et al., 2018). These studies developed robust frameworks for freight scheduling but did not account for the availability of MG energy at the home base. Similar issues were found in EV truck scheduling works by (Goeke & Schneider, 2015; Toth & Vigo, 1997; Vincent et al., 2021a), and as mentioned earlier, reference (Garrido et al., 2022). These frameworks did not consider the dynamic interaction between EV truck chargers and the MG, especially the intermittent availability of renewable energy and the variability in energy costs.

This study addresses these research gaps by integrating freight vehicle scheduling with MG energy management. It provides a comprehensive solution that includes the dynamic allocation of EV truck chargers within the MG context.

4.3 Methodology

4.3.1 Co-optimization framework

The co-optimization framework is depicted in Figure 4-1. By accounting for time-dependent power load distribution, the energy allocation algorithm estimates the recharging cost during scheduling (see Section 4.3.2). The framework aims to optimize BET fleet charging requirements while balancing the power flow among distributed energy resources (e.g., the power grid, solar PV system, and BESS). Its objective is to minimize both total energy consumption and recharging cost, considering time-of-use (TOU) electricity pricing and dynamic power load conditions.

During route planning, the BET fleet dispatching system (detailed in Section 4.3.5) estimates the required recharging time and energy demand. Given this information, the energy allocation algorithm adjusts the cleaner power flow based on solar generation and building load profiles. With the anticipated charging demand and time windows, the energy allocation algorithm can determine the time dependent power flows across available sources to optimize energy cost. The routing algorithm then adapts the dispatching strategy to reflect energy pricing, further reducing operational costs.

This iterative coordination between fleet routing and energy scheduling ensures efficient BET utilization and enhances MG resilience by prioritizing cleaner energy sources.

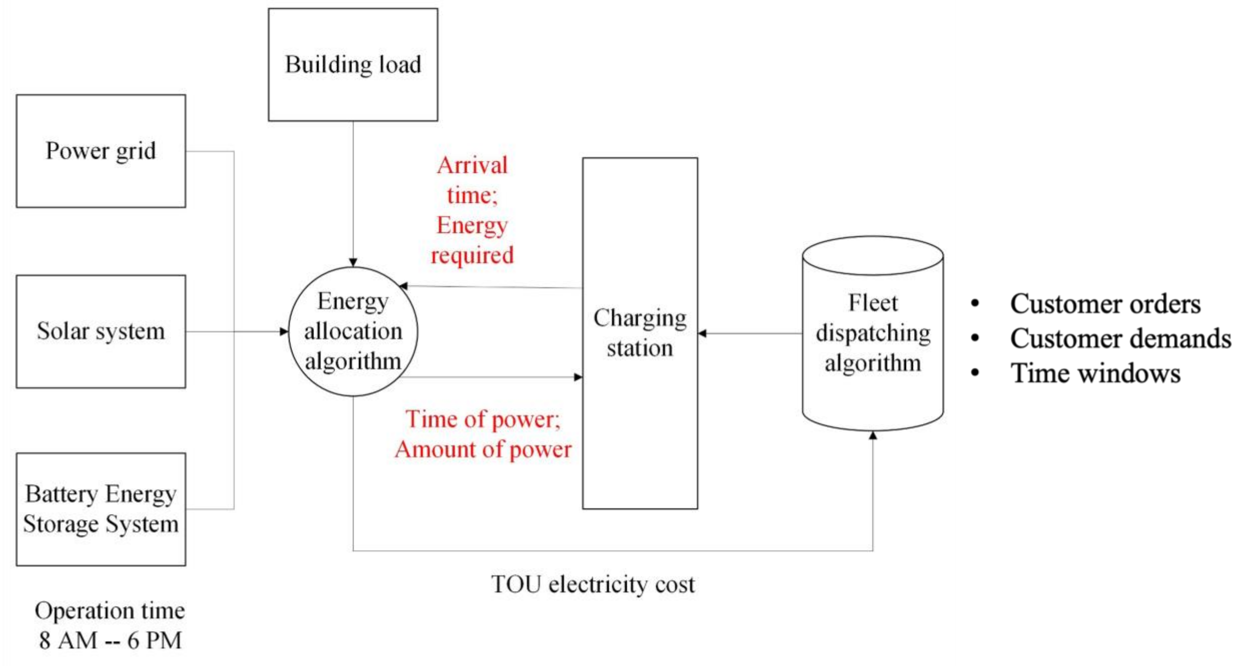

Figure 4-1. Co-optimization framework integrating MG and BET fleet dispatching.

4.3.2 Dispatch Center CS Layout

The EV truck CS located at a dispatch center comprises the building's loads (HVAC systems, lighting, 110 volt (V) outlets, and passenger vehicle chargers), a 100 kilovolt-amperes (kVA) solar inverter, a 500 kWh BESS, and an inverter for charging and discharging the BESS. Data from (Enriquez-Contreras et al., 2024) is used as a reference for the solar and an average building. Figure 4-2 illustrates the power sources connected to the truck charger alongside the other building loads.

The main breaker panel receives power from three sources: the power grid, the solar inverter, and the battery inverter. The solar inverter is unidirectional, delivering power solely to the building. In contrast, the power grid and BESS inverter are bidirectional, meaning they can supply power to the building and consume power from it. The battery trailer draws power by charging the batteries.

The truck charger consists of a 350 kW EV truck charger. While power can be sent back to the grid, this experiment prioritizes sending excess solar power to EV trucks. This setup aims to supply energy efficiently and reduce the site's overall demand.

The methodology ensures that the integrated system optimizes the use of solar power and BESS to manage the energy demands of both the building and the EV trucks, enhancing energy efficiency and cost savings.

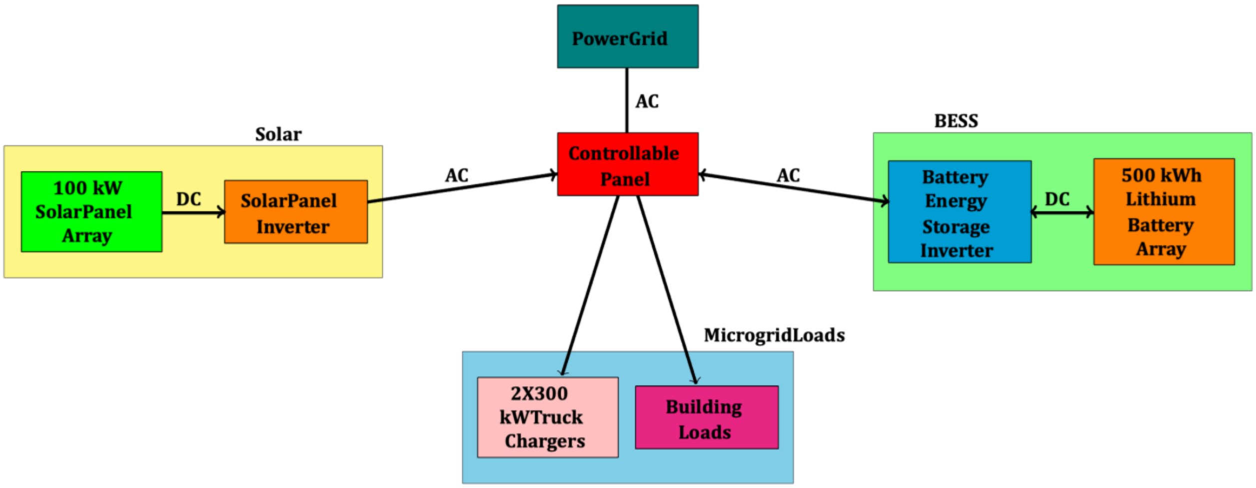

Figure 4-2. Setup for a Small Electric Truck Dispatch Center with Two EV Chargers.

4.3.3 MG Electricity Costs

The primary focus of this study is calculating costs and optimizing the MG and electric trucks, emphasizing the importance of accurately assessing and understanding billing costs. Electric rates comprise two main components: demand charges and energy charges.

The demand charge represents the maximum power value recorded within a 15-minute interval over the entire month. The energy charge, on the other hand, is the total energy consumed throughout the month.

For commercial customers, the sum of demand and energy charges constitutes the bulk of electric utility costs. These charges are further influenced by TOU rates, which vary depending on the time of day and are typically categorized into off-peak, mid-peak, on-peak, and, in some seasons, super off-peak periods.

The TOU rates used in this experiment are sourced from Southern California Edison (SCE) and are the TOU-GS-2 rate shown Table 4-1. These TOU rates apply only when power is drawn from the grid. However, since the MG in this study has abundant energy, the primary objective is to minimize power drawn from the grid, instead supplying power to the building or charging electric trucks.

Table 4-1. Weekday TOU Schedule Rates for SCE ("Schedule TOU-GS-2 Southern California Edison," 2023)

Utility	TOU Period	Energy Charge ($/kWh)	Demand Charge ($/kW)	Timeframe
Summer Rates (June 1 - September 30)				
SCE	On-Peak (Weekdays)	0.12967	24.06	4:00 p.m. - 9:00 p.m.
	Mid-Peak (Weekdays)	0.11823	N/A	8:00 a.m. - 4:00 p.m. (Winter)
	Off-Peak (All other hours)	0.07586	N/A	
	Super-Off-Peak (Weekdays)	0.04623	N/A	8:00 a.m. - 4:00 p.m. (Winter)
Weekends and Holidays	On-Peak	N/A	N/A	No on-peak period
	Mid-Peak	0.11823	6.32	4:00 p.m. - 9:00 p.m.
	Off-Peak	0.07586	1.92 N/A (SCE)	All other hours
Winter Rates (October 1 - May 31)				
SCE	Mid-Peak (Weekdays)	0.08753	6.32	4:00 p.m. - 9:00 p.m.
	Off-Peak (All other hours)	0.08806	N/A	
	Super-Off-Peak (Weekdays)	0.04623	N/A	8:00 a.m. - 4:00 p.m.
Weekends and Holidays	On-Peak	N/A	N/A	No on-peak period
	Mid-Peak	0.08753	6.32	4:00 p.m. - 9:00 p.m.
	Off-Peak	0.08806	N/A	All other hours

In certain situations, the MG may need to export power to the grid. As of April 15, 2023, the California Public Utilities Commission (CPUC) mandates that SCE utilize Net Billing Tariffs for non-grandfathered customers ("NET Energy Metering and Net Billing California Public Utilities Commission," 2023). These export rates differ from net energy metering rates, typically offering lower compensation for energy than retail rates, except during high demand periods.

By carefully considering these factors, the optimization model aims to reduce overall costs while efficiently managing the energy distribution between the MG, the building, and the electric trucks.

4.3.4 Dispatch Center MG EV Truck Charging Algorithm

This optimization function, adapted from (6) (7), minimizes the utility costs of a MG with solar PV, a BESS, building demands, and an EV CS. The objective function minimizes the sum of energy and demand costs while accounting for energy export compensation (see equation 4.1). Table 4-2 summarize the nomenclature of the MG electric truck charging algorithm.

Table 4-2. MG EV Truck Charging Algorithm Nomenclature

Symbol	Description	Symbol	Description
t	Timestep in seconds	$P_t^{B+/P_t^{B-}}$	BESS charging/discharging power at time t
Δt	Duration of each timestep	E^{B+max} $/E_t^{B-min}$	BESS maximum/minimum SOC limits t
T^{tot}	Total number of timesteps	P^{B+max} $/P_t^{B-min}$	BESS charging/discharging limits t
E_{init}^B	Initial stored energy of the BESS	P_t^G	Power drawn from the grid at time t
P_t^S	Solar generation at time t	P_t^{SB}	Solar power fed to BESS at time t
P_t^L	Load at time t	P_t^{SL}	Solar power fed to load at time t
α_{minus}	Energy charges when MG pulls power from the grid	P_t^{BL}	BESS power fed to load at time t
α_{plus}	Energy charges when MG sends power from the grid	T_t^{B1}	Energy stored at time t in Truck Battery 1
β	On/Mid/Off-Peak demand charges	P_t^{T1}	Power sent at time t to Truck Battery 1
η^{+/η^-}	Charging/discharging efficiency of BESS	T_t^{B2}	Energy stored at time t in Truck Battery 2
E_t^B	Energy stored at time t in BESS	P_t^{T2}	Power sent at time t to Truck Battery 2
P_t^B	BESS power at time t		

$$\min f(\boldsymbol{P}^G) = \sum \boldsymbol{negative}(\boldsymbol{\Delta\, t\, \alpha_{minus}}^T \boldsymbol{P}^G\,) + \sum \boldsymbol{positive}(\boldsymbol{\Delta\, t\, \alpha_{plus}}^T \boldsymbol{P}^G\,) + \max\ (\boldsymbol{\beta P}^G) \tag{4.1}$$

Subject to:

$$E_0^B = E_{\text{init}}^B \tag{4.2}$$

$$E_{t+1}^B = E_t^B + \Delta \cdot P_t^T, \forall t \in T^{tot} \tag{4.3}$$

$$\boldsymbol{E^{Bmin}} \le \boldsymbol{E_t^B} \le \boldsymbol{E^{Bmax}}, \forall \boldsymbol{t} \in \boldsymbol{T^{tot}} \tag{4.4}$$

$$\boldsymbol{0} \le \boldsymbol{P_t^{B+}} \le \boldsymbol{P^{B+max}}, \forall \boldsymbol{t} \in \boldsymbol{T^{tot}} \tag{4.5}$$

$$\boldsymbol{P^{B-max}} \le \boldsymbol{P_t^{B-}} \le \boldsymbol{0}, \forall \boldsymbol{t} \in \boldsymbol{T^{tot}} \tag{4.6}$$

$$\boldsymbol{P_t^B} = \boldsymbol{P_t^{B+}} - \boldsymbol{P_t^{B-}}, \forall \boldsymbol{t} \in \boldsymbol{T}^{\text{tot}} \tag{4.7}$$

$$\boldsymbol{0} \le \boldsymbol{P_T} \le \boldsymbol{P}_{\boldsymbol{T}_{\text{max}}} \tag{4.8}$$

$$\boldsymbol{P}_{\text{SL}} + \frac{\boldsymbol{P^{B+}}}{\boldsymbol{\eta_+}} + \frac{\boldsymbol{P^{T1}}}{\boldsymbol{\eta_+}} + \frac{\boldsymbol{P^{T2}}}{\boldsymbol{\eta_+}} = \boldsymbol{P_S} \tag{4.9}$$

$$\boldsymbol{P}_{\text{SL}} + \boldsymbol{P_G} + \boldsymbol{P_B^-} \cdot \boldsymbol{\eta_-} = \boldsymbol{P_L} \tag{4.10}$$

$$\boldsymbol{P}_{\text{SL}} \ge \boldsymbol{0} \tag{4.11}$$

$$\boldsymbol{T_t^{B1}} = \begin{cases} \text{truck\_init\_soc\_1} & \text{if } \boldsymbol{t} = \text{ truck\_arrival\_time\_1} \\ \text{truck\_final\_soc\_1} & \text{if } \boldsymbol{t} = \text{ truck\_leave\_time\_1} \\ \boldsymbol{0} & \text{if } \boldsymbol{t} < \text{ truck\_arrival\_time\_1 or } \boldsymbol{t} > \text{ truck\_leave\_time\_1} \\ \boldsymbol{T_{t-1}^{B1}} + \boldsymbol{\Delta t} \cdot \boldsymbol{P_{t-1}^{T1}} & \text{otherwise} \end{cases} \tag{4.12}$$

$$\boldsymbol{P_t^{T1}} = \boldsymbol{0}, \quad \text{if } \boldsymbol{t} < \text{ truck\_arrival\_time\_1 or } \boldsymbol{t} > \text{ truck\_leave\_time\_1} \tag{4.13}$$

$$\boldsymbol{T_t^{B2}} = \begin{cases} \text{truck\_init\_soc\_2} & \text{if } \boldsymbol{t} = \text{ truck\_arrival\_time\_2} \\ \text{truck\_final\_soc\_2} & \text{if } \boldsymbol{t} = \text{ truck\_leave\_time\_2} \\ \boldsymbol{0} & \text{if } \boldsymbol{t} < \text{ truck\_arrival\_time\_2 or } \boldsymbol{t} > \text{ truck\_leave\_time\_2} \\ \boldsymbol{T_{t-1}^{B2}} + \boldsymbol{\Delta t} \cdot \boldsymbol{P_{t-1}^{T2}} & \text{otherwise,} \end{cases} \tag{4.14}$$

$$\boldsymbol{P_t^{T2}} = \boldsymbol{0}, \quad \text{if } \boldsymbol{t} < \text{ truck\_arrival\_time\_2 or } \boldsymbol{t} > \text{ truck\_leave\_time\_2} \tag{4.15}$$

When power is pulled from the grid, the positive values are multiplied by α_{minus}, the array of TOU costs for the given period. The product of these values is summed to find the energy cost for the winter and summer rates, respectively. When power is sent to the grid, the negative values are multiplied by α_{plus}, the array of net billing tariffs for April and July. The maximum power pulled and sent to the grid calculates the demand costs.

The following constraints ensure that the optimization algorithm follows the electrical properties and that the truck battery is charged during its specified time frame. Equation 4.2 ensures that the BESS starts from an initial state of 50% SOC, or 250 kWh. After the initial state, the battery state is updated by adding the amount of power charged or discharged during the time interval (Equation 4.3), while adhering to the lowest and highest SOC limits (Equation 4.4). Equations 4.4 and 4.5 limit the amount of power that can be charged or discharged from the BESS, while Equation 4.6 combines charging and discharging into a single value for Equation 4.7. Equation 4.8 limits the amount of power that can be charged to the truck battery. The solar value provided equals the sum of the net load, truck, and battery charging (Equation 4.9). The load value provided equals the sum of the net load and battery discharging (Equation 4.10).

Equations 4.12 and 4.13 are the main contributions of this research, specifically adapted to truck routing schedules. While the electric battery in the BESS is available for the entire period with a variable final charge state, the truck battery is only available during a predetermined period set by the route scheduler, with the truck charging period following this same timeframe. The truck battery's initial and final charge states must match the values the truck scheduler sets. This optimization varies from previous work by allowing the truck scheduler to determine some of the constraints for the feedback loop. The function returns the cost value to the scheduler, which adjusts the timeframe and charge amount to reduce costs further. Equations 4.14 and 4.15 are the same formulation but are for the second truck and subsequently added to the constraints.

4.3.4 BET dispatching model description

The dispatching model follows the assumptions that include:

(1) The BET fleet dispatching follows the backhaul strategy (Toth & Vigo, 1997). The customers are divided into two groups, including linehaul customers who require delivery and backhaul customers who require pickups. For each trip, the linehaul customers should be visited first, followed by backhaul customers. A trip only containing backhaul customers is not allowed.

(2) Similar to (S. Zhang et al., 2018), a microscopic energy consumption model (Peng, Wu, et al., n.d.) is applied to estimate the energy consumption.

(3) The truck fleet is allowed to visit home-based recharging facilities at distribution center (DC) once during operation. The DC has a smart grid energy allocation strategy, to control the load distribution in terms of power grid, 100 W solar system, and ESS.

(4) The total operation time is limited. The truck fleet should start operation at T_{Start} and end serive before T_{End}. The service times, travel times and recharging time are considered.

(5) We assume the initial SOC y_0 is limited as less clean energy is generated at night. Therefore, that assumption can encourage the BET fleet to visit recharging facilities daily at DC.

4.3.5 Dispatching model formulation

The purposes of the dispatching algorithm are twofold. On the one hand, the dispatching algorithm aims to find a set of routes minimizing the total transportation energy cost. On the other hand, a favorable home-based recharging visit is determined. To estimate the energy cost of the BET fleet, we apply a real-world energy consumption model that has been used in Peng et al. (Peng, Wu, et al., 2023c). First, the required tractive power P_T can be calculated by Equation 4.16, where total vehicle weight $M = w + C_{ij}$ (vehicle weight w plus cargo weight on an arc C_{ij}), a denotes the acceleration, ρ, c_r and c_d represent the air density, the aerodynamic and rolling friction coefficients, respectively. A denotes the air density and the front area of the BET. The average speed $v_{ij} = d_{ij}/t_{ij}$ for an arc can be calculated by the corresponding travel distances and travel times. g denotes gravity.

$$\boldsymbol{P_T = \left(M \cdot a + \frac{1}{2} \cdot c_d \cdot \rho \cdot A \cdot v^2 + M \cdot g \cdot sin(\theta) + c_r \cdot M \cdot g \cdot cos\,(\theta)\right) \cdot v} \qquad 4.16$$

Adopted from Wang et al., 2022 and S. Zhang et al., 2018, the electric energy consumption E_{ij} is calculated by Equation 4.17. The discharging efficiency eff_d and the motor efficiency eff_m are considered. We use $\alpha_{ij} = a + g\sin\,\theta + gC_r\cos\,\theta$ to represent an arc-specific constant coefficient and $\beta = 0.5C_dA\rho_a$ to denote the vehicle specific constant. Additionally, constant accessory power P_{acc} is considered.

$$\boldsymbol{E_{ij} = \frac{1}{eff_d \cdot eff_m} \cdot (P_T + P_{acc}) \cdot \frac{d_{ij}}{v_{ij}} = \frac{1}{eff_d \cdot eff_m} \cdot \left\{\left[\alpha_{ij}(w + C_{ij})d_{ij} + \beta v_{ij}^2 d_{ij}\right] + P_{acc}\frac{d_{ij}}{v_{ij}}\right\}} \qquad 4.17$$

Extending the integer programming model presented in Toth & Vigo, 1997, the dispatching model can be defined in a directed graph $G = (V, A\ )$. A set of vertices is denoted by $V = O \cup \mathcal{N} \cup \mathcal{R} \cup D$, where O and D represent the depot nodes, i.e., start node and end node. The customer set $\mathcal{N}$ contains two subsets, i.e., linehaul customers L and backhaul customers B, which can be represented by $\mathcal{N} = \{L, B\}$. Similar to (Toth & Vigo, 1997) and (Peng, Wu, et al., n.d.), the arc set $\mathcal{A}$ is defined by $\mathcal{A} = A_1 \cup A_2 \cup A_3$, where a set $A_1 = \{(i,j) \in \mathcal{A}: i \in L \cup O, j \in L \cup \mathcal{R}\}$ connects all forward flows, a set $A_2 = \{(i,j) \in \mathcal{A}: i \in B \cup \mathcal{R}, j \in B \cup D\}$ represents the backward flows, and the interface arcs are represented by $A_3 = \{(i,j) \in \mathcal{A}: i \in L \cup \mathcal{R}, j \in B \cup D\}$. Let $\Delta_i^+ = \{j: (i,j) \in \mathcal{A}, i \in \mathcal{N}'_{O,D}\}$ denotes the forward flows, and $\Delta_i^- = \{j: (j,i) \in \mathcal{A}, i \in \mathcal{N}'_{O,D}\}$ denotes the backward flow arcs. Furthermore, the decision binary variable x_{ij} determines whether a vehicle travels on arc $(i,j) \in \mathcal{A}$. Battery capacity binary variable g_i decides whether a vehicle can be arrival at node $i \in V \backslash O$.

The integer linear programming model formulation for the proposed dispatching problem is as follows. In Equation 4.18, the first term $c_{offpeak}E_{ij}x_{ij}$ denotes the total energy cost during before departure, where $c_{offpeak}$ denotes the electricity factor during off-peak hours. The second term $f_{sg}(y_i, Y_i, T_{arr}, T_{dep})$ is also a convex optimization problem, representing the recharging cost at the CS (see Section 4.3.2). It should be noted that a time-variant energy allocation algorithm is incorporated into the dispatching model, which can be estimated by function $f_{sg}(y_i, Y_i, T_{arr}, T_{dep})$. The recharging cost is related to the SOC y_i when the BET arrivals at the home-based recharging station, the leaving SOC Y_i and the available recharging time window $[T_{arr}, T_{dep}]$.

$$min \sum_{i\in V\backslash D, j\in V\backslash O, i\neq j} c_{offpeak} E_{ij} x_{ij} + \sum_{i\in V, j\in V\backslash O, i\neq j} f_{sg}(y_i, Y_i, T_{arr}, T_{dep}) \tag{4.18}$$

Subject to:

$$\sum_{i\in\Delta_i^+} \boldsymbol{x_{ij} = 1}, \quad \boldsymbol{i \in \mathcal{N} \cup \mathcal{R}} \tag{4.19}$$

$$\sum_{i\in\Delta_j^-} \boldsymbol{x_{ij} = 1}, \quad \boldsymbol{j \in \mathcal{N} \cup \mathcal{R}} \tag{4.20}$$

$$\sum_{j\in \mathcal{N}'_D \cup \mathcal{R}, i\neq j} \boldsymbol{x_{ij} - x_{ji} = 0, \forall i \in V\backslash D} \tag{4.21}$$

$$\boldsymbol{y_O \leq Q_{inital}^{max}} \tag{4.22}$$

$$\sum_{j\in(D\cup\mathcal{N}\cup\mathcal{R})} \boldsymbol{x_{ij} \leq 1, \forall i \in \mathcal{R}} \tag{4.23}$$

$$\boldsymbol{0 \leq Y_i \leq Q, \forall i \in V\backslash\mathcal{R}} \tag{4.24}$$

$$\boldsymbol{e_i \leq \tau_i \leq l_i, \quad i \in D} \tag{4.25}$$

$$\boldsymbol{0 \leq u_i \leq C, \forall i \in V\backslash\mathcal{R}} \tag{4.26}$$

$$\boldsymbol{0 \leq \Big((1 - g_i)\cdot y_i + g_i \cdot Y_i - E_{ij}\Big) x_{ij} \leq Q, \forall i \in V\backslash D, j \in V\backslash O, i \neq j} \tag{4.27}$$

$$\boldsymbol{x_{ij} \in \{0,1\}, \quad \forall i, j \in \mathcal{N}'_{O,D}, i \neq j} \tag{4.28}$$

The proposed dispatching model extends (Peng, Wu, et al., n.d.). Equation 4.18 shows the objective function of the developed co-optimization framework, aiming to minimize the total energy cost. Considering the backhaul strategy, constraints 4.19 and 4.20 denote the forward and backward flows, respectively. Constraint 4.21 defines flow conservation. The initial SOC for a BET is limited and the upper bound of initial total energy is Q_{inital}^{max} as shown in constraint 4.22. Constraint 4.23 shows that a home-based recharging visit is limited to at most once per vehicle. Constraint 4.24 ensures that the battery capacity is always positive and cannot exceed the maximum capacity. The operation time is limited as indicated in constraint 4.25. Constraint 4.26 enforces the cargo payload constraints. Constraint 4.27

defines the recharging policy. A binary variable x_{ij} represents if an arc has been visited in 4.28.

4.3.6 Co-optimization framework

The co-optimization framework is depicted in Figure 4-3. Considering a time-dependent and time-dependent power load distribution, the energy allocation algorithm can estimate the recharging cost (see Section 4.3.2) when scheduling the recharging visit. The developed co-optimization framework aims to minimize the total energy use and the total recharging cost.

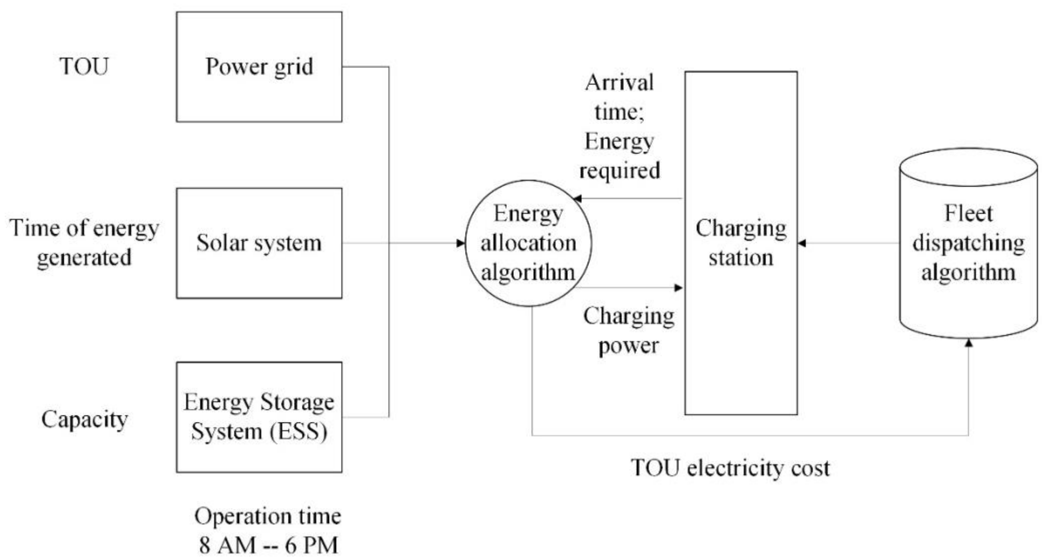

Figure 4-3. Co-optimization framework integrating MG and BET fleet dispatching.

4.3.7 BET dispatching algorithm

An ALNS-based metaheuristics algorithm (Ropke & Pisinger, 2006c, 2006a) is applied to solve the proposed dispatching problem. The ALNS metaheuristics algorithm has been widely used to solve the vehicle routing problem and its variations (see examples (Goeke & Schneider, 2015; H. Liu et al., 2024; Peng, Wu, et al., n.d., 2023c; Vincent et al., 2021b)). In this study, we developed an ALNS-based algorithm as a search engine to determine the energy-efficient route and favorable recharging schedule, which can achieve lower TOU costs.

The ALNS metaheuristic begins by generating an initial feasible solution for the BET routes. We use a modified greedy algorithm (Peng, Barth, et al., n.d.) to construct a set of initial feasible routes. At the beginning of the construction, a customer is randomly selected and inserted into a BET journey. A greedy algorithm is then employed to find a candidate customer and their optimal insertion location, determined by the lowest incremental cost. This process continues until no more customers can be added to the current BET trips due to battery capacity constraints. At this point, a recharging visit is included in the current

BET trip, allowing more customers to be added. The current BET route is completed when no additional candidate customers can be visited. Next, a new BET route starts following the same procedure. The greedy construction algorithm terminates once all customers have been inserted into the BET routes.

After generating an initial feasible solution, the ALNS-based metaheuristics algorithm is iteratively performed to find a better solution. Based on the ALNS framework built in (Peng, Wu, et al., n.d.), we modify the objective function to Equation 4.18. Next, we combine the ALNS algorithm with the energy allocation algorithm from a micro-grid perspective. The intuition behind this idea is to minimize the total energy cost. We consider the energy cost for the dispatching service and the dynamic recharging cost, which is dependent on the dynamic power load.

In this section, we only briefly introduce the framework of the ALNS-based metaheuristics algorithm for limited space, and we refer interested readers to (Peng, Wu, et al., n.d.) for more details. Similar to (Peng, Wu, et al., n.d.), we use the same five removal operators (i.e., worst removal, Shaw removal, random removal, path removal and cluster removal operators) to partially destroy the solution. Then, three reconstruction operators (i.e., greedy, regret-2, and greedy with CS insertion operators) are used to reconstruct a new solution. The weight of each operator can be updated according to the quality of the new solution. Then, a SA heuristic algorithm is implemented to determine if the new solution should be accepted. The ALNS algorithm terminates when the maximum iteration is reached. For the parameters of the ALNS algorithm, we apply the same parameters presented in (Peng, Wu, et al., n.d.), but we set the maximum iterations to 500, ensuring the time efficiency when combined with the energy allocation algorithm.

4.4 Real-world case study in San Bernardino County, California

This section presents a real-world case study to assess the performance of our co-optimization framework. Real-world dispatching data from a full-service logistics company is used in this study. The dataset can be accessed via the GitHub link: https://github.com/CurtisPeng123/Additional-material-for-the-BET-dispatching-with-MG-intergration. The dataset from a heavy-duty diesel truck fleet containing customers' historical iterations is sampled. It includes customer IDs, required weight, service types (deliveries or pickups), and locations. It is worth noting that the BET can reach the farthest fully recharged and is allowed to come back to the depot. To this end, we generate a real-world instance with 19 customers, where 14 are line-haul customers, and the rest are back-haul customers. Table 4-3 summarizes the problem parameters.

Table 4-3. Summary of Problem parameters

Notation	Description	Value
A	Frontal surface area of a BET $[m^2]$	10
C	BET usable battery capacity [kWh]	265
Q	BET payload capacity [lbs..]	37,000
eff_m	Motor efficiency	0.7
eff_d	Discharging efficiency	0.91
c_r	Rolling resistance coefficient	0.008
c_d	Aerodynamic drag coefficient	0.7
w	Vehicle curb weight [lbs.]	8,000
g	Gravitational constant $[m/s^2]$	9.81
ρ_a	Air density (km/m^3)	1.2041
θ	Road angle	0°
a	Acceleration	0
Q_{inital}^{max}	Initial battery capacity [kWh]	100, 150
P_{Acc}	Accessory power [kW]	5.6

We devise three dispatching scenarios to investigate the solutions under different power load conditions, which is shown in the following:

- **Scenario I (Baseline)**: In this scenario, we assume that the BET dispatching does not consider the micro-grid energy allocation algorithm. The BET can be recharged at the CS as needed. The energy is directly obtained from the power grid. Additionally, the TOU rates in different seasons are taken into account, denoted by Scenario I (Baseline-Apr-TOU) and Scenario I (Baseline-Aug-TOU).
- **Scenario II**: Dispatching by co-optimization framework during one day in April. The (micro-grid) energy allocation algorithm is applied to reduce the recharging cost according to real-world load data in April.
- **Scenario III**: Dispatching by co-optimization framework during one day in August. The (micro-grid) energy allocation algorithm is applied to reduce the recharging cost according to real-world load data in August.

For all dispatching scenarios, we assume that the BET fleet is partially recharged during the night with off-peak rate since there is no solar energy during the night. We set the upper bound of the initial battery capacity Q_{inital}^{max} to 100 kWh and 150 kWh. Then we compare the total energy cost among those three dispatching scenarios.

Table 4-4 summarizes the detailed energy consumption in different dispatching scenarios. In contrast to the baseline strategy (dispatching without smart grid integration). The proposed co-optimization can significantly reduce the operation cost and recharging cost, especially during April (i.e., winter season). Take Scenario I with less initial battery capacity as an example. Considering the energy allocation algorithm can reduce the total energy cost by 71.09% and 52.32% in April and August compared with baseline, respectively. The reason is that August puts a more significant strain on the power grid compared to April since the other loads (e.g., HVACs). Therefore, the BET fleet prefers to charge the battery with a high amount of charge with off-peak rate compared to April.

Table 4-4. Experiment results on different dispatching scenarios.

Scenarios	Total energy Consumption [kWh]	Total energy cost [USD]	Total initial energy [kWh]	Off-peak TOU cost [USD]	Total en route charge [kWh]	En route charging cost [USD]
Initial maximum battery capacity = 100 kWh						
Scenario I (Baseline-Apr-TOU)	259.96	13.18	123.95	6.34	136.00	6.83
Scenario I (Baseline-Aug-TOU)	259.96	21.78	123.95	10.38	136.00	11.39
Scenario II (Apr)	308.71	3.81	74.45	3.81	234.25	0.00
Scenario III (Aug)	259.96	10.38	123.95	10.38	136.00	0.00
Initial maximum battery capacity = 150 kWh						
Scenario I (Baseline-Apr-TOU)	211.11	10.80	211.11	10.80	0.00	0.00
Scenario I (Baseline-Aug-TOU)	211.11	17.69	211.11	17.69	0.00	0.00
Scenario II (Apr)	308.71	3.81	74.45	3.81	234.25	0.00
Scenario III (Aug)	211.11	17.69	211.11	17.69	0.00	0.00

In contracts of the different amount of upper bound of initial battery capacity, the case study shows that larger battery capacity of the BET fleet leads to lower total energy consumption cost. For instance, the total energy consumption in baseline scenario is 259.95 kWh when the upper bound initial battery capacity is 100-kWh, increasing by 18.78% compared to the 150-kWh initial battery capacity. When the initial battery capacity is lower, the BET fleet needs to detour for the recharging during the operation. Also, it is worth knowing that the total operation cost is relatively higher during the summer season for the baseline scenario, even though the total energy consumption is the same. Because the summer TOU rate is higher than the winter season.

Additionally, the total energy consumption in Scenario I is relatively lower than in other dispatching scenarios because the impacts of micro-grid load and dynamic TOU rates are not considered. The BET fleet aims to find the most energy-efficient dispatching solutions. However, considering power loads and time-varying TOU rates in Scenarios II and III, the decision-makers should consider a better recharging schedule to optimize the charging costs, such as using clearer energy from solar systems or the ESS as much as possible. Figure 4-4 show the experiments results of the dispatching solutions. Each colored line represents a BET route.

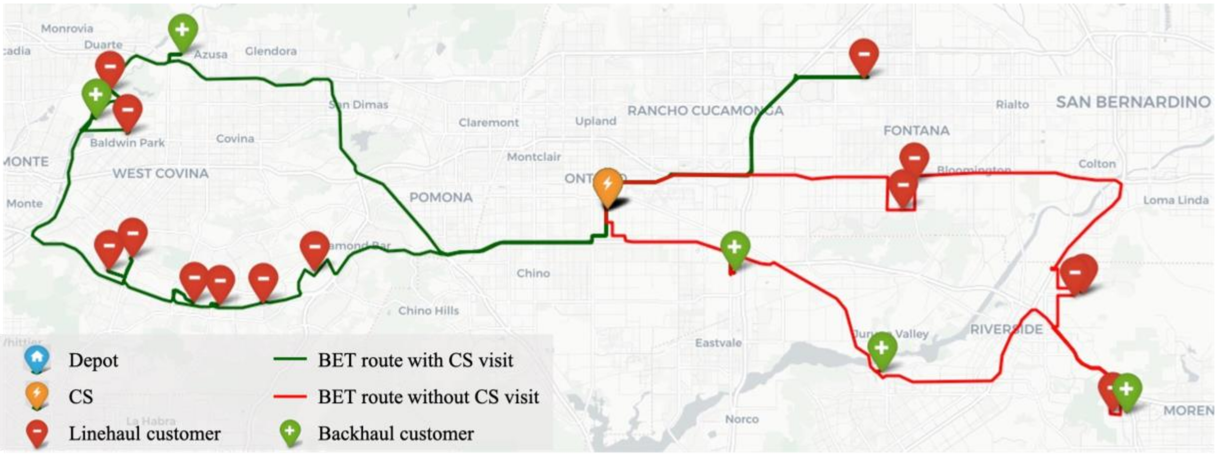

(a). Routes for Scenario I baseline with 100 kWh maximum battery energy (April and August).

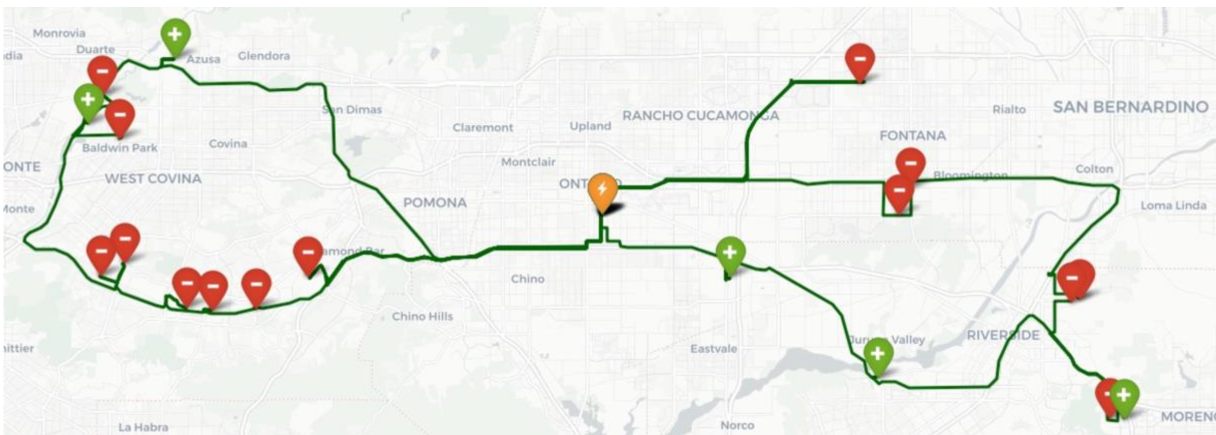

(b). Routes for Scenario II (April) with 100 kWh maximum battery energy.

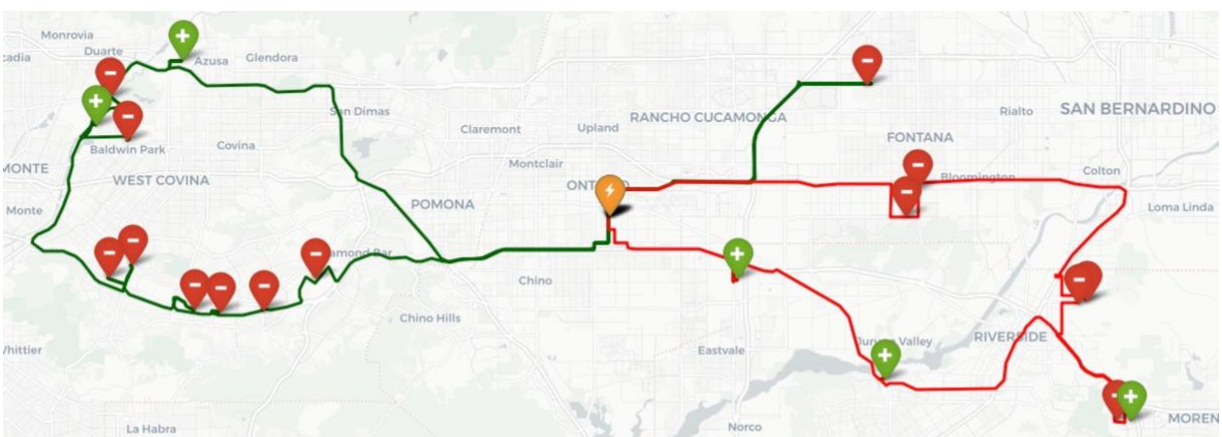

(c). Routes for Scenario III (August) with 100 kWh maximum battery energy.

Figure 4-4. Visualization of BET routes in different dispatching scenarios. Each colored line represents a BET route.

4.5 Sensitivity analysis on the impact of the co-optimization framework across different TOU electricity rate seasons

This section presents a sensitivity analysis on the impact of the co-optimization framework across different TOU electricity rate seasons (winter and summer). Figure 4-5 and Figure 4-6 show the MG loads on a typical day in April (under the winter TOU rate) and August (under the summer TOU rate), respectively. The results demonstrate that the proposed co-optimization framework can significantly reduce peak power demand from the grid.

Take Figure 4-5 as an example. If we only consider a MG management system, i.e., a non-optimized system, the BET fleet is recharged directly with the maximum charging power of 300 kWh. Under this scenario, the MG must draw up to 497.33 kW from the grid to meet charging demand, resulting in an additional charging cost of $6.83.

In contrast, if we consider a co-optimization framework, i.e., the MG management system has the future charging information. It can intelligently allocate charging power based on the time-dependent load profile. As shown in Figure 4-5, co-optimized output, the power drawn from the grid is effectively reduced to zero. Cleaner energy sources within the MG are sufficient to dynamically meet the charging needs of the BET fleet in response to load variations.

Figure 4-6 illustrates the MG load during a typical summer day. Notably, due to higher TOU rates and increased building loads, the system discourages frequent fleet charging. Consequently, only one BET is charged at the station, requiring a maximum power of 242.60 kW. Nevertheless, the co-optimization framework continues to demonstrate superior performance in allocating distributed energy resources and achieving a smoother power transition.

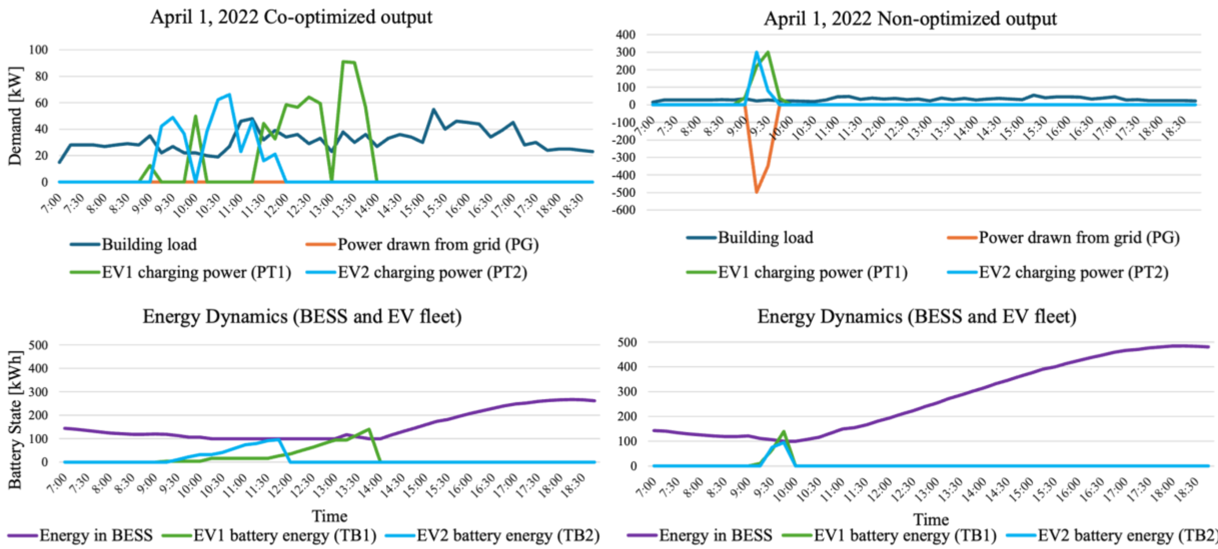

Figure 4-5. Visualization of the co-optimized and non-optimized MG load and battery state on April 1, 2022.

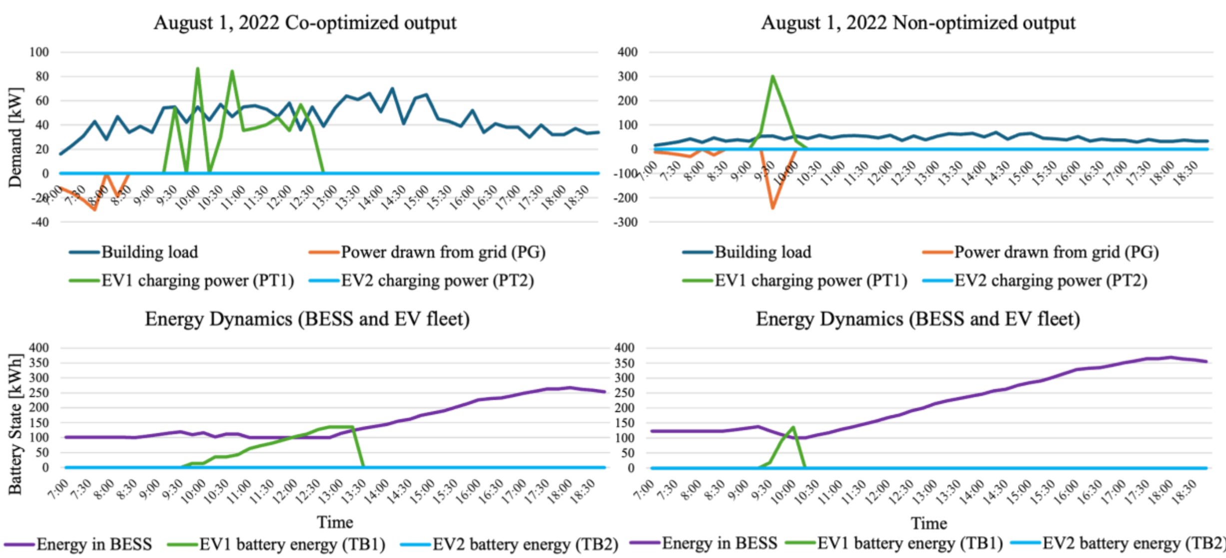

Figure 4-6. Visualization of the co-optimized and non-optimized MG load and battery state on August 1, 2022.

4.6 Conclusions and future work

The proposed truck scheduling algorithm significantly enhances the efficiency and flexibility of the MG system. Unlike traditional methods, where trucks charge until complete, regardless of the energy demand or cost, our algorithm determines the precise amount required for each truck, preventing unnecessary energy use. It also imposes constraints on the charging timeframes, ensuring that trucks charge only during predefined periods. This targeted approach allows for more effective utilization of available energy resources and cost savings.

The MG algorithm is designed to adapt to the scheduling information provided by the truck algorithm. It ensures that each truck battery's desired SOC is achieved within the specified timeframe. During these designated charging periods, the MG prioritizes truck batteries, which may temporarily cease MG battery charging. This prioritization ensures that the energy needs of the trucks are met without compromising the overall system stability.

In contrast, the baseline scenario for the MG operates without any coordinated input from the truck scheduling algorithm. Trucks arrive and charge based on their lowest cost preference, disregarding SOC constraints. The MG charges the trucks without prioritizing them over the MG battery, leading to sub-optimal energy use and higher costs. This uncoordinated approach often results in inefficient energy distribution and missed opportunities for cost savings.

The implementation of the co-optimized scheduling algorithm demonstrates significant improvements over the baseline. With each optimization iteration, the scheduler refines the charging times to align with lower TOU periods, thereby reducing energy costs. Additionally, the algorithm effectively manages the energy demand, ensuring that a significant portion of the required energy is supplied by solar power. This reduces reliance on grid energy and leverages renewable energy sources, enhancing the sustainability of the MG system.

The results indicate that the co-optimized method achieves a more balanced energy distribution and substantially saves costs. The dynamic adaptation of the MG to the truck scheduling algorithm allows for a synergistic relationship between the two systems, maximizing overall efficiency. This integrated approach represents a significant advancement in MG and transportation energy management, offering a scalable solution for future smart grid applications.

This integrated approach resolves key issues in EV charging management, providing a more reliable and efficient solution. The system can dynamically adapt to varying conditions by leveraging co-optimization, reducing demand costs, and optimizing energy usage. This method demonstrates significant potential for broader application in smart grid and transportation systems, paving the way for more sustainable and cost-effective energy management solutions. The results show clear benefits of integrating scheduling algorithms with MG operations. This synergy leads to more efficient energy distribution, cost savings, and grid stability.

4.7 Future work

Future research will focus on several key areas to enhance the MG energy allocation algorithm. First, we aim to extend the algorithm's capability to handle a dynamic set of constraints. This involves developing an adaptable framework that can accommodate a variable number of trucks dispatched to the EV CS. Currently, the algorithm operates under fixed constraints, but incorporating dynamic constraints will improve its flexibility and applicability to real-world scenarios where the number of trucks may fluctuate.

In addition to this, we plan to introduce a prioritization algorithm to address non-optimal solutions. This enhancement will enable operators to choose which trucks to dispatch based on a set of prioritization criteria when energy availability is limited. The prioritization algorithm will consider factors such as the SOC of each truck's battery, the urgency of their energy needs, and their operational schedules. By implementing this feature, the system will offer multiple methods for making dispatch decisions, thus optimizing the utilization of available energy and improving overall operational efficiency.

By addressing these areas, the proposed advancements aim to significantly improve the efficiency and adaptability of MG energy allocation systems, contributing to more sustainable and practical transportation energy management.

References

Agra, A., Christiansen, M., Figueiredo, R., Hvattum, L. M., Poss, M., & Requejo, C. (2013). The robust vehicle routing problem with time windows. *Computers & Operations Research*, *40*(3), 856–866. https://doi.org/10.1016/j.cor.2012.10.002

Alkaabneh, F., & Diabat, A. (2023). A multi-objective home healthcare delivery model and its solution using a branch-and-price algorithm and a two-stage meta-heuristic algorithm. *Transportation Research Part C: Emerging Technologies*, *147*, 103838. https://doi.org/10.1016/j.trc.2022.103838

Ames, A. D., Coogan, S., Egerstedt, M., Notomista, G., Sreenath, K., & Tabuada, P. (2019). Control barrier functions: Theory and applications. *2019 18th European Control Conference (ECC)*, 3420–3431.

Amiri, A., Zolfagharinia, H., & Amin, S. H. (2023). A robust multi-objective routing problem for heavy-duty electric trucks with uncertain energy consumption. *Computers & Industrial Engineering*, *178*, 109108. https://doi.org/10.1016/j.cie.2023.109108

Andreoni, M. (2023, June 23). Power Grids Are Teetering Worldwide. Here's Why. *The New York Times*. https://www.nytimes.com/2023/06/23/climate/texas-heat-power-grid.html

Basso, R., Kulcsár, B., & Sanchez-Diaz, I. (2021). Electric vehicle routing problem with machine learning for energy prediction. *Transportation Research Part B: Methodological*, *145*, 24–55. https://doi.org/10.1016/j.trb.2020.12.007

Ben-Tal, A., Ghaoui, L. E., & Nemirovski, A. (2009). *Robust Optimization*. Princeton University Press.

Ben-Tal, A., & Nemirovski, A. (1998). Robust Convex Optimization. *Mathematics of Operations Research*, *23*(4), 769–805. https://doi.org/10.1287/moor.23.4.769

Bezzi, D., Ceselli, A., & Righini, G. (2023). A route-based algorithm for the electric vehicle routing problem with multiple technologies. *Transportation Research Part C: Emerging Technologies*, *157*, 104374. https://doi.org/10.1016/j.trc.2023.104374

Bongiovanni, C., Kaspi, M., Cordeau, J.-F., & Geroliminis, N. (2022). A machine learning-driven two-phase metaheuristic for autonomous ridesharing operations. *Transportation Research Part E: Logistics and Transportation Review*, *165*, 102835. https://doi.org/10.1016/j.tre.2022.102835

Bongiovanni, C., Kaspi, M., & Geroliminis, N. (2019). The electric autonomous dial-a-ride problem. *Transportation Research Part B: Methodological*, *122*, 436–456. https://doi.org/10.1016/j.trb.2019.03.004

Boriboonsomsin, K., Vu, A., Hao, P., Wei, Z., Brown, D., Barth, M., Zhang, Y., Alasiri, F., Vital, F., & Ioannou, P. (2022). *Development and Application of Environmentally Friendly Intelligent Transportation System (ECO-ITS) Freight Strategies*. https://escholarship.org/uc/item/7262s64x

Brandão, J. (2016). A deterministic iterated local search algorithm for the vehicle routing problem with backhauls. *Top*, *24*(2), 445–465.

California Energy Commission. (2023). *Medium- and heavy-duty zero-emission vehicles in California*. https://www.energy.ca.gov/data-reports/energy-almanac/zero-emission-vehicle-and-infrastructure-statistics-collection/medium

Chen, P., Ioannou, P., & Dessouky, M. (2022). Mixed Freight Dynamic Routing Using a Co-Simulation Optimization Approach. *IEEE Transactions on Intelligent Transportation Systems*, *23*(8), 12833–12845. IEEE Transactions on Intelligent Transportation Systems. https://doi.org/10.1109/TITS.2021.3117931

Clean Vehicles Directive—European Commission. (n.d.). Retrieved August 19, 2024, from https://transport.ec.europa.eu/transport-themes/clean-transport/clean-and-energy-efficient-vehicles/clean-vehicles-directive_en

Desaulniers, G., Errico, F., Irnich, S., & Schneider, M. (2016). Exact Algorithms for Electric Vehicle-Routing Problems with Time Windows. *Operations Research*, *64*(6), 1388–1405. https://doi.org/10.1287/opre.2016.1535

Enriquez-Contreras, L., Barth, M., & Ula, S. (2024). CO\textsubscript2 and Cost Impact Analysis of a Microgrid with Electric Vehicle Charging Infrastructure: A Case Study in Southern California. *IEEE 27th International Conference on Intelligent Transportation Systems (ITSC)*.

Erdoğan, S., & Miller-Hooks, E. (2012). A green vehicle routing problem. *Transportation Research Part E: Logistics and Transportation Review*, *48*(1), 100–114.

Federal Motor Carrier Safety Administration. (n.d.). *Hours of service regulations*. https://www.fmcsa.dot.gov/regulations/hours-service

Fernando Enriquez-Contreras, L., Jahid Hasan, A. S. M., Yusuf, J., Garrido, J., & Ula, S. (2022). Microgrid Demand Response: A Comparison of Simulated and Real Results. *2022 North American Power Symposium (NAPS)*, 1–6. https://doi.org/10.1109/NAPS56150.2022.10012248

Freightquote. (n.d.). *Shipping to Long Beach*. https://www.freightquote.com/freight/rates/metro/long-beach-to-san-francisco/

Garrido, J., Hidalgo, E., Barth, M., & Boriboonsomsin, K. (2022). En-Route Opportunity Charging for Heavy-Duty Battery Electric Trucks in Drayage Operations: Case Study at the Southern California Ports. *2022 IEEE Vehicle Power and Propulsion Conference (VPPC)*, 1–6. https://doi.org/10.1109/VPPC55846.2022.10003273

Goeke, D., & Schneider, M. (2015). Routing a mixed fleet of electric and conventional vehicles. *European Journal of Operational Research*, *245*(1), 81–99.

Goetschalckx, M., & Jacobs-Blecha, C. (1989). The vehicle routing problem with backhauls. *European Journal of Operational Research*, *42*(1), 39–51. https://doi.org/10.1016/0377-2217(89)90057-X

Gounaris, C. E., Wiesemann, W., & Floudas, C. A. (2013). The Robust Capacitated Vehicle Routing Problem Under Demand Uncertainty. *Operations Research*. https://doi.org/10.1287/opre.1120.1136

Hasan, A. J., Enriquez-Contreras, L. F., Yusuf, J., & Ula, S. (2023). A universal optimization framework for commercial building loads using DERs from utility tariff perspective with tariff change impacts analysis. *Energy Reports*, *9*, 6088–6101.

Hu, C., Lu, J., Liu, X., & Zhang, G. (2018a). Robust vehicle routing problem with hard time windows under demand and travel time uncertainty. *Computers & Operations Research*, *94*, 139–153. https://doi.org/10.1016/j.cor.2018.02.006

Hu, C., Lu, J., Liu, X., & Zhang, G. (2018b). Robust vehicle routing problem with hard time windows under demand and travel time uncertainty. *Computers & Operations Research*, *94*, 139–153. https://doi.org/10.1016/j.cor.2018.02.006

Hussein, A. A., & Rakha, H. A. (2021). Vehicle platooning impact on drag coefficients and energy/fuel saving implications. *IEEE Transactions on Vehicular Technology*, *71*(2), 1199–1208.

Jeong, J., Ghaddar, B., Zufferey, N., & Nathwani, J. (2024). Adaptive robust electric vehicle routing under energy consumption uncertainty. *Transportation Research Part C: Emerging Technologies*, *160*, 104529.

Keskin, M., & Çatay, B. (2016a). Partial recharge strategies for the electric vehicle routing problem with time windows. *Transportation Research Part C: Emerging Technologies*, *65*, 111–127. https://doi.org/10.1016/j.trc.2016.01.013

Keskin, M., & Çatay, B. (2016b). Partial recharge strategies for the electric vehicle routing problem with time windows. *Transportation Research Part C: Emerging Technologies*, *65*, 111–127.

Keskin, M., Çatay, B., & Laporte, G. (2021). A simulation-based heuristic for the electric vehicle routing problem with time windows and stochastic waiting times at recharging stations. *Computers & Operations Research*, *125*, 105060. https://doi.org/10.1016/j.cor.2020.105060

Keskin, M., Laporte, G., & Çatay, B. (2019). Electric Vehicle Routing Problem with Time-Dependent Waiting Times at Recharging Stations. *Computers & Operations Research*, *107*, 77–94. https://doi.org/10.1016/j.cor.2019.02.014

Koç, Ç., & Laporte, G. (2018). Vehicle routing with backhauls: Review and research perspectives. *Computers & Operations Research*, *91*, 79–91.

Kuo, R. J., Wibowo, B. S., & Zulvia, F. E. (2016). Application of a fuzzy ant colony system to solve the dynamic vehicle routing problem with uncertain service time. *Applied Mathematical Modelling*, *40*(23), 9990–10001. https://doi.org/10.1016/j.apm.2016.06.025

Lamontagne, S., Carvalho, M., Frejinger, E., Gendron, B., Anjos, M. F., & Atallah, R. (2023). Optimising Electric Vehicle Charging Station Placement using Advanced Discrete Choice Models. *INFORMS Journal on Computing*, *35*(5), 1195–1213. https://doi.org/10.1287/ijoc.2022.0185

Lee, Z. J., Chang, D., Jin, C., Lee, G. S., Lee, R., Lee, T., & Low, S. H. (2018). Large-Scale Adaptive Electric Vehicle Charging. *2018 IEEE International Conference on Communications, Control, and Computing Technologies for Smart Grids (SmartGridComm)*, 1–7. https://doi.org/10.1109/SmartGridComm.2018.8587550

Li, Z., Yang, A., Chen, G., Tashakor, N., Zeng, Z., Peterchev, A. V., & Goetz, S. M. (2023). A smart adaptively reconfigurable DC battery for higher efficiency of electric vehicle drive trains. *arXiv Preprint*.

Lin, B., Ghaddar, B., & Nathwani, J. (2021). Electric vehicle routing with charging/discharging under time-variant electricity prices. *Transportation Research Part C: Emerging Technologies*, *130*, 103285.

Lin, S. (1965). Computer solutions of the traveling salesman problem. *Bell System Technical Journal*, *44*(10), 2245–2269.

Liu, H., Hao, P., Liao, Y., Tanvir, S., Boriboonsomsin, K., & Barth, M. J. (2024). Eco-Friendly Crowdsourced Meal Delivery: A Dynamic On-Demand Meal Delivery System with a Mixed Fleet of Electric and Gasoline Vehicles. *IEEE Transactions on Intelligent Transportation Systems*. https://ieeexplore.ieee.org/abstract/document/10457861/

Liu, X., Wang, D., Yin, Y., & Cheng, T. C. E. (2023). Robust optimization for the electric vehicle pickup and delivery problem with time windows and uncertain demands. *Computers & Operations Research*, *151*, 106119. https://doi.org/10.1016/j.cor.2022.106119

Lourenço, H. R., Martin, O. C., & Stützle, T. (n.d.). *ITERATED LOCAL SEARCH*.

Luke, J., Salazar, M., Rajagopal, R., & Pavone, M. (2021). Joint Optimization of Autonomous Electric Vehicle Fleet Operations and Charging Station Siting. *2021 IEEE International Intelligent Transportation Systems Conference (ITSC)*, 3340–3347. https://doi.org/10.1109/ITSC48978.2021.9565089

Markus, F. (2024, September). *EV battery technology: What’s coming now, tomorrow, and the far future*. https://www.motortrend.com/news/ev-battery-technology-future-emerging/

McCallen, R., Couch, R., Hsu, J., Browand, F., Hammache, M., Leonard, A., Brady, M., Salari, K., Rutledge, W., Ross, J., & al, et. (1999). *Progress in reducing aerodynamic drag for higher efficiency of heavy duty trucks (class 7-8)*. SAE Technical Paper.

McKinsey & Company. (2024, September). *How batteries will drive the zero-emission truck transition*. https://www.mckinsey.com/industries/automotive-and-assembly/our-insights/how-batteries-will-drive-the-zero-emission-truck-transition

Mingozzi, A., Giorgi, S., & Baldacci, R. (1999). An Exact Method for the Vehicle Routing Problem with Backhauls. *Transportation Science*, *33*, 315–329. https://doi.org/10.1287/trsc.33.3.315

Montoya, A., Guéret, C., Mendoza, J. E., & Villegas, J. G. (2017a). The electric vehicle routing problem with nonlinear charging function. *Transportation Research Part B: Methodological*, *103*, 87–110. https://doi.org/10.1016/j.trb.2017.02.004

Montoya, A., Guéret, C., Mendoza, J. E., & Villegas, J. G. (2017b). The electric vehicle routing problem with nonlinear charging function. *Transportation Research Part B: Methodological*, *103*, 87–110.

Morehouse, C. (2022, December 26). *Physical attacks on power grid surge to new peak*. POLITICO. https://www.politico.com/news/2022/12/26/physical-attacks-electrical-grid-peak-00075216

NET energy metering and net billing California Public Utilities Commission. (2023). In *California Public Utilities Commission*. https://www.cpuc.ca.gov/industries-and-topics/electrical-energy/demand-side-management/customer-generation/net-energy-metering-and-net-billing

Norrby, D. (2014). *A CFD study of the aerodynamic effects of platooning trucks*.

OR, I. (n.d.). *Traveling Salesman Type Combinatorial Problems and Their Relation to the Logistics of Regional Blood Banking.* [Ph.D., Northwestern University]. Retrieved July 2, 2024, from https://www.proquest.com/docview/302812391/citation/C01A84EFE0E94317PQ/1

Palhazi Cuervo, D., Goos, P., Sörensen, K., & Arráiz, E. (2014). An iterated local search algorithm for the vehicle routing problem with backhauls. *European Journal of Operational Research*, *237*(2), 454–464. https://doi.org/10.1016/j.ejor.2014.02.011

Parragh, S. N., Doerner, K. F., & Hartl, R. F. (2008). A survey on pickup and delivery problems. *Journal Für Betriebswirtschaft*, *58*(1), 21–51. https://doi.org/10.1007/s11301-008-0033-7

Pelletier, S., Jabali, O., & Laporte, G. (2019). The electric vehicle routing problem with energy consumption uncertainty. *Transportation Research Part B: Methodological*, *126*, 225–255.

Peng, D., Barth, M., & Boriboonsomsin, K. (n.d.). Addressing the Robust Battery Electric Truck Dispatching Problem with Backhauls and Time Windows under Travel Time Uncertainty. *In 2024 IEEE 27th International Conference on Intelligent Transportation Systems (ITSC). IEEE.*

Peng, D., Wu, G., & Boriboonsomsin, K. (n.d.). The Bi-objective Battery Electric Truck Dispatching Problem with Backhauls and Time Windows. *Transportation Research Record*. https://doi.org/10.1177/03611981241246270

Peng, D., Wu, G., & Boriboonsomsin, K. (2023a). Energy-Efficient Dispatching of Battery Electric Truck Fleets with Backhauls and Time Windows. *SAE International Journal of Electrified Vehicles*, *13*(1), Article 14-13-01–0009. https://doi.org/10.4271/14-13-01-0009

Peng, D., Wu, G., & Boriboonsomsin, K. (2023b). Energy-efficient dispatching of battery electric truck fleets with backhauls and time windows. *SAE International Journal of Electrified Vehicles*, *13*(14-13-01–0009). https://www.sae.org/publications/technical-papers/content/14-13-01-0009/

Peng, D., Wu, G., & Boriboonsomsin, K. (2023c). Energy-Efficient Dispatching of Battery Electric Truck Fleets with Backhauls and Time Windows. *SAE International Journal of Electrified Vehicles*, *13*(14-13-01–0009). https://www.sae.org/publications/technical-papers/content/14-13-01-0009/

Peng, D., Zhao, Z., Wu, G., & Boriboonsomsin, K. (2023). Bi-Level Fleet Dispatching Strategy for Battery-Electric Trucks: A Real-World Case Study. *Sustainability*, *15*(2), Article 2. https://doi.org/10.3390/su15020925

Potvin, J.-Y., & Rousseau, J.-M. (1995). An exchange heuristic for routeing problems with time windows. *Journal of the Operational Research Society*, *46*(12), 1433–1446.

Public Safety Power Shutoffs. (n.d.). Retrieved February 6, 2025, from https://www.cpuc.ca.gov/PSPS/

Purvins, A., Covrig, C.-F., & Lempidis, G. (2018). Electric vehicle charging system model for accurate electricity system planning. *IET Generation, Transmission & Distribution*, *12*(17), 4053–4059.

Ropke, S., & Pisinger, D. (2006a). A unified heuristic for a large class of Vehicle Routing Problems with Backhauls. *European Journal of Operational Research*, *171*(3), 750–775. https://doi.org/10.1016/j.ejor.2004.09.004

Ropke, S., & Pisinger, D. (2006b). A unified heuristic for a large class of Vehicle Routing Problems with Backhauls. *European Journal of Operational Research*, *171*(3), 750–775. https://doi.org/10.1016/j.ejor.2004.09.004

Ropke, S., & Pisinger, D. (2006c). An adaptive large neighborhood search heuristic for the pickup and delivery problem with time windows. *Transportation Science*, *40*(4), 455–472.

Santos, M. J., Amorim, P., Marques, A., Carvalho, A., & Póvoa, A. (2020). The vehicle routing problem with backhauls towards a sustainability perspective: A review. *Top*, *28*(2), 358–401.

Savelsbergh, M. W. (1992). The vehicle routing problem with time windows: Minimizing route duration. *ORSA Journal on Computing*, *4*(2), 146–154.

Schedule TOU-GS-2 Southern California Edison. (2023). In *Southern California Edison*. https://edisonintl.sharepoint.com/teams/Public/TM2/Shared%20Documents/Forms/AllItems.aspx?ga=1&id=%2Fteams%2FPublic%2FTM2%2FShared%20Documents%2FPublic%2FRegulatory%2FHistorical%2DSCE%20Historical%20Books%2FElectric%2F2023%2FSchedules%2FGeneral%20Service%20%26%20Industrial%20Rates%2FELECTRIC%5FSCHEDULES%5FTOU%2DGS%2D2%2Epdf&parent=%2Fteams%2FPublic%2FTM2%2FShared%20Documents%2FPublic%2FRegulatory%2FHistorical%2DSCE%20Historical%20Books%2FElectric%2F2023%2FSchedules%2FGeneral%20Service%20%26%20Industrial%20Rates

Schneider, M., Stenger, A., & Goeke, D. (2014). The electric vehicle-routing problem with time windows and recharging stations. *Transportation Science*, *48*(4), 500–520.

Shaw, P. (1998). Using Constraint Programming and Local Search Methods to Solve Vehicle Routing Problems. In M. Maher & J.-F. Puget (Eds.), *Principles and Practice of Constraint Programming—CP98* (pp. 417–431). Springer. https://doi.org/10.1007/3-540-49481-2_30

Shen, Y., Yu, L., & Li, J. (2022). Robust Electric Vehicle Routing Problem with Time Windows under Demand Uncertainty and Weight-Related Energy Consumption. *Complex System Modeling and Simulation*, *2*(1), 18–34. https://doi.org/10.23919/CSMS.2022.0005

Shi, Y., Boudouh, T., & Grunder, O. (2019). A robust optimization for a home health care routing and scheduling problem with consideration of uncertain travel and service times. *Transportation Research Part E: Logistics and Transportation Review*, *128*, 52–95. https://doi.org/10.1016/j.tre.2019.05.015

Szilagyi, E., Petreus, D., Paulescu, M., Patarau, T., Hategan, S.-M., & Sarbu, N. A. (2023). Cost-effective energy management of an islanded microgrid. *Energy Reports*, *10*, 4516–4537.

The U.S. National Blueprint for Transportation Decarbonization: A Joint Strategy to Transform Transportation. (n.d.). Energy.Gov. Retrieved August 19, 2024, from https://www.energy.gov/eere/us-national-blueprint-transportation-decarbonization-joint-strategy-transform-transportation

Toth, P., & Vigo, D. (1997). An Exact Algorithm for the Vehicle Routing Problem with Backhauls. *Transportation Science*, *31*(4), 372–385. https://doi.org/10.1287/trsc.31.4.372

Uddin, M., Mo, H., Dong, D., Elsawah, S., Zhu, J., & Guerrero, J. M. (2023). Microgrids: A review, outstanding issues and future trends. *Energy Strategy Reviews*, *49*, 101127.

U.S. Energy Information Administration. (2023). *California leads the United States in electric vehicles and charging infrastructure*. https://www.eia.gov/todayinenergy/detail.php?id=61082

Vegendla, P., Sofu, T., Saha, R., Kumar, M. M., & Hwang, L.-K. (2015). *Investigation of aerodynamic influence on truck platooning*. SAE Technical Paper.

Verbruggen, F., Hoekstra, A., & Hofman, T. (2018). Evaluation of the state-of-the-art of full-electric medium and heavy-duty trucks. *Proceedings of the 2018 World Electric Vehicle Symposium and Exhibition (EVS31)*, *30*.

Vincent, F. Y., Jodiawan, P., & Gunawan, A. (2021a). An Adaptive Large Neighborhood Search for the green mixed fleet vehicle routing problem with realistic energy consumption and partial recharges. *Applied Soft Computing*, *105*, 107251.

Vincent, F. Y., Jodiawan, P., & Gunawan, A. (2021b). An Adaptive Large Neighborhood Search for the green mixed fleet vehicle routing problem with realistic energy consumption and partial recharges. *Applied Soft Computing*, *105*, 107251.

Vital, F., & Ioannou, P. (2019). Long-haul truck scheduling with driving hours and parking availability constraints. *2019 IEEE Intelligent Vehicles Symposium (IV)*, 620–625. https://ieeexplore.ieee.org/abstract/document/8814011/

Vital, F., & Ioannou, P. (2021a). Effects of Working Hour Regulations and Parking Shortages on Truck Electrification. *2021 IEEE International Intelligent Transportation Systems Conference (ITSC)*, 3360–3365. https://doi.org/10.1109/ITSC48978.2021.9564810

Vital, F., & Ioannou, P. (2021b). Scheduling and shortest path for trucks with working hours and parking availability constraints. *Transportation Research Part B: Methodological*, *148*, 1–37.

Vital, F., Ioannou, P., & Gupta, A. (2020). Survey on intelligent truck parking: Issues and approaches. *IEEE Intelligent Transportation Systems Magazine*, *13*(4), 31–44.

Wang, C., Hao, P., Boriboonsomsin, K., & Barth, M. (2022). Developing a Mesoscopic Energy Consumption Model for Battery Electric Trucks Using Real-World Diesel Truck Driving Data. *2022 IEEE Vehicle Power and Propulsion Conference (VPPC)*, 1–6. https://doi.org/10.1109/VPPC55846.2022.10003335

Waqas, M., Nuzzo, P., & Ioannou, P. (2024). Provably Safe Design Methodology for Automatic Longitudinal Control of Autonomous Vehicles. *IEEE Transactions on Intelligent Vehicles*. https://ieeexplore.ieee.org/abstract/document/10416395/

Wu, G., Peng, D., & Boriboonsomsin, K. (2024). *Developing an Efficient Dispatching Strategy to Support Commercial Fleet Electrification*. https://escholarship.org/uc/item/2qz0n2gv

Xiao, J., Du, J., Cao, Z., Zhang, X., & Niu, Y. (2023). A diversity-enhanced memetic algorithm for solving electric vehicle routing problems with time windows and mixed backhauls. *Applied Soft Computing*, *134*, 110025. https://doi.org/10.1016/j.asoc.2023.110025

Yang, S., Ning, L., Tong, L. C., & Shang, P. (2022a). Integrated electric logistics vehicle recharging station location–routing problem with mixed backhauls and recharging strategies. *Transportation Research Part C: Emerging Technologies*, *140*, 103695.

Yang, S., Ning, L., Tong, L. (Carol), & Shang, P. (2022b). Integrated electric logistics vehicle recharging station location–routing problem with mixed backhauls and recharging strategies. *Transportation Research Part C: Emerging Technologies*, *140*, 103695. https://doi.org/10.1016/j.trc.2022.103695

Yu, V. F., Aloina, G., Jodiawan, P., Gunawan, A., & Huang, T.-C. (2023). The vehicle routing problem with simultaneous pickup and delivery and occasional drivers. *Expert Systems with Applications*, *214*, 119118. https://doi.org/10.1016/j.eswa.2022.119118

Yu, V. F., Anh, P. T., & Baldacci, R. (2023). A robust optimization approach for the vehicle routing problem with cross-docking under demand uncertainty. *Transportation Research Part E: Logistics and Transportation Review*, *173*, 103106. https://doi.org/10.1016/j.tre.2023.103106

Yu, V. F., Jodiawan, P., & Gunawan, A. (2021). An Adaptive Large Neighborhood Search for the green mixed fleet vehicle routing problem with realistic energy consumption and partial recharges. *Applied Soft Computing*, *105*, 107251. https://doi.org/10.1016/j.asoc.2021.107251

Zhang, S., Gajpal, Y., Appadoo, S. S., & Abdulkader, M. M. S. (2018). Electric vehicle routing problem with recharging stations for minimizing energy consumption. *International Journal of Production Economics*, *203*, 404–413. https://doi.org/10.1016/j.ijpe.2018.07.016

Zhang, X., & Li, H. (2021). Battery range innovations for long-haul trucks. *Transportation Research Part D: Transport and Environment*, *90*, 102665.

Data Summary

Products of Research

For long-haul trucking study (Chapter 1 and Chapter 2), this study utilized multiple datasets to develop a comprehensive optimization model for electric truck routing and charging along the Long Beach to San Francisco corridor. The key data categories collected and analyzed include:

- **CS Data:** Locations and availability of CSs were observed using **TruckMap** and supplemented by distance data obtained from **Google Maps**.
- **Electric Truck Operational Data:** Includes battery characteristics, SOC, and energy consumption rates. Data related to truck range limitations and estimated charging speeds were sourced and estimated from the **Run on Less website**.

Driver and Regulatory Data: Compliance with HOS requirements, driving schedules, and rest periods were collected from the relevant HOS website.

In this project, real-world dispatching data were collected from a local full-service logistics company to support the numerical experiments in Sections 3.7 and 4.4. Additionally, Section 3.6 introduces a novel hypothetical EV routing problem with backhauls and time windows (EVRPBTW) benchmark dataset.

The datasets, along with detailed descriptions, are summarized in Table 5-0-1Table 5-0-1. Dataset description and format (Chapter 3 and . Both the datasets and their solutions have been uploaded to the Dryad data repository. The dataset URL is provided in the Data Access and Sharing Section.

Table 5-0-1. Dataset description and format (Chapter 3 and Chapter 4).

Data Files	Data description	File Format
Section_3_new_EVRPBTW_data.zip	The new EVRPTWB benchmark dataset contains 60 instances, with 20 instances including 25 customers, 20 instances including 50 customers, and 20 instances including 100 customers. The instances are provided as CSV files. We store the problem instances and detailed solutions in the compressed ZIP file, named “Section_3_2_EVRPBTW_benchmark_instances”.	.zip

Section_3_BKS_data_ with_solutions.zip	The Zip file contains benchmark dataset obtained from (Toth & Vigo, 1997) and our solutions. The TV89 instance set comprises 36 problem instances with customer sizes ranging from 21 to 100. Detailed solutions are also documented in Excel files.	.zip
Section_3_real_world_data _with_solutions.zip	The real-world dispatching data is stored in the Zip file, which includes a CSV file for an instance with 47 customers and an Excel file containing detailed solutions.	.zip
Section_4_ real_world_data _with_solutions.zip	We generate a real-world instance with 19 customers, where 14 are line-haul customers, and the rest are back-haul customers. The Zip file includes the problem instance and the detailed results in PDF format.	.zip

Data Format and Content

The collected data is stored and processed in various formats to suit analytical needs, including:

- **CSV Files:** Battery SOC, truck-specific operational details, and estimated charging durations.
- **TXT Files:** HOS compliance rules, driving logs, and rest period schedules.

The data format and content utilized in Chapters 4 and 5 are detailed in Table 5-0-1.

Data Access and Sharing

TruckMap, Google Maps, and HOS regulations should be free to access. The data from Run on Less may need to have a limitation on access.

https://runonless.com/run-on-less-electric-depot-reports/

https://www.fmcsa.dot.gov/regulations/hours-of-service

The data used in Chapter 3 can be openly access via Dryad repository link: https://doi.org/10.5061/dryad.6hdr7srbv.

The data used in Chapter 4 can be openly access via GitHub repository link: https://github.com/CurtisPeng123/Additional-material-for-the-BET-dispatching-with-microgrid-intergration.

Reuse and Redistribution

The data used in this study were sourced directly from publicly available websites, including Google Maps, TruckMap, and Run on Less. Due to the terms of service and usage restrictions of these data sources, the raw data cannot be redistributed or made publicly available. However, the processed outputs derived from this data are available for review in the report and related publications. The raw data from external websites were used solely for research purposes in accordance with the terms of service of the respective data providers. The original data from Google Maps, TruckMap, and Run on Less are subject to their respective licensing agreements and cannot be shared or redistributed by the authors. Any reuse of processed results from this project must include proper attribution to this report and its authors.

The data should be restricted for research use only. If the data are used, our work should be properly cited as:

Dongbo Peng, Matthew Barth, Kanok Boriboonsomsin (2023), Routing short-haul trucks under the uncertainties of travel time and service time [supporting dataset], Project Funded by NCST 2024-2025, UC Riverside, Dataset, https://doi.org/10.5061/dryad.6hdr7srbv

Appendix A

Algorithm 1 Overview of the two-phase metaheuristics

Input: An initial feasible solution S generated by initialization phase
Output: Global Best solution S^{best}

$S^{init} \leftarrow$ $generate\_inital\_solution(\,)$; $S^{current} \leftarrow S^{init}$; $S^{best} \leftarrow S^{init}$;
$S^{current} \leftarrow S^{init}$; $S^{best} \leftarrow S^{init}$;
Phase I: Perform the ALNS metaheuristics algorithm on S^{init} to solve a deterministic model
while stop criteria of ALNS is not meet **do**
  {select a destroy operator $\zeta^{-} \in \Pi^{-}$ by $P(\omega_i^{-})$}
  Remove n vertex from current solution $S^{current}$ with ζ^{-}
  $S^{new} \leftarrow$ ApplyDestroyedOperator($S^{current}$)
  {select a repair operator $\zeta^{+} \in \Pi^{+}$ by $P(\omega_i^{+})$}}
  $S^{new} \leftarrow$ ApplyRepairOperator(S^{new})
    if $f^{DM}(S^{new}) \leq f^{DM}(S^{best})$ **then**
      $S^{best} \leftarrow S^{new}$; $S^{current} \leftarrow S^{new}$
    else
      Generate a random number $\mathrm{p} \in [0,1]$
      if $\exp[(f^{DM}(S^{new}) - f^{DM}(S^{best}))/T] \geq \mathrm{p}$ **then**
        $S^{current} \leftarrow S^{new}$
  Update: $\omega^{-}, \omega^{+}, T$
end while
Phase 2: Perform ILS process to refine S^{best} and find robust dispatching solutions
Repeat
  $S^{current} \leftarrow$ Apply perturbation process on S^{best}
  $S^{new} \leftarrow$ Apply LS on $S^{current}$
    if $f^{SRO}(S^{new}) \leq f^{SRO}(S^{best})$ **then**
      $S^{best} \leftarrow S^{new}$
Until ILS termination condition met
return S^{best}

Algorithm 2 Construction of the initial feasible solution

Input: Unvisited customers pool $N^{unvisited}$, list of CSs;
Output: An initial feasible solution S^{init}

1: **Initialization**: Total number of BEVs $K = \infty$; Potential initial solution $S^{init} = \{\}$
2: **while** iterations ς is not reached **do**
3:   **if** unvisited customers exist in $N^{unvisited}$ **then**
4:     A new route S_k^{init} starts:
5:       Randomly select a customer i from the unvisited customers pool and remove i from $N^{unvisited}$
5:       Add customer i to the new route S_k^{init}
6:       Find a favorable customer i into S_k^{init} at position x by a greedy heuristic, which leading the minimal increasing cost $\Delta cost = f^{DM}\left(S_k^{init}\right) - f^{DM}\left(S_{k,-i,x}^{init}\right)$
7:       **if** a favorable customer i exists **then**
8:         Insert customer i at position x; Update unvisited customers pool $N^{unvisited}$.
        Continue to **line 6**
9:       **else**
10:         **if** no favorable customer i can be inserted into route S_k^{init} due to limited driving range and no recharging schedule **then**
11:           Find a favorable customer r into S_k^{init} at position x by a greedy heuristic, which leading the minimal increasing cost $\Delta cost = f^{DM}\left(S_k^{init}\right) - f^{DM}\left(S_{k,-r,x}^{init}\right)$
          Continue to **line 6**
12:         **else**
13:           Continue to **line 3**
14:   **if** $K \leq \left|S^{init}\right|$ **then**
15:     **Update:** Total number of BEVs $K = \left|S^{init}\right|$, if $K \leq \left|S^{init}\right|$; $S^{init} = \{S_1^{init}, \dots, S_k^{init}\}$
16: **Update:** $\varsigma = \varsigma + 1$
17: **end while**
18: **return** S^{init}

Appendix B

Table B-1. Final parameters setting of two-phase metaheuristics used in numerical studies

ALNS Notation	Value	Description
ς	100	Maximum iteration in the construction of initial feasible solution.
ϕ	(0.5, 0.25, 0.25)	Parameter vector in Shaw removal operator.
T_{init}	10	Initial temperature in the SA heuristic.
T_{init}	0.05	End temperature in the SA heuristic.
δ	0.9998	Cooling rate in the SA heuristic.
λ	0.8	Decay parameter in the ALNS metaheuristics.
η_{ALNS}^{max}	2000	Maximum iterations in the ALNS metaheuristics.
$\eta_{non\_improve}$	750	Non-improved iterations in the ALNS metaheuristics.
ψ	(15, 9, 8, 5)	Score vector in the ALNS metaheuristics.
ILS		
η_{ILS}^{max}	50	Maximum iterations in the ILS metaheuristics.

Table B-2. Results for the standard VRPB on TV89 instances. Columns "N, L, B" represent the number of customers, linehaul and backhaul customers, respectively. The column "M" represents the number of vehicles. We compare our proposed ALNS to the BKS and the result

Instances	N	L	B	M	BKS	ILSA (B16)	Our proposed ALNS		
							Best sol.	Best sol. gap (%)	Time (Sec.)
eil22_50	21	11	10	3	371	371	371	0.00%	6.09
eil22_66	21	14	7	3	366	366	366	0.00%	5.56
eil22_80	21	17	4	3	375	375	375	0.00%	6.43
eil23_50	22	11	11	2	682	682	682	0.00%	6.75
eil23_66	22	15	7	2	649	656	649	0.00%	7.02
eil23_80	22	18	4	2	623	623	623	0.00%	7.15
eil30_50	29	15	14	2	501	501	501	0.00%	14.29
eil30_66	29	20	9	3	537	538	537	0.00%	14.75
eil30_80	29	24	5	3	514	519	514	0.00%	12.79
eil33_50	32	16	16	3	738	738	738	0.00%	18.00
eil33_66	32	22	10	3	750	750	750	0.00%	15.81
eil33_80	32	26	6	3	736	736	736	0.00%	32.24
eil51_50	50	25	25	3	559	560	559	0.00%	40.10
eil51_66	50	34	16	4	548	548	548	0.00%	46.05
eil51_80	50	40	10	4	565	565	573	1.42%	43.65
eilA76_50	75	37	38	6	739	739	739	0.00%	110.17
eilA76_66	75	50	25	7	768	768	769	0.13%	198.52

Instances	N	L	B	M	BKS	ILSA (B16)	Our proposed ALNS		
							Best sol.	Best sol. gap (%)	Time (Sec.)
eilA76_80	75	60	15	8	781	793	889	13.83%	256.03
eilB76_50	75	37	38	8	801	801	801	0.00%	178.14
eilB76_66	75	50	25	10	873	875	891	2.06%	177.01
eilB76_80	75	60	15	12	919	928	940	2.29%	185.28
eilC76_50	75	37	38	5	713	714	713	0.00%	157.88
eilC76_66	75	50	25	6	734	734	735	0.14%	174.44
eilC76_80	75	60	15	7	733	737	739	0.82%	147.15
eilD76_50	75	37	38	4	690	690	690	0.00%	153.89
eilD76_66	75	50	25	5	715	715	715	0.00%	59.00
eilD76_80	75	60	15	6	694	695	702	1.15%	101.90
eilA101_50	100	50	50	4	831	847	842	1.32%	364.86
eilA101_66	100	67	33	6	846	855	846	0.00%	282.47
eilA101_80	100	80	20	6	856	891	885	3.39%	456.19
eilB101_50	100	50	50	7	923	940	940	1.84%	388.28
eilB101_66	100	67	33	9	982	1028	1105	12.41%	406.15
eilB101_80	100	80	20	11	1008	1016	1068	5.95%	429.09
Average					700.6	705.9	713.1		136.46
Number of optimal solutions					33	16	20		